



Institute for Soil Mechanics  
and Foundation Engineering



# MASTER THESIS

---

## NUMERICAL STUDY ON THE LONG-TERM BEHAVIOUR OF WOODEN PILE FOUNDATIONS IN VENICE

---

**CHRISTIANA KÖPPL**

Submitted at the  
Institute for Soil Mechanics and Foundation Engineering  
Graz University of Technology

Advisors:

**Ao.Univ.-Prof. Helmut F. Schweiger**

Institute for Soil Mechanics and Foundation Engineering  
Graz University of Technology

**Dipl.-Ing. Franz Tschuchnigg**

Institute for Soil Mechanics and Foundation Engineering  
Graz University of Technology

**Prof. Paolo Simonini**

Geomechanics Group, Department IMAGE  
University of Padova

Graz, October 2012

## **DECLARATION**

I hereby declare that this submission is my own work and that, to the best of my knowledge and belief, it contains no material previously published or written by another person nor material which to a substantial extent has been accepted for the award of any other degree or diploma of the university or other institute of higher learning, except where due acknowledgment has been made in the text.

Graz, October 2012

Christiana Köppl

## **ACKNOWLEDGEMENTS**

At first, I would like to thank my primary advisors Prof. Helmut Schweiger and Dipl.-Ing. Franz Tschuchnigg for the excellent support and guidance during the writing process and for the thorough review of my thesis.

Further, I want to acknowledge the contributions of my secondary advisor Prof. Paolo Simonini, who proposed this topic to me, and of Francesca Ceccato. I appreciate their support in getting this thesis started and the profit of our cooperation.

I am deeply grateful to Samir Omerović. Thanks for his encouragement and advice, especially during the past few months, and for keeping me grounded.

Finally, I want to express my gratitude to my family. Thanks for giving me the opportunity to pursue my goals and for supporting me during the years of study.

---

## ABSTRACT

According to recent studies, wooden foundation piles degrade also in anoxic conditions. This represents a serious problem for the preservation of the cultural heritage of Venice, as wooden piles were commonly used for supporting the loads of Venetian buildings. Based on these facts, it is necessary to investigate and describe the phenomenon of pile degradation, and to quantify its effect on the stability of the foundation and of the superstructure.

For this purpose, numerical analyses are carried out in 2D and 3D. The 2D analyses focus on the identification of a representative model capturing the degradation process, and on mechanically describing the interaction between single piles and adjacent soil during this process. In this regard, different parameter sets for the soil as well as different constitutive models for the same are applied. The 3D analyses are dedicated to the foundation of the Frari bell tower in Venice, which is facing the problem of wooden pile degradation. Within both 2D and 3D analyses, also the visco-plastic behaviour of the lagoon soil is taken into account.

By means of the 2D single-pile model, it was possible to simulate the typical behaviour of a group pile. The performed analyses give a valuable insight in the distribution of stresses and their redistribution with pile degradation, which is essentially different for the tested degradation methods. In this regard, a reduction of interface parameters represents a reasonable approach for simulating pile degradation in the early stages. In case of advanced degradation, a modification of pile parameters should additionally be incorporated in the model.

During the single-pile analyses, the effect of interface degradation caused a significant increase in settlements compared to the amount of secondary settlements. In contrast, in the 3D analyses the interface degradation hardly affected the results. Moreover, those settlements resulted even smaller than the settlements due to creeping. Consequently, the response of the foundation during degradation has to be verified.

Based on the results presented in this thesis, further analyses have to be conducted including the time-dependent behaviour of both wooden pile and soil. For this purpose, more advanced models should be applied for representing pile degradation and the peculiarities of Venetian subsoil. Thus, it might be possible to quantitatively describe the effects of the degradation phenomenon not only in case of the Frari tower; quantitative statements would play a decisive role in evaluating if foundations in Venice fulfill the stability requirements and, if this is not the case, their need for safeguarding measures. Moreover, a further development of degradation models would be beneficial also for other European cities facing the same problem of wooden pile degradation, such as for example Amsterdam.

Keywords: Venice, wooden pile foundations, pile degradation, time-dependent behaviour, long-term behaviour, computational geotechnics, finite element analysis

---

## KURZFASSUNG

Laut jüngsten Studien zersetzen sich Gründungspfähle aus Holz auch in sauerstofffreien Milieu. Das stellt ein ernstzunehmendes Problem für die Erhaltung des Kulturerbes von Venedig dar, da Holzpfähle üblicherweise zum Abtragen von Gebäudelasten eingesetzt wurden. Aufgrund dieser Tatsachen ist es notwendig, das Phänomen Pfahldegradation zu untersuchen und zu beschreiben.

Zu diesem Zweck werden numerische Berechnungen in 2D und 3D durchgeführt. Bei den 2D-Berechnungen liegt der Schwerpunkt darauf, ein repräsentatives Modell zur Darstellung des Degradationsprozesses zu finden und die Interaktion zwischen einzelnen Pfählen und dem angrenzenden Boden während dieses Prozesses mechanisch zu beschreiben. In diesem Zusammenhang werden verschiedene Parameter und Materialmodelle angewandt. Die 3D-Berechnungen beziehen sich auf die Gründung des Frari-Glockenturms in Venedig, welche mit dem Problem der Holzpfehldegradation konfrontiert ist. In den 2D- und 3D-Berechnungen wird weiters das visko-plastische Verhalten des Lagunenbodens berücksichtigt.

Durch das 2D Einzelpfehl-Modell war es möglich, das typische Verhalten eines Gruppenpfahls zu simulieren. Die durchgeführten Berechnungen ermöglichen einen wertvollen Einblick in die Spannungsverteilung und deren Umverteilung mit fortschreitender Pfehldegradation, welche sich für die getesteten Degradationsmethoden grundlegend unterschiedlich ergeben. Hierbei stellt eine Reduktion der Interfaceparameter einen sinnvollen Ansatz zur Modellierung der Degradation im Frühstadium dar. Bei fortgeschrittener Degradation sollte zusätzlich eine Veränderung der Pfehlparameter selbst in das Modell eingebunden werden.

Im Zuge der Einzelpfehl-Berechnungen verursachte die Interface-Degradation einen starken Anstieg der Setzungen verglichen mit dem Betrag der Sekundärsetzungen. Im Gegensatz dazu hatte die Interface-Degradation im 3D-Modell kaum Auswirkungen auf die Ergebnisse. Darüber hinaus waren die resultierenden Setzungen geringer als die Sekundärsetzungen. Daher ist die Reaktion der Gründung auf die Degradation noch zu bestätigen.

Ausgehend von den Ergebnissen der vorliegenden Masterarbeit müssen weitere Berechnungen durchgeführt werden, die das zeitabhängige Verhalten sowohl der Holzpfähle als auch des Bodens einschließen. Zu diesem Zweck sollten erweiterte Modelle zur Darstellung der Pfehldegradation und der Besonderheiten des Lagunenbodens eingesetzt werden. Auf diese Weise wäre es möglich, die Auswirkungen der Degradation nicht nur im Fall des Frari-Turmes zahlenmäßig zu erfassen; eine quantitative Aussage wäre ein entscheidendes Kriterium um bewerten zu können, ob Gründungen in Venedig die Stabilitätsanforderungen erfüllen, und, wenn das nicht der Fall ist, deren Bedarf an Instandsetzungsmaßnahmen zu ermitteln. Darüber hinaus wäre eine Weiterentwicklung von Degradationsmodellen auch für andere Europäische Städte nützlich, wie beispielsweise Amsterdam, die ebenfalls mit dem Problem der Holzpfehldegradation konfrontiert sind.

Schlüsselwörter: Venedig, Holzpfehlgründungen, Pfehldegradation, zeitabhängiges Verhalten, Langzeitverhalten, numerische Geotechnik, Finite Element Methode

---

# TABLE OF CONTENTS

1	Introduction .....	1
2	Historic foundations in Venice .....	3
2.1	Foundation types and pile-driving techniques .....	3
2.2	Foundation of the Frari bell tower .....	7
2.3	Pile degradation .....	11
3	Geologic formation and characteristics of Venice lagoon soils .....	13
4	Numerical modelling in geotechnical engineering .....	16
4.1	Introduction.....	16
4.2	Specific features of numerical modelling.....	16
4.2.1	Soil models .....	16
4.2.2	Interface .....	17
4.2.3	Initial stresses .....	18
5	Preliminary study on single pile .....	19
5.1	Introduction.....	19
5.2	Geometry and input in Plaxis 2D.....	20
5.3	Material parameters.....	23
5.3.1	Soil parameters.....	23
5.3.2	Pile.....	26
5.3.3	Raft .....	30
5.4	Calculations .....	31
5.4.1	Pile degradation .....	32
5.4.2	Interface degradation.....	64
5.4.3	Conclusion .....	84
6	Numerical analysis of the foundation of the Frari bell tower .....	87
6.1	Introduction.....	87
6.2	Geometry and Input in Plaxis 3D Foundation .....	87
6.3	Material parameters.....	91
6.3.1	Soil .....	91
6.3.2	Piles .....	92
6.3.3	Raft .....	93
6.3.4	Masonry footing .....	93
6.3.5	Temporary support system for construction pit .....	93
6.4	Calculations .....	94

---

6.4.1	Drained analysis.....	94
6.4.2	Consolidation analysis .....	104
6.4.3	Conclusion .....	108
7	Final remarks.....	109
8	Future prospect.....	111
9	References.....	113

## FIGURES

<i>Figure 1: Foundation of Palazzo Ducale [by Malvezzi (1874), see Ceccato (2011)]</i> .....	3
<i>Figure 2: Foundation of new San Marco bell tower [by Donghi (1913), see Colombo et al. (1997)]</i> .....	3
<i>Figure 3: Section and top view of the foundation of the Sant’Agnese tower [by Casoini (1851), see Marchi et al. (2006)]</i> .....	5
<i>Figure 4: Watercolour by Grevembroch, G. (18<sup>th</sup> century), which illustrates two workers driving wooden piles into the subsoil using a battipalo [see Trovò (2012)]</i> .....	6
<i>Figure 5: Battipalo, Venice, Procurators office [see Maggi (2002)]</i> .....	6
<i>Figure 6: Battipalo driven by water wheel (18th century) [see Trovò (2012)]</i> .....	6
<i>Figure 7: View of Venice and location of the Frari basilica (source: google maps)</i> .....	7
<i>Figure 8: Frari basilica with bell tower and adjacent cloister (source: google maps)</i> .....	7
<i>Figure 9: The foundation of the Frari bell tower – (a) photography from the intervention of 1904 and (b) section of original foundation including enlargement [see Marchi et al. (2006)]</i> .....	9
<i>Figure 10: Stratigraphy of the Frari site and location of the original foundation</i> .....	10
<i>Figure 11: Oak (a) and alder (b) samples from the foundation of the Frari tower [from Bertolini et al. (2006)]</i> .....	11
<i>Figure 12: Conceptual model of the degradation of a single pile [see Ceccato (2011)]</i> .....	12
<i>Figure 13: Stratigraphy of lagoon soil in the historic centre of Venice, passing through the Isle of Giudecca, Canal Grande, San Marco and Sant’Elena according to Zezza (2007)</i> .....	15
<i>Figure 14: Single-pile (dimensions given in meters)</i> .....	20
<i>Figure 15: Axisymmetric model of a single pile</i> .....	21
<i>Figure 16: Generated meshes including details of pile head and foot refinements for single pile</i> .....	22
<i>Figure 17: Elastic modulus and Compressive strength of a clear-wood specimen as a function of Wood moisture [see Schickhofer (2006)]</i> .....	26
<i>Figure 18: Stress-strain curve for a clear-wood specimen subjected to compression and idealized curve [based on illustration in Schickhofer (2006)]</i> .....	27
<i>Figure 19: Compressive strength and corresponding shear strength for the wood specimen</i> .....	28
<i>Figure 20: Overview of performed calculations (Single-pile analysis)</i> .....	31
<i>Figure 21: Node for settlement curves</i> .....	35
<i>Figure 22: Gradual reduction of <math>c</math>, Development of plastic points</i> .....	36
<i>Figure 23: Change of stress state due to strength reduction</i> .....	37
<i>Figure 24: Load transfer, Soil 1 – Gradual reduction of stiffness and strength</i> .....	38
<i>Figure 25: Cross-section below foundation slab</i> .....	38
<i>Figure 26: Distribution of total normal stresses, Soil 1 – Gradual reduction of stiffness and strength.</i>	39
<i>Figure 27: Development of base and skin resistance, Soil 1 – Gradual reduction of stiffness and strength</i> .....	40
<i>Figure 28: Resistance-settlement curve, Soil 1 – Gradual reduction of stiffness and strength</i> .....	40
<i>Figure 29: Distribution of total normal stresses, Soil 1 – Gradual reduction of stiffness</i> .....	41
<i>Figure 30: Total displacements <math>u_y</math> for Method A and B, Soil 1 – Reduction of stiffness and strength</i> ...	44
<i>Figure 31: Load transfer for Method A and B, Soil1 – Reduction of stiffness and strength</i> .....	45
<i>Figure 32: Cartesian total stresses <math>\sigma_{yy}</math> for Method A and B, Soil1 – Reduction of stiffness and strength</i> .....	46
<i>Figure 33: Relative shear stresses for Method A and B, Soil1 – Reduction of stiffness and strength</i> ...	47

<i>Figure 34: Direction of total principal stresses <math>\sigma_1</math> for Method A and B, Soil1 – Reduction of stiffness and strength .....</i>	<i>48</i>
<i>Figure 35: Distribution of total normal stresses for Method A, Soil 1 – Reduction of stiffness and strength (repetition) .....</i>	<i>48</i>
<i>Figure 36: Distribution of total normal stresses for Method B, Soil 1 – Reduction of stiffness and strength .....</i>	<i>49</i>
<i>Figure 37: Distribution of total normal stresses for Method B, Soil 1 – Reduction of stiffness .....</i>	<i>49</i>
<i>Figure 38: Stress distributions for soil and pile having the same stiffness of 30 MPa (K=1) .....</i>	<i>50</i>
<i>Figure 39: Load transfer, Soil 1 &amp; 2 – Gradual reduction of stiffness and strength .....</i>	<i>51</i>
<i>Figure 40: Development of base and skin resistance, Soil 1 &amp; 2 – Gradual reduction of stiffness and strength .....</i>	<i>52</i>
<i>Figure 41: Development of plastic points, Soil 1, Gradual analysis .....</i>	<i>53</i>
<i>Figure 42: Development of plastic points, Soil 2, Gradual analysis .....</i>	<i>54</i>
<i>Figure 43: Resistance-settlement curve, Soil 2 – Gradual reduction of stiffness and strength .....</i>	<i>55</i>
<i>Figure 44: Formation of plastic points in dependence of placing of geometry lines, for interface extension of (a) 10 cm, (b) 0 cm, (c) 20 cm and (d) 10 cm with additional horizontal geometry line ..</i>	<i>56</i>
<i>Figure 45: Load transfer for Method A and B, Soil 2 – Reduction of stiffness and strength .....</i>	<i>57</i>
<i>Figure 46: Stress distributions for Method A, Soil 2 – Reduction of stiffness and strength .....</i>	<i>58</i>
<i>Figure 47: Stress distributions for Method B, Soil 2 – Reduction of stiffness and strength .....</i>	<i>58</i>
<i>Figure 48: Load transfer for Method A and B, Soil 1 – Reduction of stiffness and strength (repetition) .....</i>	<i>59</i>
<i>Figure 49: Load transfer for Method B, Soil 1 – Reduction of strength (a) and of stiffness (b) .....</i>	<i>59</i>
<i>Figure 50: Load transfer for Method A and B, Soil 2 – Reduction of stiffness and strength (repetition) .....</i>	<i>60</i>
<i>Figure 51: Load transfer for Method B, Soil 2 – Reduction of strength (a) and of stiffness (b) .....</i>	<i>60</i>
<i>Figure 52: Stress distributions for Method A, Soil 1 and 2 – Reduction of stiffness and strength (repetition) .....</i>	<i>62</i>
<i>Figure 53: Load transfer, Soil 1 – Interface degradation .....</i>	<i>66</i>
<i>Figure 54: Development of base and skin resistance, Soil 1 – Interface degradation .....</i>	<i>67</i>
<i>Figure 55: Resistance-settlement curve, Soil 1 - Interface degradation .....</i>	<i>68</i>
<i>Figure 56: Load transfer, Soil 2 – Interface degradation .....</i>	<i>68</i>
<i>Figure 57: Development of base and skin resistance, Soil 2 – Interface degradation .....</i>	<i>69</i>
<i>Figure 58: Resistance-settlement curve, Soil 2 – Interface degradation .....</i>	<i>69</i>
<i>Figure 59: Influence of the raft's stiffness on load transfer, Soil 2 – Interface degradation .....</i>	<i>70</i>
<i>Figure 60: Influence of the raft's stiffness on Pile resistance, Soil 2 – Interface degradation .....</i>	<i>70</i>
<i>Figure 61: Influence of the raft's stiffness on Resistance-settlement curve, Soil 2 – Interface degradation .....</i>	<i>71</i>
<i>Figure 62: Influence of the model size on load transfer, Soil 2 – Interface degradation .....</i>	<i>72</i>
<i>Figure 63: Influence of the model size on load transfer, Soil 2 – Interface degradation .....</i>	<i>72</i>
<i>Figure 64: Influence of the model size on load transfer, Soil 2 – Interface degradation .....</i>	<i>73</i>
<i>Figure 65: Load transfer, Frari soil - SSC model .....</i>	<i>74</i>
<i>Figure 66: Development of base and skin resistance, Frari soil – SSC model .....</i>	<i>74</i>
<i>Figure 67: Resistance-settlement curve, Frari soil – SSC model .....</i>	<i>75</i>
<i>Figure 68: Time-settlement curve, Frari soil – SSC model .....</i>	<i>75</i>
<i>Figure 69: Time-settlement curve with and without interface degradation, Frari soil – SSC model .....</i>	<i>76</i>
<i>Figure 70: Load transfer, Frari soil – SSC vs. SS model .....</i>	<i>77</i>

---

<i>Figure 71: Development of base and skin resistance, Frari soil – SSC vs. SS model .....</i>	<i>77</i>
<i>Figure 72: Resistance-settlement curve, Frari soil – SS model .....</i>	<i>78</i>
<i>Figure 73: Load transfer, Frari soil – SS vs. HS model.....</i>	<i>80</i>
<i>Figure 74: Development of base and skin resistance, Frari soil – SS vs. HS model.....</i>	<i>81</i>
<i>Figure 75: Resistance-settlement curve, Frari soil – HS model.....</i>	<i>81</i>
<i>Figure 76: Load transfer, Frari soil – Combined analysis.....</i>	<i>85</i>
<i>Figure 77: Development of base and skin resistance, Frari soil – Combined analysis.....</i>	<i>85</i>
<i>Figure 78: Resistance-settlement curve, Frari soil – Combined analysis .....</i>	<i>86</i>
<i>Figure 79: Top view of the geometry.....</i>	<i>87</i>
<i>Figure 80: Section of the geometry, situated in symmetry axis .....</i>	<i>88</i>
<i>Figure 81: Three-dimensional view of the model including detail on foundation.....</i>	<i>88</i>
<i>Figure 82: Top view of the mesh with detail on narrow element-cluster representing the interface ...</i>	<i>89</i>
<i>Figure 83: Front view of the mesh .....</i>	<i>90</i>
<i>Figure 84: Construction sequence of the Frari bell tower.....</i>	<i>95</i>
<i>Figure 85: Position of node for displacement curves.....</i>	<i>95</i>
<i>Figure 86: Time-settlement behaviour during construction period.....</i>	<i>96</i>
<i>Figure 87: ‘Load’-displacement curve for OCR 1.1 and 1.35 .....</i>	<i>97</i>
<i>Figure 88: Time-settlement curve for OCR 1.1 and 1.35 .....</i>	<i>97</i>
<i>Figure 89: Deformed mesh at the end of the observation (scaled up 5 times) .....</i>	<i>98</i>
<i>Figure 90: Detail on Figure 89 .....</i>	<i>98</i>
<i>Figure 91: Total settlements at the end of the observation .....</i>	<i>99</i>
<i>Figure 92: Detail on foundation and interface cluster.....</i>	<i>101</i>
<i>Figure 93: Change of interface material during degradation .....</i>	<i>101</i>
<i>Figure 94: Time-settlement curves showing influence of interface degradation .....</i>	<i>102</i>
<i>Figure 95: Detail on Figure 94 .....</i>	<i>102</i>
<i>Figure 96: Time-displacement curve before load application .....</i>	<i>106</i>
<i>Figure 97: Time-displacement curve after construction of foundation .....</i>	<i>107</i>

# TABLES

<i>Table 1: Stratigraphy of the Frari site.....</i>	<i>9</i>
<i>Table 2: Overview of soils and constitutive models used during single-pile analyses.....</i>	<i>19</i>
<i>Table 3: Mesh information .....</i>	<i>21</i>
<i>Table 4: Parameters of Soil 1.....</i>	<i>23</i>
<i>Table 5: Parameters of Soil 2.....</i>	<i>23</i>
<i>Table 6: Parameters of clay layer – SSC model.....</i>	<i>24</i>
<i>Table 7: Parameters of sand layer – HSS model.....</i>	<i>25</i>
<i>Table 8: Initial parameters of the pile .....</i>	<i>28</i>
<i>Table 9: Parameters of the raft (single-pile analysis).....</i>	<i>30</i>
<i>Table 10: Degradation steps for pile degradation.....</i>	<i>32</i>
<i>Table 11: Further degradation steps for pile degradation .....</i>	<i>32</i>
<i>Table 12: Calculation phases for gradual analysis .....</i>	<i>33</i>
<i>Table 13: Calculation phases for single analyses .....</i>	<i>34</i>
<i>Table 14: Soil 1, Gradual analysis, Settlements.....</i>	<i>35</i>
<i>Table 15: Settlements, Soil 1 – Single analyses .....</i>	<i>42</i>
<i>Table 16: Settlements of the pile head, Soil 2, Gradual analysis.....</i>	<i>51</i>
<i>Table 17: Settlements, Soil 2 – Single analyses .....</i>	<i>57</i>
<i>Table 18: Reduced interface parameters of Soil 1 and Soil 2 .....</i>	<i>64</i>
<i>Table 19: Reduced interface parameters of soil of Frari site.....</i>	<i>65</i>
<i>Table 20: Calculation phases for gradual interface degradation.....</i>	<i>65</i>
<i>Table 21: Variation of initial pore ratio and stiffness parameters .....</i>	<i>73</i>
<i>Table 22: Stiffness parameters for SS model and HS model.....</i>	<i>79</i>
<i>Table 23: Soil parameters of the HS model .....</i>	<i>79</i>
<i>Table 24: Calculation steps for a combined interface and pile degradation analysis.....</i>	<i>84</i>
<i>Table 25: Stratigraphy of the Frari site.....</i>	<i>91</i>
<i>Table 26: Soil parameters for layer representing alternating strata (Frari bell tower).....</i>	<i>91</i>
<i>Table 27: Parameters of the block representing the piles (Frari bell tower).....</i>	<i>92</i>
<i>Table 28: Parameters of the planking (Frari bell tower) .....</i>	<i>93</i>
<i>Table 29: Parameters of Masonry (Frari bell tower) .....</i>	<i>93</i>
<i>Table 30: Wall parameters (Frari bell tower) .....</i>	<i>93</i>
<i>Table 31: Calculation phases of pure creep analysis in drained conditions (Frari bell tower) .....</i>	<i>94</i>
<i>Table 32: Creep-settlements due to self-weight of the soil after 1 year .....</i>	<i>96</i>
<i>Table 33: Calculation phases for combined creep and degradation analysis .....</i>	<i>100</i>
<i>Table 34: Friction angle for interface cluster.....</i>	<i>101</i>
<i>Table 35: Permeability coefficients .....</i>	<i>104</i>
<i>Table 36: Calculation phases for pure creep analysis in undrained conditions.....</i>	<i>104</i>

# 1 INTRODUCTION

The historic city of Venice is facing several problems, which have become serious in the course of the last decades. Main problems comprise the rising of the eustatic sea level, land subsidence and consequently increasing frequency of flooding. Reasons for subsidence can be found in the peculiar properties of Venetian subsoil as well as in human action.

The old fabric of Venetian buildings paired with these hazards represents the key challenge in preserving the cultural heritage of Venice. In this context, several safeguarding projects have been initiated. Apart of large-scale projects, such as the MOSE-project, also smaller studies and interventions are conducted, aiming for the stabilization and restoration of single buildings. These include current research programs directed by CORILA<sup>1</sup>, which focus on the wooden foundations of Venetian buildings and their preservation. For a long time, the relevance of wooden foundations for the maintenance of historic building fabric was underestimated and neglected. This is due to their limited accessibility and due to the common assumption that submerged wooden elements would not be subjected to degradation. Breaking that myth, recent investigations prove however that the wooden piles degrade also in quasi-anoxic conditions due to the action of bacteria.

Hence, describing the behaviour of degrading wooden piles with time and the consequences for the stability of the foundation and superstructure is of major importance, and is a key issue within the on-going CORILA project *Guidelines for reinforcement measures on wooden pile foundations* (Italian *Linee guida per gli interventi di consolidamento di fondazioni basate su palificazioni in legno*, translated by the author). In this regard, studies have been conducted at the Department IMAGE, University of Padova, for analyzing the mechanical behaviour of Venetian pile foundations under the specific aspect of pile degradation [see Baglioni (2009), Ceccato (2011) and Ceccato (2012)]. Within these studies, numerical models for typical pile foundations in Venice are developed and first approaches for modelling pile degradation are presented.

The present master thesis represents a continuation of the studies performed, and is realized in collaboration with Prof. Simonini and PhD student Francesca Ceccato (both University of Padova). The main intention is to further investigate and describe the effect of pile degradation on wooden pile foundations. In particular, main interest lies on the investigation of stress-redistribution between pile and adjacent soil due to the pile's degradation, and, in a larger scale, the resulting modification of the load bearing and settlement behaviour of an entire foundation.

For conducting a thorough study on wooden pile foundations and their long-term behaviour, an intensive literature study is necessary concerning wooden pile foundations and their degradation and the nature of Venetian lagoon soils. In this regard, in Chapter 2 and 3, basic information on historical foundations in Venice and on lagoon soils in the Venetian basin is presented, and the phenomenon of pile degradation is introduced.

In Chapter 4, numerical modelling in geotechnical engineering is introduced and specific features are explained, serving as preparation for the main Chapters 5 and 6 of this thesis. The latter deal with the generation of the models and the results obtained from numeric analyses.

---

<sup>1</sup> Consortium for the coordination of research activities concerning the Venice lagoon system, see [www.corila.it](http://www.corila.it)

---

The numeric analyses are carried out in 2D and 3D using finite element based software. By means of an axisymmetric single-pile model, a preliminary study is carried out for finding a representative method for modelling degradation. Within this study, the effects of different pile degradation methods on pile resistance and stress-distribution are investigated and compared. For each degradation method, various parameter sets are used representing the degradation of the pile or the interface between pile and surrounding soil respectively. Moreover, different parameter sets for the soil as well as different constitutive models for the same are applied for studying their influence on system behaviour. Besides, also the time-dependent behaviour of the Venetian subsoil itself is implemented in the model. For this purpose, apart of the Mohr-Coloumb model also the Soft Soil Creep and further the Hardening Soil model are used for modelling the behaviour of the soil.

Chapter 7 is dedicated to the analysis of a specific building in Venice. This is the bell tower of the gothic basilica *Santa Maria Gloriosa dei Frari*, whose foundation piles partially show severe degradation due to bacterial attack. The foundation is simulated within a 3D model, whereas piles and intermediate soil are represented by a block. The time factor is taken into account in the model, concerning the degradation of the piles as well as the visco-plastic behaviour of the subsoil.

For concluding this thesis, final remarks on the results obtained from the 2D and 3D analysis are given (Chapter 8) and possible starting points for future researches are presented (Chapter 9).

## 2 HISTORIC FOUNDATIONS IN VENICE

### 2.1 FOUNDATION TYPES AND PILE-DRIVING TECHNIQUES

The Venice lagoon bears some peculiar boundary conditions for constructing, such as the extreme water conditions as well as strong heterogeneity and low stiffness of the lagoon soils. Due to these complex conditions, the possibilities in constructing were - and still are in a lesser extent - restricted, and led to the development of construction types and methods which are particular for the Venetian lagoon.

In the following, a possible classification for foundation types is presented in Ceccato (2011):

- Shallow foundations: This type of foundation consists of several layers of wooden planks, installed in a depth of 2 - 3 m below surface level, and a stone masonry which is resting on the planking. Compare Figure 1.
- Deep foundations: These are wooden pile foundations with piles of small dimension, which were installed very close to each other. On the pile heads, a wooden planking was located, on which the masonry footing is resting. Compare Figure 2.

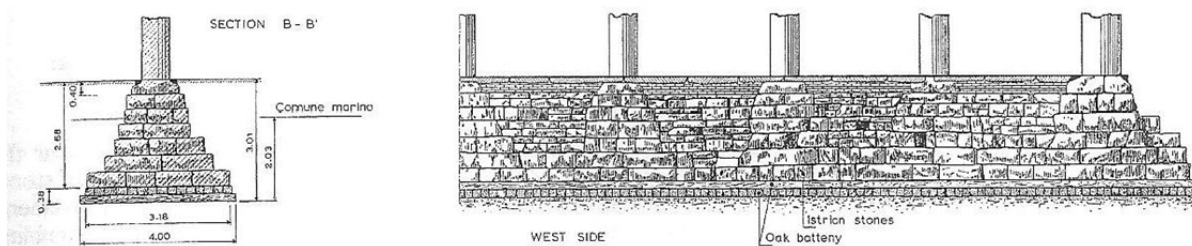


Figure 1: Foundation of *Palazzo Ducale* [by Malvezzi (1874), see Ceccato (2011)]

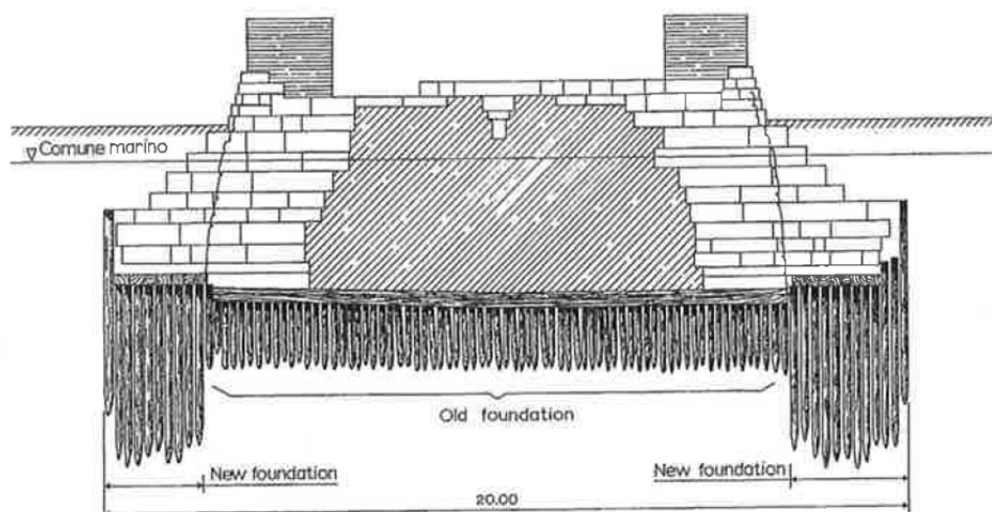


Figure 2: Foundation of new *San Marco* bell tower [by Donghi (1913), see Colombo et al. (1997)]

---

Since the bell tower of the Frari basilica is founded on wooden piles, in the following only the pile foundation is discussed further.

As already mentioned before, the pile foundations consist of the three components masonry footing, wooden planking and wooden piles. The wooden piles were installed with small intermediate distance (even touching each other), having a length of 1.5 to 3 m and a diameter of 10 to 20 cm. The planking (Venetian *madieri*) was laid on top of the pile heads, and was installed in several layers. On the planking, the masonry of stone blocks was situated. In some cases, the planking is missing. Further, in the core of a lot of foundations the masonry, the planking as well as the piles are missing due to economic reasons [compare Biscontin et al. (2009)].

Because of the small distance between single piles and their limited dimensions, in literature this type of 'foundation' is also referred to as soil improvement (Italian *pali di costipamento*, German *Spickpfahlgründung*). Actually, the primary goal was to improve the mechanical properties of the soft subsoil rather than to transfer the load from the superstructure to deeper layers [compare for example Marchi et al. (2006) and Wichert (1988)].

An example for Venetian pile foundations is the one of the *Sant'Agnese* bell tower [compare Marchi et al. (2006)]. This tower was demolished in the 19<sup>th</sup> century, which enabled Giovanni Casoni studying the tower's foundation. In Casoni (1851), the author documented the geometry and dimensions of the foundation – compare Figure 3. The geometry is very similar to the one of the Frari bell tower, which is explained subsequently.

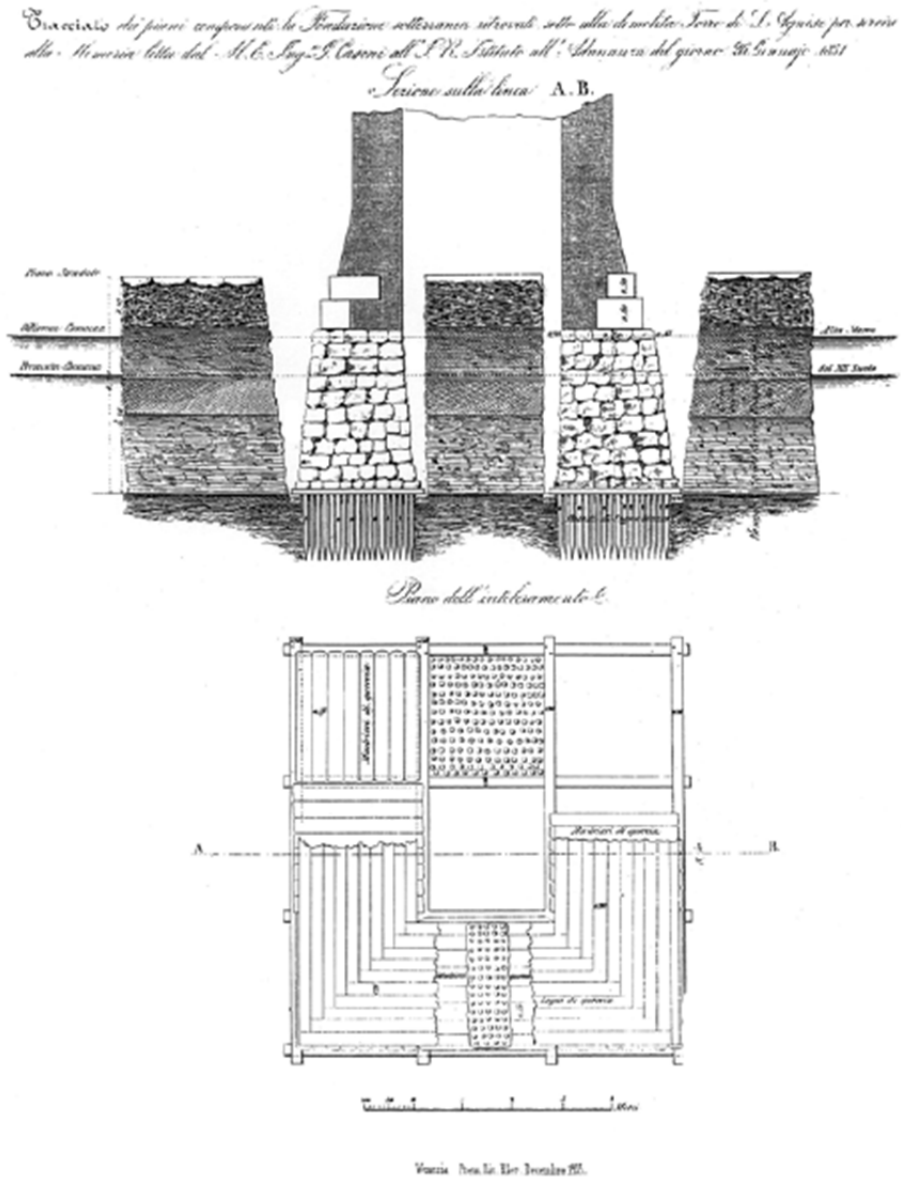


Figure 3: Section and top view of the foundation of the Sant'Agnese tower [by Casoini (1851), see Marchi et al. (2006)]

For driving the piles into the subsoil, different driving devices (Italian *battipali*) were used. Their application is illustrated in Figure 4 to Figure 6. It is reported that exterior piles of a pile group were driven first in order to confine the soil, so that the compaction achieved by the installation of the interior piles was increased through this confinement. However, the used technique and its consequences (such as modification of soil properties during the construction of the foundation) are not considered during the calculations for the Frari tower.



Figure 4: Watercolour by Grevembroch, G. (18<sup>th</sup> century), which illustrates two workers driving wooden piles into the subsoil using a *battipalo* [see Trovò (2012)]

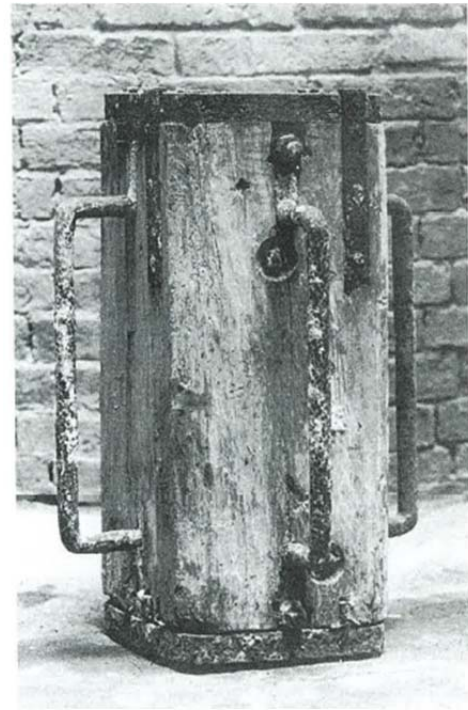


Figure 5: *Battipalo*, Venice, Procurators office [see Maggi (2002)]

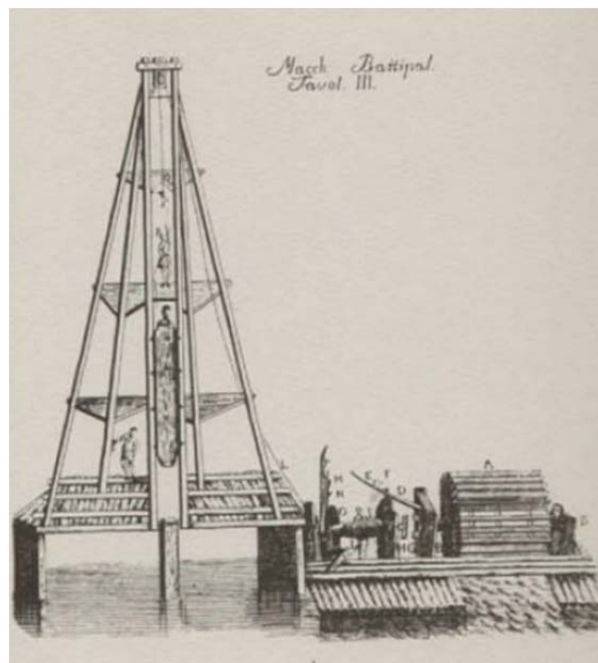


Figure 6: *Battipalo* driven by water wheel (18th century) [see Trovò (2012)]

## 2.2 FOUNDATION OF THE FRARI BELL TOWER

The gothic basilica of *Santa Maria Gloriosa dei Frari*, short basilica *dei Frari*, is situated in the district of *San Polo* in Venice (Italy). Its location is marked with the red dot in Figure 7.



Figure 7: View of Venice and location of the Frari basilica (source: google maps)

The Frari complex consists of the basilica, the bell tower and the buildings of two former cloisters. The square in front and alongside the basilica is called *Campo dei Frari*. The whole complex of buildings is illustrated in Figure 8.



Figure 8: Frari basilica with bell tower and adjacent cloister (source: google maps)

The bell tower of the basilica was completed in 1396, after a construction period of 35 years. With a height of 65 m, this tower represents the second tallest in Venice after the tower of the famous basilica *San Marco*. Since its construction, the tower has experienced settlements in the order of

60 cm. In order to prevent the basilica and the tower itself from (further) damage, several interventions have been undertaken to stabilize the tower.

In the following, back-ground data of the Frari bell tower is given. The collected data represents a compendium of information, presented in Italian literature: Lionello (2008), Marchi et al. (2006), Gottardi et al. (2008), Biscontin et al. (2009) and Bertolini et al. (2006).

### Geometry of foundation

The information obtained from historic documents and from an investigation conducted in 2003 allowed reconstructing the geometry of the Frari tower: The foundation consists of a massive footing of stone masonry, resting on horizontal layers of wooden planks, which in turn are founded on wooden piles. The masonry footing is quadratic in plan and trapezoidal in section. Its side length at ground level is about 9.3 m, whereas at foundation surface the length amounts to 11.0 m approximately. The wooden planks (Venetian *madieri*) form a layer with a total height of 45 to 60 cm. Between the planking and the piles, a sand layer of 5 to 10 cm was found. The piles have a diameter of 15 to 20 cm and were installed with a distance of several centimeters. With a length of 1.7 to 2.2 m, the piles are founded in the clay layer. In the middle of the foundation, in a square with side length of 3 m at ground level and 1.5 m at foundation surface, neither masonry nor piles or planks could be detected. Compare foundation of Sant'Agnese tower, illustrated in Figure 3.

### Settlement history and interventions

The settlements of the Frari bell tower since its construction are estimated in the order of 60 cm, compared to a total load of 57 MN and a momentum of 30 MNm due to the tower's inclination. In the course of a leveling which was carried out in 1902, the differential settlements between the tower and the adjacent basilica were measured around 40 cm. According to Lionello (2008), the relative settlements showed an increase of about 10 cm in the last century.

Until the beginning of the 20<sup>th</sup> century, the settlements of the tower did not interfere with the stability of the basilica, as the tower was originally built as autonomous structure. In this way, the two buildings could settle independently. However, in the course of maintenance measures the tower was structurally connected to the basilica, which caused problems in the interaction between the tower and the basilica.

Also the rotation of the tower has contributed to these problems. In 1904, the overhang of the tower towards the *Campo dei Frari* amounted to about 76.5 cm compared to a reference height of 42.5 m. In order to control the settlements as well as the rotation, maintenance measures were conducted in 1904. Beside the mentioned connection of tower and basilica, these measures included an enlargement of the pre-existing foundation, which was realized at the one side of the tower facing the square. The enlargement consisted of the installation of piles made from larch with a diameter of 20 cm and a length of 3.8 m and the placing of concrete in layers of 15 cm. Comparing the results of the leveling in 1902 and the results of measurements conducted regularly since the year 2000, the average settlement-rate ranges between 0.5 and 1 mm per annum. According to Marchi et al. (2006), it was further observed that the sense of rotation goes into reverse towards the basilica, which actually might be traced back to these measures.

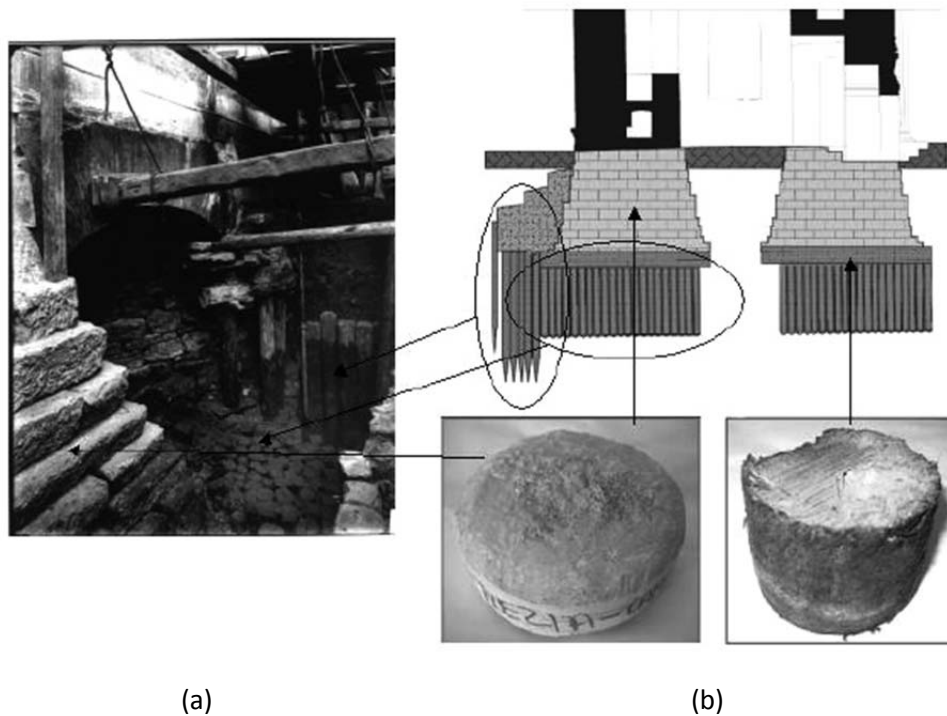


Figure 9: The foundation of the Frari bell tower – (a) photography from the intervention of 1904 and (b) section of original foundation including enlargement [see Marchi et al. (2006)]

In the years of 2005 and 2006, another major intervention was undertaken, which consisted in the injection of cement mortar via sleeve pipes in a depth of 2 to 12 m under ground level. In preparation for that intervention, a thorough investigation was carried out in 2003 by the Venetian agency of historic preservation (*Soprintendenza B.A.P. di Venezia e Laguna*, translated by the author). The investigation included sampling of soil specimen and specimen of the foundation via core-drilling, static cone penetration tests (CPT-u), dynamic standard penetration tests (SPT) and dilatometer measurements (DMT) [see Lionello (2008)].

### Stratigraphy

By means of the performed investigation, it was possible to determine the stratigraphy and the groundwater level [compare Lionello (2008)]. The soil profile is described in Table 1 and illustrated in Figure 10.

Table 1: Stratigraphy of the Frari site

<i>Depth</i>	<i>Description</i>
$\pm 0.0 \div -3.2 \text{ m}$	Anthropogenic filling, composed of sand and silt, poorly compacted, fragments of bricks, boulders
$-1.0 \text{ m}$	Level of water table
$-3.2 \text{ m} \div 6.8 \text{ m}$	Clay, slightly silty to silty, dark gray, with low plasticity, from normalconsolidated (NC) to slightly overconsolidated (OC), local inclusions of organic material

-4.5 m ÷ -5.5 m	Large quantity of shell fragments in the size of centimeters
-6.2 m ÷ -6.5 m	Silt layer, clayey to sandy, of medium plasticity, coloured yellow
-6.8 m ÷ -14.5 m	Sand, coloured grey, medium-textured, clean, compacted to heavily compacted
-14.5 m ÷ -25.5 m	Alternating layers of silty clay and sand

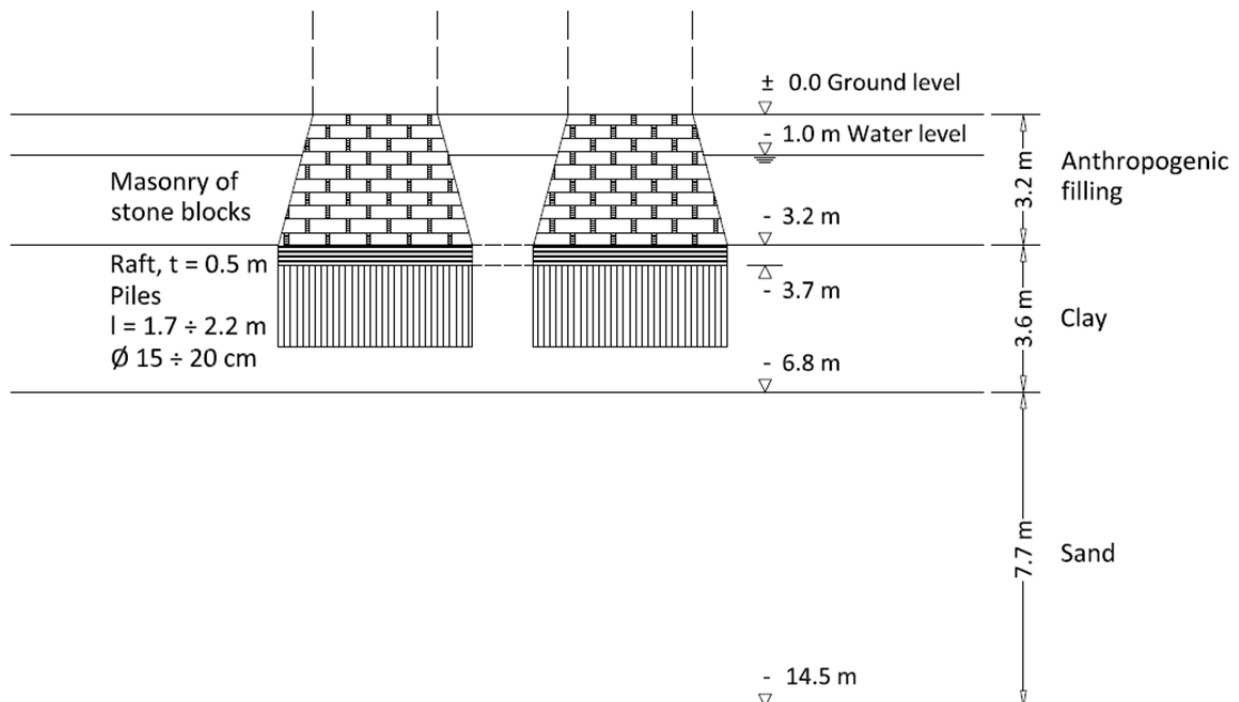


Figure 10: Stratigraphy of the Frari site and location of the original foundation

As the original piles are founded in the soft clay layer, and do not embed in the compacted sand layer, this foundation represents a floating foundation. The longer piles installed during the intervention in 1904 are founded *on* the sand layer. The original configuration of the tower's foundation can be seen from Figure 10.

### State of conservation

The samples of the foundation also allowed studying composition and condition of the masonry footing and the wooden foundation elements. The masonry footing consists of 10 layers of Istria stone, with little intermediate mortar left. The timber used for the planks is larch, and for the piles primarily elder, but also oak was used. According to Biscontin et al. (2009), the planks were found well preserved, whereas the piles, especially those of elder, turned out to be in very bad condition.

### Causes for settlements

According to Lionello (2008), the settlements occurred in the past century respectively the estimated current settlement rate of 0.5 to 1 mm p.a. cannot be explained solely with the secondary

settlements experienced by the soft soil in confined state. Rather, plastic ‘outflow’ of soil from highly stressed areas due to the lack of confinement could explain the ongoing settlements. Further, the degradation of the wooden piles could represent another explanation.

## 2.3 PILE DEGRADATION

For a long time it was assumed that the foundation piles in Venice would not experience any degradation. This assumption was based on the fact that the piles, driven into the soft subsoil, are permanently waterlogged. Due to these quasi-anoxic conditions, fungi, insects or other aerobic xylophagous organisms do not find a suitable environment to live in.

However, in the course of the investigations at the Frari site in 2003, samples of the piles partially showed a severe degradation, especially in case of piles made from alder. This is shown in Figure 11, where oak (a) and alder (b) samples deriving from the Frari tower are illustrated.



Figure 11: Oak (a) and alder (b) samples from the foundation of the Frari tower [from Bertolini et al. (2006)]

Until then, it was generally believed that alder piles would be very durable in the described conditions, and consequently might have been used for a lot of foundations in Venice. Hence, the problem of degraded foundation piles may not be limited to the Frari tower, which was the crucial factor for further initiatives.

In the frame of a research project conducted by the consortium *CORILA (Consortium for Coordination of Research Activities Concerning the Venice Lagoon System)*, foundations of different buildings in Venice were investigated [see Biscontin et al. (2009)]. The investigations concentrated on evaluating the actual state of conservation of the piles. The results demonstrate that the examined wooden foundation piles had experienced similar degradation as observed in case of the Frari bell tower. Further, erosion bacteria turned out to be responsible for the degradation, which actually manage to live in these quasi-anoxic conditions. This species of bacteria ‘erodes’ certain parts of the cell wall of the wood, which represents a very slow degradation-mechanism. This in turn explains why this type of degradation becomes relevant only after several centuries of service.

However, with the information obtained it is neither possible to describe the degree of degradation with time, nor to mechanically describe the actual state of conservation.

One suggestion for modeling the degradation is presented by Ceccato (2011). To simplify matters, it is assumed in this work that the *degradation is advancing radially from the outside to the inside of the pile, with the degradation being uniform in longitudinal direction*. The development of the mechanical properties with degradation is described as follows [compare Ceccato (2011)]: *At the*

beginning of the pile's service life, the outer part of the pile section might be degraded comparatively fast due to the action of fungi that live on the remaining oxygen. In this phase, the elastic modulus and the compressive strength of the whole cross-section are reduced by the increasing water content. However, the pile is still in good conditions. The stress-distribution is assumed rather uniformly, with a slight reduction at the border. Compare Figure 12 (a). Once the oxygen is consumed, the degradation-rate is strongly reducing, as the bacteria provoke only a very slow decay. In this phase, the stresses are not distributed uniformly anymore, as the decay is supposed to decrease towards the pile's core. A possible distribution is illustrated in (b). The bacterial decay will lead into a critical state just after several decades or centuries of service. In this state, the whole pile would be affected by the degradation, and over the whole cross-section the residual strength and stiffness would be strongly reduced compared to the initial values. See Figure 12 (c).

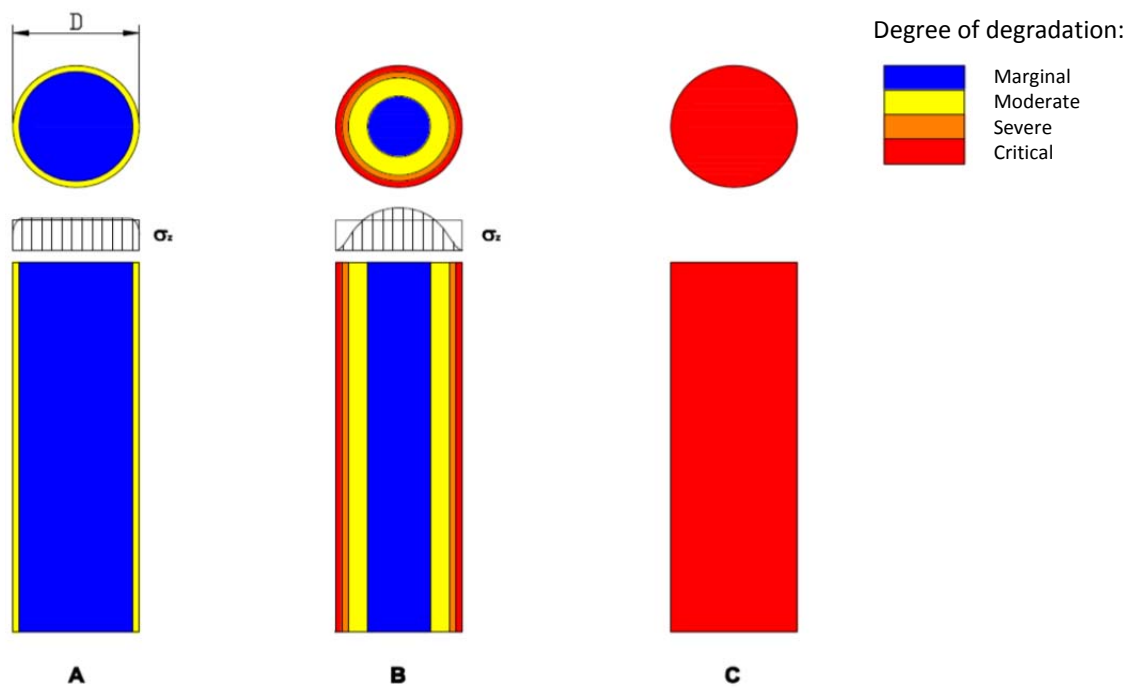


Figure 12: Conceptual model of the degradation of a single pile [see Ceccato (2011)]

### 3 GEOLOGIC FORMATION AND CHARACTERISTICS OF VENICE LAGOON SOILS

In the following, a short introduction on the geological history of Venice lagoon soils and their basic composition and characteristics is given, referencing Cola & Simonini (2002) and Ricceri et al. (2002).

*The depositional patterns of the Venetian sediments are rather complex due to the combined effects of geological history and human action, which modified significantly the morphology of the lagoon, inlets and channels over the past several centuries.*

*The sediments of the Quaternary Basin comprising the whole Venetian Lagoon area, reach depths of approximately 800 m, and were deposited over the past 2 million years. In particular, the subsurface soils of the Venice Lagoon down to 50 to 60 m, the depth of interest here, are characterized by a complex system of interbedded sands, silts, and silty clays deposited during the last glacial period of Pleistocene (Würm) when the rivers transported fluvial material from the Alpine ice fields. The Holocene is only responsible for the shallowest lagoon deposits, about 5 to 15 m thick.*

*The top layer of Würmian deposits is composed of a crust of highly overconsolidated (OC) clay, commonly referred to as 'caranto'. It was subjected to a process of overconsolidation as a result of oxidation during the 10 000-year emergence of the last Pleistocenic glaciation. The OC crust of caranto, lying at depths ranging between 5 and 12 m below mean sea level, shows thicknesses varying from a few centimetres to some metres.*

Note: Until the last century, it was generally believed that most Venetian foundations would have been founded on this *caranto* layer, which shows good mechanical properties due to its overconsolidation. However, results from geotechnical investigations demonstrate that the extent of this layer is limited to about half of the historic city [according to Biscontin et al. (2009)].

*Subsurface profiles are characterized by irregular alternation of three soil types, sand, silt and very silty clay, which constitute over 95% of the Venetian soils, a few thin layers of compacted peat and medium plasticity clay. The main feature of Venetian soils is the presence of a predominantly silty fraction, being a consequence of mechanical degradation of the original sand particles. The silt is always combined with clay and/or sand, forming a chaotic interbedding of different sediments, whose basic mineralogical characteristics vary however in a relatively narrow range due to their common mineralogical origin and depositional environment.*

*Based on the predominance of the silty fraction and the low influence of clay minerals, the overall response of the Venice lagoon soils is governed by mechanical rather than electrochemical interaction between soil particles, with the exception of a few cases due to plastic clays.*

In the course of the last decades, numerous geological investigations have been conducted in Venice and its lagoon. However, the extreme heterogeneity of Venice lagoon soils due to the complex depositional history still represents a challenge for setting up a general classification and stratigraphy

of Venetian subsoil and describing its behaviour mechanically. Moreover, through the soil's irregularities, interpreting measurement data from investigations performed, also within a limited area, becomes particularly interesting and requires profound knowledge.

In Figure 13, one section through the historic centre of Venice is illustrated exemplarily together with the explored stratigraphy. This section is passing through the Isle of Giudecca, Canal Grande, San Marco and Sant'Elena, and shows the extreme heterogeneity of the subsoil discussed above.

An approach for describing the mechanical behaviour of the lagoon silts is presented by Cola & Simonini (2002). This approach is based on the fact that *all of the Venetian sediments are originated from one common basic material, namely siliceous-calcareous sand, by crushing and sedimentation*, through which their mechanical behaviour can be described by the interaction between soil particles, unaffected by electrochemical actions. Therefore, the authors established relationships between the mechanical properties and the grading characteristics.

For representing the grading characteristics, Cola & Simonini introduced a new material parameter, the so-called grain-size index  $I_{GS}$ , which is defined as

$$I_{GS} = \frac{D_{50}/D_0}{U} \quad (3.1)$$

The used notations are:

- $D_{50}$  Grain diameter at 50% passing
- $D_0$  Reference diameter equal to 1 mm for normalizing the index
- $U$  Coefficient of uniformity, defined as

$$U = \frac{D_{60}}{D_{10}} \quad (3.2)$$

$D_{60}$  and  $D_{10}$  are the grain diameters at 60% and 10% passing respectively.

Correlations were set-up between the  $I_{GS}$ , representing grain-size distribution, and several parameters of the Venetian soils at large and very small strains, such as critical state angle and very small strain stiffness. A detailed description and explanation of these correlations would exceed the scope of this chapter. Interested readers are therefore referred to Cola & Simonini (2002).

Another key aspect of Venetian lagoon silts is their time-dependent behaviour, which was for example observed during various in-situ measurements at the Treporti Test site [see Jamiolkowski et al. (2009)]. An approach for modeling this time-dependent, visco-plastic behaviour of the lagoon silts is presented by Berengo et al. (2008). Numerical calculations were carried out based on different constitutive models, which are the known *Soft Soil Creep model* on the one hand, and on the other hand, the so-called *Anisotropic creep model for soft soils (ACM)*, presented by Leoni et al. (2008). The latter model actually accounts for fabric anisotropy, which is inherent in Venetian soils due to their natural formation.

Further, within the safeguarding project MOSE in Venice, another creep model called *Visco-clay* was used for estimating long-term settlements, which was presented in Rocchi et al. (2003).

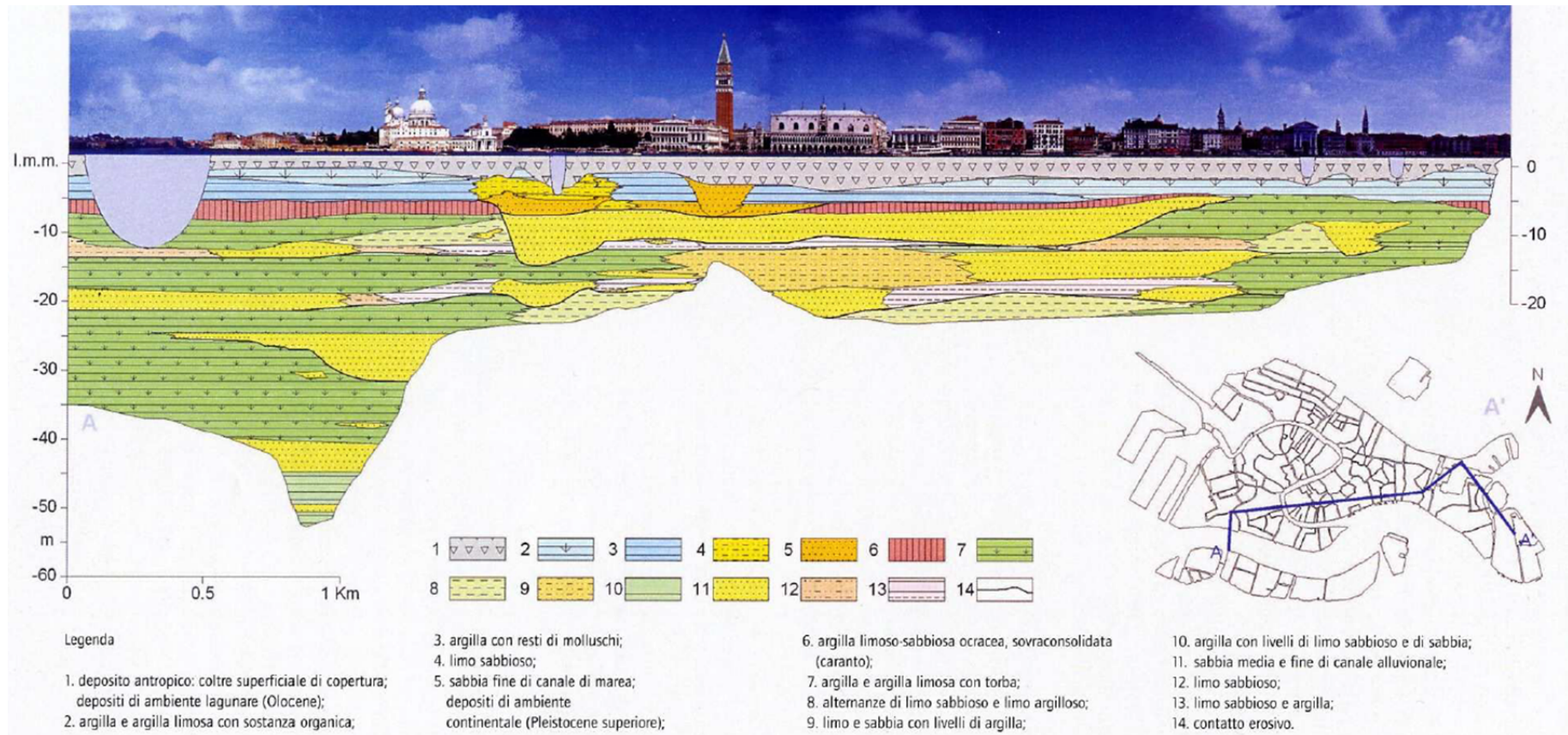


Figure 13: Stratigraphy of lagoon soil in the historic centre of Venice, passing through the Isle of Giudecca, Canal Grande, San Marco and Sant'Elena according to Zezza (2007)

Legend (translated by the author):

- |   |   |   |
|---|---|---|
| 1. Anthropogenic filling: pavement, deposits from lagoon environment (Holocene) | 5. Fine-grained sand from tideway; deposits from continental environment (Late Pleistocene) | 10. Clay with levels of sandy silt and sand |
| 2. Clay and silty clay with organic material                                    | 6. Silty, sandy clay, coloured ochre, OC ( <i>Caranto</i> )                                 | 11. Fine- and medium-grained sand           |
| 3. Clay with remains of molluscs  | 7. Clay and silty clay with peat  | 12. Sandy silt                              |
| 4. Sandy silt   | 8. Alternations of sandy silt and clayey silt   | 13. Sandy silt and clay                     |
|   | 9. Silt and sand with clay levels   | 14. Erosional discontinuity                 |

## 4 NUMERICAL MODELLING IN GEOTECHNICAL ENGINEERING

### 4.1 INTRODUCTION

Beside the application of analytical methods, numerical modelling has become an essential feature in modern soil mechanics. This is based on the development of the *finite element method* [see Zienkiewicz et al. (2005)], and on the progress made in material modelling over the last decades. Nowadays, complex material models are available which consider many features of real soil behaviour. However, one has to be aware of their limitations and range of application.

In general, assumptions are necessary when establishing a numerical model of a geotechnical problem. Due to the soil's inherent heterogeneity, its nonlinear material behaviour and various other aspects, making assumptions is the key challenge in modelling soil behaviour. Thus, a lot of experience and profound knowledge in various subjects is required, such as soil mechanics, constitutive modelling and finite element theory. Last but not least, engineers have to be familiar with the applied software and its theoretical background.

Assumptions comprise for example the used model parameters. Their identification has to be done with great care, as they have a decisive influence on the results. In any case, a critical assessment of the assumptions as well as of the obtained results is of major importance.

### 4.2 SPECIFIC FEATURES OF NUMERICAL MODELLING

The numerical calculations of the present Master Thesis are performed with the finite element based calculation programs provided by Plaxis bv. The 2D, axisymmetric models were generated within the Plaxis 2D versions 2010.01 (Build 6019) and 2011.01 (Build 6604); the 3D model was created with the Plaxis 3DF version 2.2 (Build 382).

In this regard, specific features of numerical modelling of soils and soil-structure interaction are addressed in the following, which might be necessary for understanding the performed calculations. The information given in sections 4.2.2 and 4.2.3 is basically reproduced according to (Plaxis bv).

#### 4.2.1 SOIL MODELS

For modelling soil behaviour, different material models exist that are generally applied according to the nature of the soil under examination. Also the desired accuracy of the results might influence the choice. For a preliminary study or in case of limited information on the subsoil, for instance, it might be useful applying the elastic-perfectly plastic Mohr-Coulomb model, instead of one of the more advanced models. The latter are basically more time-consuming and computationally intensive, and require therefore more computational resources. However, it has to be considered that real soil behaviour is rather captured with the advanced models, presuming their proper use.

In this thesis, different constitutive models are used for modelling the behaviour of various types of soils. These models are:

- Mohr-Coulomb model
- Hardening Soil model
- Hardening Soil model with small-strain stiffness
- Soft Soil model
- Soft Soil Creep model

However, a description of the single models would go beyond the dimensions of this work. A basic introduction is provided by (Plaxis bv). The input-parameters required within these models are specified in Chapters 5 and 6.

### 4.2.2 INTERFACE

Interfaces are used for describing the contact behaviour between structural elements, such as for example piles, and the adjacent soil. For this purpose, the interface is located along the structural element, but within the soil layer. The main interface parameter is the so-called strength reduction factor  $R_{inter}$ . Through this parameter, the interface properties can be derived from the soil properties of the corresponding soil layer, and are defined as

$$c_i = R_{inter} * c_{Soil} \quad (4.1)$$

$$\tan \varphi_i = R_{inter} * \tan \varphi_{Soil} \quad (4.2)$$

$$\psi_i = 0^\circ \text{ for } R_{inter} < 1, \text{ otherwise } \psi_i = \psi_{Soil} \quad (4.3)$$

The default value of  $R_{inter}$  is 1. The smoother the surface of the structural element is, the smaller the  $R_{inter}$  should be. A typical value is 0.7.

For simulating the behaviour of the interface, an elastic-perfectly plastic material model is used, whereas the limit shear stress indicates the transition from elastic to plastic behaviour.

The elastic behaviour is given by the following inequation:

$$|\tau| < \sigma_N * \tan \varphi_i + c_i \quad (4.4)$$

The plastic behaviour is given by the following equation:

$$|\tau| = \sigma_N * \tan \varphi_i + c_i \quad (4.5)$$

### 4.2.3 INITIAL STRESSES

The initial stresses are of major importance for describing the mechanical behaviour of the soil. They are defined by means of vertical stresses,  $\sigma'_{v,0}$ , which are dependent on the weight of the overlying soil layers and on the soil's formation and preloading history. The initial horizontal stresses,  $\sigma'_{h,0}$ , are defined by the following relationship:

$$\sigma'_{h,0} = k_0 * \sigma'_{v,0} \quad (4.6)$$

$k_0$  is the coefficient of lateral earth pressure.

Within the calculations performed, the initial stresses are generated by using the so-called *k<sub>0</sub>-procedure*. Strains are not generated within this procedure.

In case of using advanced models, namely the HS or the SS model, additionally the so-called *overconsolidation ratio (OCR)* can be applied for generating pre-consolidation pressures. According to (Plaxis bv), the OCR is defined as *the ratio of greatest effective vertical stress previously reached,  $\sigma_p$ , and the in-situ effective vertical stress,  $\sigma'_{yy}$* :

$$OCR = \frac{\sigma_p}{\sigma'_{yy}} \quad (4.7)$$

## 5 PRELIMINARY STUDY ON SINGLE PILE

### 5.1 INTRODUCTION

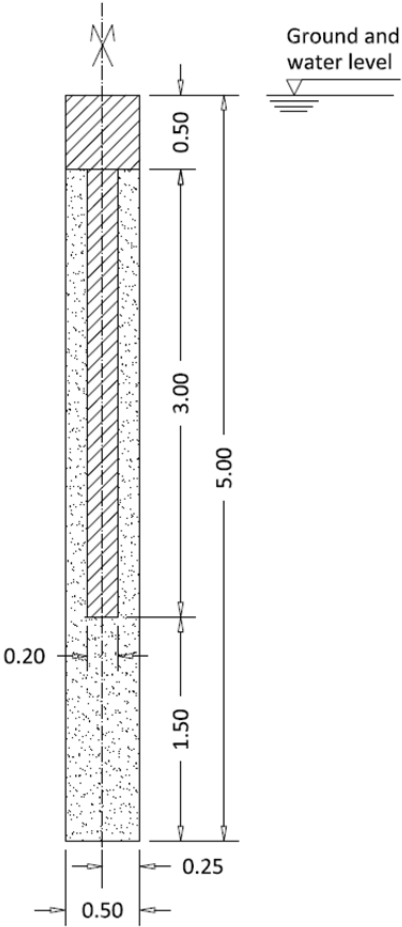
Preliminary calculations are conducted on a single pile in order to study its behaviour in detail. This study focuses on load distribution and load transfer between pile and raft and on the development of pile resistance, consisting of base and skin resistance, with on-going degradation of the pile. The degradation is simulated in two different ways – either ‘degrading’ the whole cross-section of the pile or just the interface between pile and adjacent soil – in order to find the most realistic system response.

The dimensions and parameters used for the preliminary study do not refer to a specific project; the dimensions are based on those of typical historic foundations in Venice. During the study, soil parameters and also constitutive models are changed. A general overview of soils and relative models used is given in Table 2.

Table 2: Overview of soils and constitutive models used during single-pile analyses

<i>Denomination</i>	<i>Description</i>	<i>Constitutive model</i>
Soil 1	e.g. Stiff sand	Mohr-Coulomb
Soil 2	e.g. Soft and weak silty clay	Mohr-Coulomb
Frari	Layering of Frari Site: Clay & sand layer	Soft Soil Creep, Hardening Soil Small

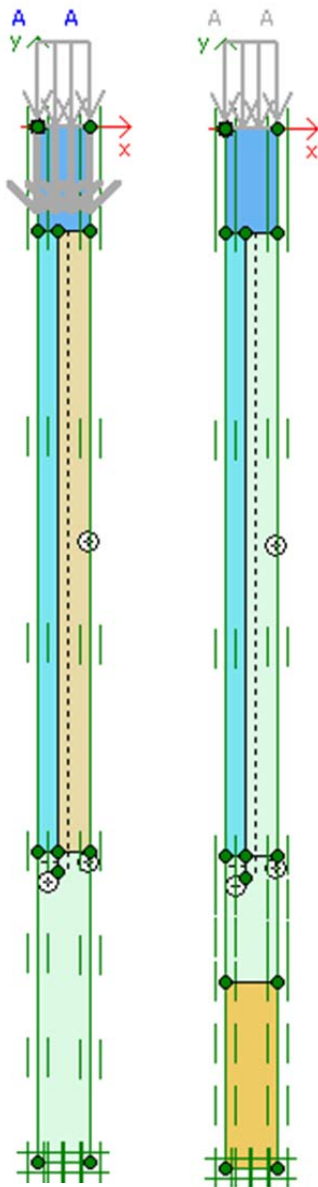
### 5.2 GEOMETRY AND INPUT IN PLAXIS 2D



The pile has a length of 3 m and a diameter of 20 cm. The axial distance between two piles is assumed to be 50 cm. The raft has a thickness of 50 cm. This leads to a total model width of 25 cm and height of 5 m, with the lower model boundary being 1.5 m below the pile foot. The water table coincides with the upper model boundary. See Figure 14.

In the 2D calculation, the pile is defined with an axisymmetric model with the axis of symmetry coinciding with the left boundary. The axisymmetric model allows simulating a centre pile of a pile group by using a single pile in a model with specific lateral fixities and limited model width. For this purpose, the boundary conditions are activated in standard mode, which means that vertical boundaries obtain a horizontal fixity ( $u_x = 0$ ), and the lower boundary obtains a full fixity ( $u_x = u_y = 0$ ), as can be seen in Figure 15.

Figure 14: Single-pile (dimensions given in meters)



(a) Model for Soil 1 and 2 (b) Model for Frari site

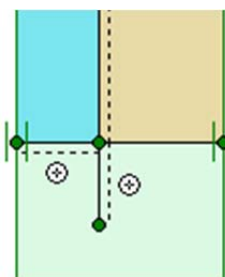
The interfaces, which are tools for simulating the contact behaviour between soil and pile, are situated along the shaft and under the pile foot. In order to minimize the influence of stress peaks at the pile foot, the interface between pile shaft and soil is 10 cm longer than the pile itself.

Down to a depth of -3.5 m, which coincides with the bottom line of the pile, the interface parameter  $R_{inter}$  is either 0.7 or 1.0, underneath it is 1.0. The  $R_{inter}$  of 0.7 is used in case of the so-called 'pile degradation', the  $R_{inter}$  of 1.0 for the so-called 'interface degradation'. See section 5.4, 'Calculations', for an explanation of the degradation methods.

To generate the mesh, about 2 000 15-noded elements are used. See Table 3. Besides the soil itself, the pile as well as the raft is modelled with 2D elements. The global coarseness is set to medium for Soil 1 and 2 as well as for the Frari model, with local refinements in the head and foot area of the pile. Compare Figure 16. By generating refinements more accurate results in areas with high stress gradients are obtained.

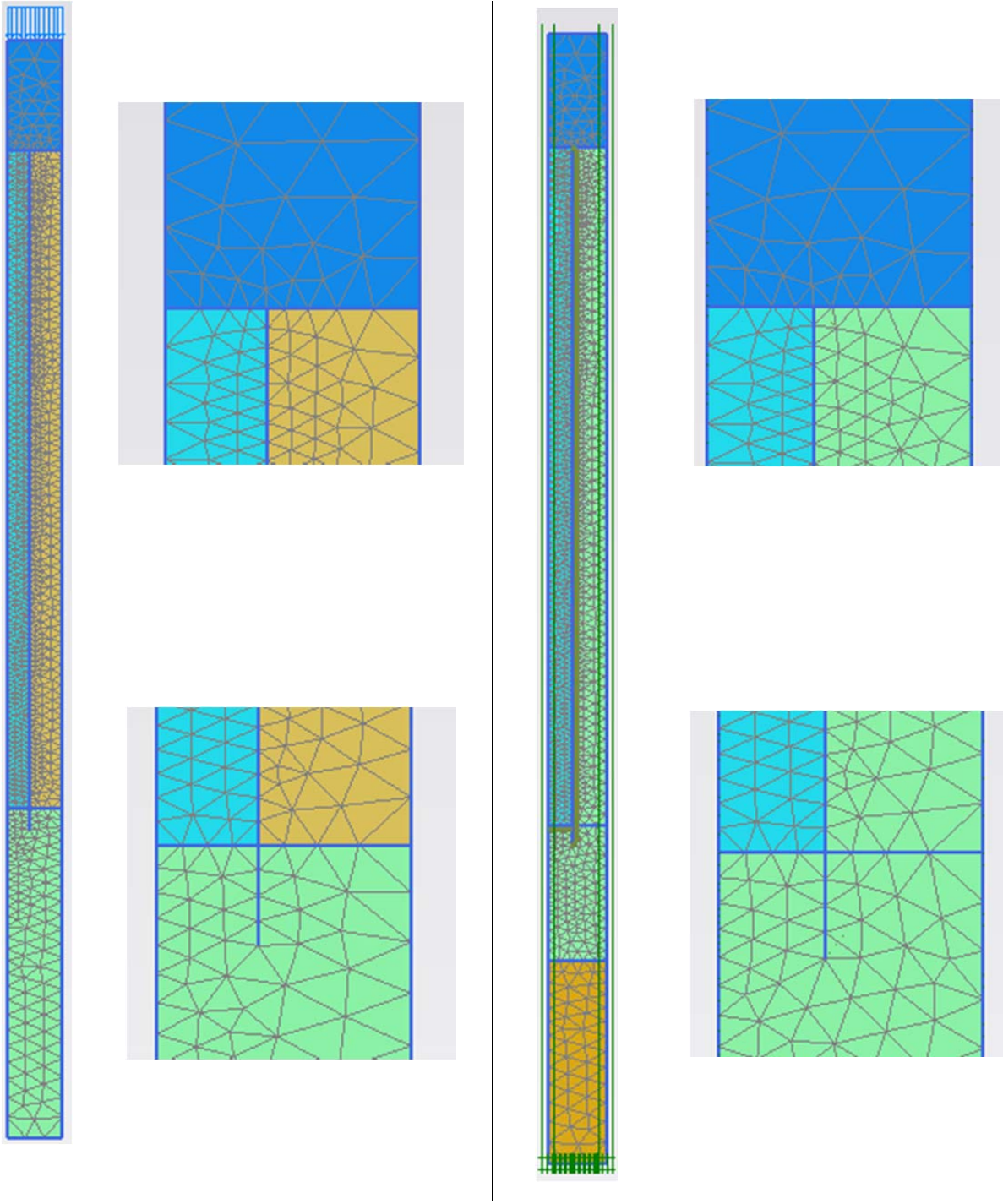
Table 3: Mesh information

<i>Calculation</i>	<i>Number of Elements</i>	<i>Number of Nodes</i>
Soil 1 and Soil 2	1 948	16 669
Frari	2 027	17 311



(c) Detail of Interface

Figure 15: Axisymmetric model of a single pile



(a) Mesh for Soil 1 and 2

(b) Mesh for soil of the Frari site

Figure 16: Generated meshes including details of pile head and foot refinements for single pile

## 5.3 MATERIAL PARAMETERS

### 5.3.1 SOIL PARAMETERS

At first, two very different soils are used to see the impact of soil properties on system behaviour: Soil 1, which has a high strength and a high stiffness, and on the contrary Soil 2, which represents a rather weak and soft soil. The calculations are performed in the same way for Soil 1 and 2. The constitutive model used for these soils is the Mohr-Coulomb model. The corresponding parameters are summarized in Table 4 and Table 5.

Table 4: Parameters of Soil 1

<i>Parameter</i>	<i>Unit</i>	<i>Explanation</i>	<i>Value</i>
$\gamma_{\text{unsat}} = \gamma_{\text{sat}}$	[kN/m <sup>3</sup> ]	Unit weight (unsaturated, saturated)	19
$\varphi'$	[°]	Friction angle	30
$c'$	[kN/m <sup>2</sup> ]	Cohesion	7
$\psi$	[°]	Dilatancy angle	0
$\nu$	[-]	Poisson's ratio	0.3
$E'$	[MN/m <sup>2</sup> ]	Young's Modulus	30

Table 5: Parameters of Soil 2

<i>Parameter</i>	<i>Unit</i>	<i>Explanation</i>	<i>Value</i>
$\gamma_{\text{unsat}} = \gamma_{\text{sat}}$	[kN/m <sup>3</sup> ]	Unit weight (unsaturated, saturated)	19
$\varphi'$	[°]	Friction angle	22
$c'$	[kN/m <sup>2</sup> ]	Cohesion	0
$\psi$	[°]	Dilatancy angle	0
$\nu$	[-]	Poisson's ratio	0.3
$E'$	[MN/m <sup>2</sup> ]	Young's Modulus	3

### Layering of the Frari site

A similar study is conducted with the soil layering of the Frari site. In this case, two parameter sets are used: one representing an upper layer of clay (to depth of -4.1 m below ground level), and another set for a lower layer consisting of sand. This can also be seen in Figure 15 (b).

For simulating the behaviour of the two types of soil, the Soft Soil Creep model (SSC) for the clay layer and the Hardening Soil Small model (HSS) for the sand layer are used. In Table 6 and Table 7, one can find the parameters corresponding to the constitutive models.

When using the clay parameters, it has to be considered that they are not the result of soil testing at the Frari site. Rather, these parameters represent realistic estimations for Venice lagoon clay in general. The parameters of the sand layer also are roughly estimated, based on the verbal description of the subsoil given in Table 1. Therefore, results of calculations performed with these parameters just give a qualitative idea of the load-bearing and settlement behaviour.

Table 6: Parameters of clay layer – SSC model

<i>Parameter</i>	<i>Unit</i>	<i>Explanation</i>	<i>Value</i>
$\gamma_{\text{unsat}} = \gamma_{\text{sat}}$	[kN/m <sup>3</sup> ]	Unit weight (unsaturated, saturated)	19
$\varphi'$	[°]	Friction angle	32.9
$c'$	[kPa]	Cohesion	0
$\psi$	[°]	Dilatancy angle	0
$e_{\text{init}}$	[-]	Initial void ratio	0.9
$\lambda^*$	[-]	Modified compression index	0.06316
$\kappa^*$	[-]	Modified swelling index	0.01053
$\mu^*$	[-]	Modified creep index	0.00347
$\nu_{\text{ur}}$	[-]	Poisson's ratio for unloading-reloading	0.15
$K_0^{\text{nc}}$	[-]	Coefficient of earth pressure at rest (NC)	0.4568
OCR	[-]	Over-consolidation ratio	1.1

Table 7: Parameters of sand layer – HSS model

<i>Parameter</i>	<i>Unit</i>	<i>Explanation</i>	<i>Value</i>
<i>Standard Parameters for Hardening Soil Model</i>			
$\gamma_{\text{unsat}} = \gamma_{\text{sat}}$	[kN/m <sup>3</sup> ]	Unit weight (unsaturated, saturated)	19
$\phi'$	[°]	Friction angle (Mohr-Coulomb)	36
$c'$	[kN/m <sup>2</sup> ]	Cohesion (Mohr-Coulomb)	0.1
$\psi$	[°]	Dilatancy angle	0
$\nu_{\text{ur}}$	[-]	Poisson's ratio for unloading-reloading	0.2
$E_{50}^{\text{ref}}$	[kPa]	Secant modulus for un- and reloading	45 000
$E_{\text{oed}}^{\text{ref}}$	[kPa]	Tangent modulus for oedometric loading	45 000
$E_{\text{ur}}^{\text{ref}}$	[kPa]	Secant modulus for un- and reloading	130 000
$m$	[-]	Exponent of the Ohde/Janbu law	0.5
$p^{\text{ref}}$	[kPa]	Reference stress for the stiffness parameters	100
$K_0^{\text{nc}}$	[-]	Coefficient of earth pressure at rest (NC)	0.4568
$R_f$	[-]	Failure ratio	0.90
$\sigma_{\text{Tension}}$	[kPa]	Tensile strength	0
<i>Supplemental parameters for Small strain stiffness</i>			
$G_0^{\text{ref}}$	[kPa]	Initial or very small strain shear modulus	170 000
$\gamma_{0,7}$	[kN/m <sup>3</sup> ]	Reference shear strain where $G_{\text{sec}}=0.7 \cdot G_0$	0.00015

## 5.3.2 PILE

### 5.3.2.1 PRELIMINARIES

With today's technology it is possible to take samples of wooden foundation piles and test the specimens. Comparable to soil-sampling, the challenge is to generalize this local information to a larger area. In this case, information obtained from certain piles has to be generalized to the entire foundation. It has to be considered that also within the foundation of a single building different wood species could have been used (such as alder and oak in case of the Frari tower) and that single piles could very much differ from each other in their properties.

Another challenge is to assess the impact of time on wooden piles. As already discussed, the submerged pile can actually degrade during its life-cycle, which means that after decades and centuries of service its initial properties have changed.

In a first approximation to this problem, the initial strength and stiffness properties needed in the numeric calculation are estimated. The estimation is based on tabular values for oak and alder, which are commonly used wood species for piles in Venice. By applying tabular values for compressive strength and elastic modulus, beside other factors loading direction, water content and size of the pile have to be accounted for, as they have a strong influence on the mechanical behaviour. The influence of wood moisture on compressive strength and stiffness can be seen in Figure 17. The values for strength and stiffness are strongly decreasing with increasing wood moisture. The compressive strength, for example, amounts to about 50 N/mm<sup>2</sup> at a water content of 12 %, reaching a stable value of about 25 N/mm<sup>2</sup> starting from a water content of 30 to 40 %.

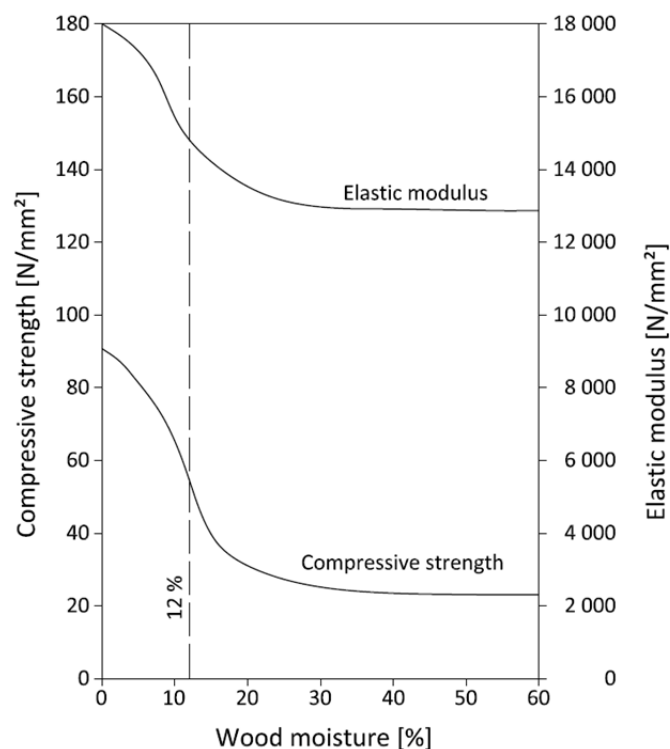


Figure 17: Elastic modulus and Compressive strength of a clear-wood specimen as a function of Wood moisture [see Schickhofer (2006)]

It is worth mentioning that the orthotropic material behaviour of wood is neglected, as the Mohr-Coulomb model including isotropic elasticity is used. This is justified by the fact that the main loading direction and the main load-bearing direction are parallel to the pile axis and therefore the mechanical behaviour in this direction is predominant. Orthotropy is however reflected in a further reduction of the parameters.

When approximating the pile's behaviour through the Mohr-Coulomb Model, it has to be considered that a wood specimen under uniaxial compression at first shows linear elastic behaviour, but involves also a non-linear stress-strain relation with considerable plastic strains before reaching failure [compare Schickhofer (2006)]. In Figure 18 (a), the stress-strain curve for a clear-wood specimen (=wood specimen free from defects) is shown, which is subjected to compression parallel to the wood fibre. The limit of proportionality  $f_{c,p,0}$  indicates the stress level up to which the behaviour is linear-elastic. In comparison, (b) shows the simplified curve describing the linear elastic – perfectly plastic Mohr-Coulomb model.

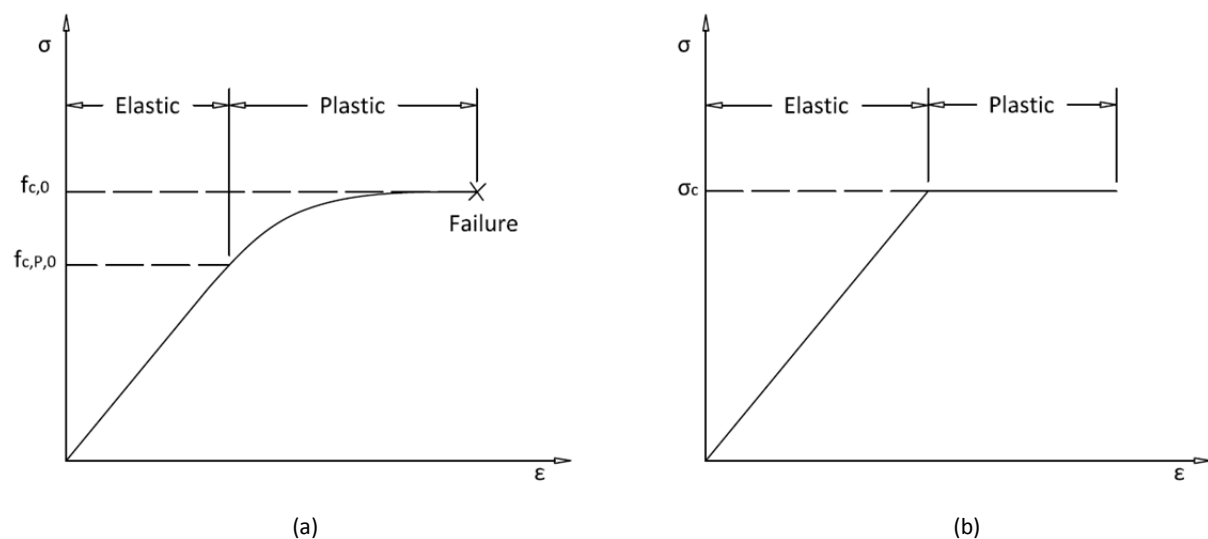


Figure 18: Stress-strain curve for a clear-wood specimen subjected to compression and idealized curve [based on illustration in Schickhofer (2006)]

In Figure 18, the notations are:

- $f_{c,0}$  Compressive strength parallel to the wood fibre
- $f_{c,p,0}$  Limit of proportionality when compressed parallel to the wood fibre, stress level limiting the elastic region where Hooke's law is valid
- $\sigma_c$  Compressive strength (isotropic material)

The unit weight in partially saturated state is assumed to be  $8 \text{ kN/m}^3$ . As the pile starts extracting the water from the surrounding soil after its installation and is permanently waterlogged, the unit weight changes during the pile's service. The period for full saturation depends amongst other things on the permeability of the surrounding soil. Besides, a centre pile needs more time for being fully saturated than a pile at the edge, as the latter can extract the water mainly from below. The indicated value is

therefore just realistic for the initial period. However, the unit weight is assumed constant during the whole calculation, as the pile weight has a negligible influence on the results.

### 5.3.2.2 MATERIAL PARAMETERS

The parameters of the pile in initial state used during the numeric calculation are summarized in Table 8. Besides, the pile is assumed to be non-porous.

Table 8: Initial parameters of the pile

<i>Parameter</i>	<i>Unit</i>	<i>Explanation</i>	<i>Value</i>	<i>K: Soil 1/ Soil 2</i>
$\gamma$	[kN/m <sup>3</sup> ]	Unit weight	8	
$\varphi'$	[°]	Friction angle	0	
$c_0'$	[kN/m <sup>2</sup> ]	Initial cohesion	7 000	
$\psi$	[°]	Dilatancy angle	0	
$\nu$	[-]	Poisson's ratio	0.4	
$E_0'$	[MN/m <sup>2</sup> ]	Initial elastic modulus	7 000	233 / 2333

As one can see from Table 8, the shear strength of the pile is given by the cohesion, which is half of the estimated initial compressive strength of 14 000 kN/m<sup>2</sup>. In Figure 19, this is shown by means of the Mohr's circle in unconfined state.

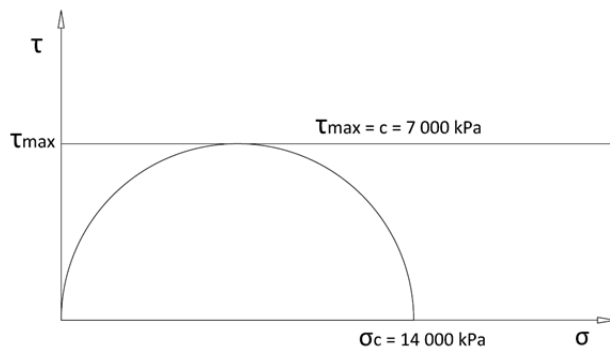


Figure 19: Compressive strength and corresponding shear strength for the wood specimen

It has to be considered that the wood specimen is tested in an unconfined state, as the uniaxial compression test is carried out for determining its strength and stiffness. Applied to pile foundations, this hypothesis would correspond to an end-bearing pile, with the skin resistance being negligibly small.

In case of Soils 1 and 2, as for these soils the Mohr-Coulomb model with a single stiffness parameter is used, the so-called relative stiffness parameter  $K$  is introduced, which is the ratio of stiffness of the pile to stiffness of the soil, as can be seen from Equation 5.1.

$$K = \frac{E_{pile}}{E_{soil}} \quad (5.1)$$

---

If the relative stiffness is smaller than 1, being  $E_{\text{pile}}$  smaller than  $E_{\text{soil}}$ , the effect of the pile, which under normal conditions acts as soil improvement, is lost.

### 5.3.2.3 DEGRADATION

In the moment, there is no model available to describe the decay of wooden piles in Venice. Punctual information about the actual state of conservation of the piles exists for sites where investigations have been conducted, such as at the Frari site. Nevertheless, the information obtained from these investigations is insufficient to set up a model for the development of mechanical properties with time, or for the actual state of conservations in mechanical terms. Therefore, different methods to simulate the degradation mechanism are studied during the analyses with the single-pile model:

- Reduction of pile parameters within the pile-degradation analysis
- Reduction of interface parameters within the interface-degradation analysis

See more detailed in Chapter 5.4.

### 5.3.3 RAFT

As described in Chapter 2, historic foundations do vary in their type of construction. For example, in some cases wooden planks forming a raft were used which could distribute the load and transfer the same to the pile heads. In other cases, such as at the bell tower of *Santo Stefano*, no planking was used, but the stone blocks of the foundation masonry rest directly on the piles respectively on the soil.

Since the study will later focus on the foundation of the bell tower of the Frari basilica, which actually includes planking, the single-pile analyses are performed with a raft. In first approximation, the foundation raft is assumed to have the following parameters, which could be those of a concrete slab:

Table 9: Parameters of the raft (single-pile analysis)

<i>Parameter</i>	<i>Unit</i>	<i>Explanation</i>	<i>Value</i>
E	[MN/m <sup>2</sup> ]	Elastic modulus	30 000
$\nu$	[-]	Poisson's ratio	0.2
$\gamma$	[kN/m <sup>3</sup> ]	Unit weight	25

The raft is defined as non-porous. For describing its mechanical behaviour the linear elastic constitutive model is used.

In general it is assumed that the raft does not experience severe degradation. Consequently, the parameters are kept constant during the analyses. Nevertheless, a reduction of the raft's stiffness is discussed on page 70 in order to evaluate its influence.

### 5.4 CALCULATIONS

As mentioned before, the degradation mechanism is simulated in two different ways:

- Degradation of the pile itself, which implies a reduction of stiffness and/or strength of the pile material (done for both Soil 1 and 2)
- Degradation of the interface, which implies a reduction of strength of the interface material (done for Soil 1 and 2 and Soil of Frari site)

Figure 20 gives an overview of the performed calculations. The differentiation between gradual analysis and single analyses during pile degradation is explained in 5.4.1.2.

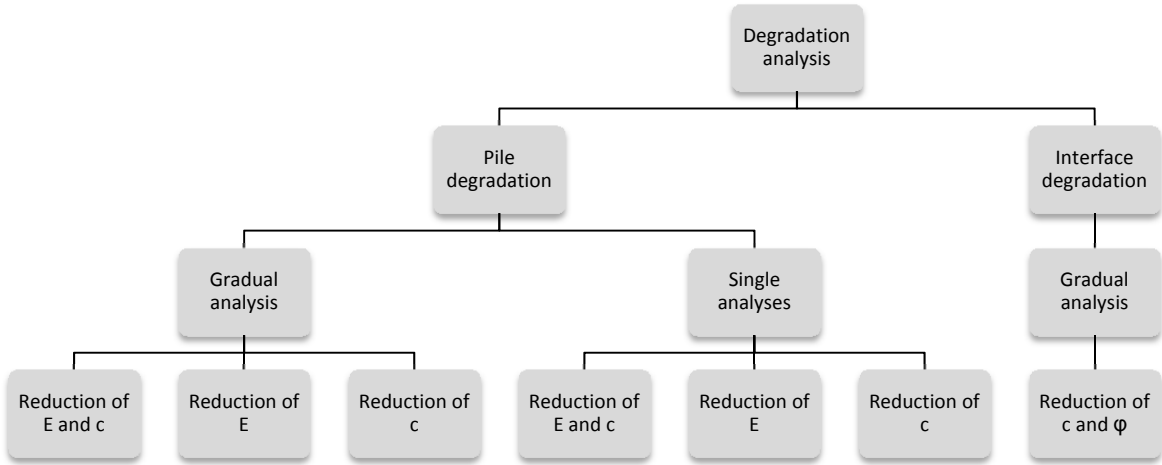


Figure 20: Overview of performed calculations (Single-pile analysis)

The analyses for Soil 1 and Soil 2 as well as those for the Frari site are carried out drained.

## 5.4.1 PILE DEGRADATION

### 5.4.1.1 PARAMETER REDUCTION

In first approximation, the degradation of the wooden pile is assumed to be uniform over the whole cross-section. This is simulated by reducing the pile's strength and stiffness, given by the parameters cohesion  $c$  and Elastic modulus  $E$  respectively.

The properties of a pile in service are reducing continuously, but as the reduction can only be simulated step by step, different degradation steps have to be assumed. The chosen steps and the relative values for cohesion and Elastic modulus are summarized in Table 10. In some cases, also the degradation steps from Table 11 are used. The reduction is done according to Equations 5.2 and 5.3, whereas for every degradation step the parameters are multiplied by the same percentage, using the *Multiplier* from Table 10 and Table 11 respectively.

$$c_{Pile,n} = x * c_{Pile,0} \quad (5.2)$$

$$E_{Pile,n} = x * E_{Pile,0} \quad (5.3)$$

The interface parameter  $R_{inter}$  is 0.7 during the whole calculation.

The pile's degradation is carried out until the degradation step of 1/1000 and until reaching a Relative stiffness of 1. The observation is stopped at this stage as the issue would completely change if the Relative stiffness was lower than 1. In this case, it would be assumed that the soil instead of the pile would be the stiffer element.

Table 10: Degradation steps for pile degradation

<i>Multiplier</i>	<i>Parameter</i>	<i>Unit</i>	<i>Value</i>	<i>K: Soil 1/ Soil 2</i>
1/10	E	[MN/m <sup>2</sup> ]	700	23 / 233
	c	[kN/m <sup>2</sup> ]	700	
1/100	E	[MN/m <sup>2</sup> ]	70	2.3 / 23.3
	c	[kN/m <sup>2</sup> ]	70	
1/1000	E	[MN/m <sup>2</sup> ]	7	0.23 / 2.3
	c	[kN/m <sup>2</sup> ]	7	

Table 11: Further degradation steps for pile degradation

<i>Multiplier</i>	<i>Parameter</i>	<i>Unit</i>	<i>Value</i>	<i>K: Soil 1/ Soil 2</i>
1/11	E	[MN/m <sup>2</sup> ]	$6.36 * 10^5$	21.21 / 212.1
	c	[kN/m <sup>2</sup> ]	636.36	
1/12	E	[MN/m <sup>2</sup> ]	$5.83 * 10^5$	19.44 / 194.4
	c	[kN/m <sup>2</sup> ]	583.3	
1/13	E	[MN/m <sup>2</sup> ]	$5.38 * 10^5$	17.94 / 179.4
	c	[kN/m <sup>2</sup> ]	538	

1/14	E	[MN/m <sup>2</sup> ]	$5 \cdot 10^5$	16.67 / 166.7
	c	[kN/m <sup>2</sup> ]	500	
1/15	E	[MN/m <sup>2</sup> ]	$4.7 \cdot 10^5$	15.56 / 155.6
	c	[kN/m <sup>2</sup> ]	466.6	
1/20	E	[MN/m <sup>2</sup> ]	$3.5 \cdot 10^5$	11.67 / 116.7
	c	[kN/m <sup>2</sup> ]	350	
1/35	E	[MN/m <sup>2</sup> ]	$2 \cdot 10^5$	6.67 / 66.7
	c	[kN/m <sup>2</sup> ]	200	
1/50	E	[MN/m <sup>2</sup> ]	$1.4 \cdot 10^5$	4.67 / 46.7
	c	[kN/m <sup>2</sup> ]	140	
1/70	E	[MN/m <sup>2</sup> ]	$10^5$	3.33 / 33.3
	c	[kN/m <sup>2</sup> ]	100	

#### 5.4.1.2 PERFORMED ANALYSES AND RELATIVE CALCULATION PHASES

Regardless of the type of soil (Soil 1 or 2), two different types of analysis are performed:

- *Method A - Gradual analysis:* One continuous calculation is done. The pile degrades gradually, which means that during the calculation every single degradation step starts with the results obtained from the previous step. This procedure represents in a very simplified way the natural decay of wooden piles.
- *Method B – Single analyses:* In this case the single degradation steps start, independently of the one before, from the *Initial phase*. This procedure is needed to examine and understand the influence of the pile's history (see explanation on page 42).

In Table 12 and Table 13, the calculation phases of the two pile-reduction methods are listed as to give a better understanding of the difference between the methods:

Table 12: Calculation phases for gradual analysis

<i>Identification</i>	<i>Phase no.</i>	<i>Start from Phase no.</i>	<i>Explanation</i>
Initial phase	0	N/A	K0-procedure
Pile and slab activation	1	0	Activation of pile with initial parameters and of slab
Load	2	1	Application of 200 kPa at the top edge of the slab
Pile degradation 1/10	3	2	Change of pile-material for simulating the pile's degradation: The initial values for stiffness and/or strength are replaced by parameters reduced to a tenth of the initial ones.

Pile degradation 1/100	4	3	The pile parameters are further changed from a tenth to a hundredth of the initial parameters.
Pile degradation 1/1000	5	4	The pile parameters are further changed from a hundredth to a thousandth of the initial parameters.

Table 13: Calculation phases for single analyses

<i>Identification</i>	<i>Phase no.</i>	<i>Start from Phase no.</i>	<i>Explanation</i>
Initial phase	0	N/A	K0-procedure
Pile and slab activation	1	0	Activation of pile with initial parameters and of slab
Load	2	1	Application of 200 kPa at the top edge of the slab
Pile degradation 1/10 and slab activation	3	0	Installation of pile with minor stiffness and/or strength (a tenth of the initial parameters) and activation of the slab
Load	4	3	Application of 200 kPa at the top edge of the slab
Pile degradation 1/100 and slab activation	5	0	Installation of pile with minor stiffness and/or strength (a hundredth of the initial parameters) and activation of the slab
Load	6	5	Application of 200 kPa at the top edge of the slab
Pile degradation 1/1000 and slab activation	7	0	Installation of pile with minor stiffness and/or strength (a thousandth of the initial parameters) and activation of the slab
Load	8	7	Application of 200 kPa at the top edge of the slab

For the two types of analyses above mentioned, the effect of changing either both parameters elastic modulus  $E$  and cohesion  $c$  or just one of them is studied. Hence, the following scenarios are run through:

- Reduction of  $E$  and  $c$
- Reduction of  $c$
- Reduction of  $E$

In the following, the most important results of the three scenarios for gradual and single analyses for Soil 1 and 2 are summarized. A detailed explanation of data interpretation is given by the example of the gradual analysis with Soil 1.

### 5.4.1.3 SOIL 1 – RESULTS OF GRADUAL ANALYSIS

#### Settlements:

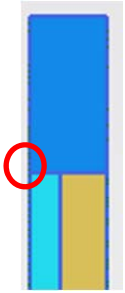


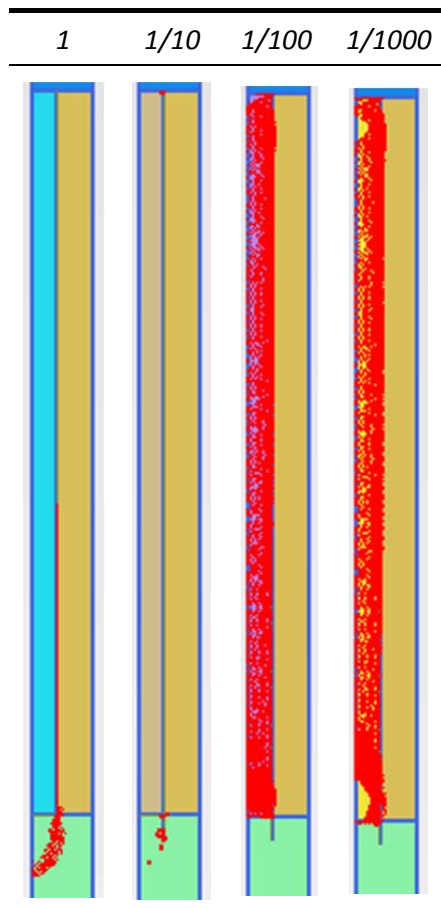
Figure 21:  
Node for  
settlement  
curves

The settlements  $u_y$  [cm] are measured in a *Node* at the centre of the pile head, which is shown in Figure 21, and are summarized in Table 14: On the left side, the results for reducing both parameters with the corresponding values for  $E$  and  $c$  as well as the relative stiffness  $K$  are shown. In the middle, the settlements for reducing the cohesion and the relative values for the same are listed. In this case, the relative stiffness remains constant, as the elastic modulus is not modified.

One can note that there is no difference in settlement behaviour of the pile head when reducing either both parameters or just the cohesion, which means that the influence of any reduction of the elastic modulus on settlements in this case is negligibly small.

Table 14: Soil 1, Gradual analysis, Settlements

<i>Multiplier</i>	$K$	$c$	$E$	$u_y$	$K$	$c$	$u_y$	$K$	$E$	$u_y$
	<i>[-]</i>	<i>[kPa]</i>	<i>[kPa]</i>	<i>[cm]</i>	<i>[-]</i>	<i>[kPa]</i>	<i>[cm]</i>	<i>[-]</i>	<i>[kPa]</i>	<i>[cm]</i>
1	233	7000	$7 \cdot 10^6$	1.0	233	7000	1.0	233	$7 \cdot 10^6$	1.0
1/10	23	700	$7 \cdot 10^5$	1.0	233	700	1.0	23	$7 \cdot 10^5$	1.0
1/100	2.3	70	$7 \cdot 10^4$	2.0	233	70	2.0	2.3	$7 \cdot 10^4$	1.0
1/1000	0.23	7	$7 \cdot 10^3$	2.1	233	7	2.1	0.23	$7 \cdot 10^3$	1.0



By using a reduced cohesion, however, the yield surface – in this case the Mohr-Coulomb failure criterion – is reached at a lower stress level, resulting in (higher) plastic deformations. This can also be seen from Figure 22, which shows the development of plastic points with decay: To a degradation of 1/10 of the initial pile parameters, no plastic points occur in the pile's region, which implies that the behaviour of the pile is still completely (linear) elastic. At 1/100 and 1/1000, on the other hand, the cohesion is reduced at such a rate that the yield criterion is reached in stress points over the whole pile length, increasing the settlement of the pile head from 1.0 cm to 2.0 cm respectively 2.1 cm.

Figure 22: Gradual reduction of  $c$ ,  
Development of plastic points

On the right side of Table 14, finally, the results for a modified elastic modulus are given with corresponding values of  $E$  and  $K$ . This modification does not provoke further settlements in comparison to the initial ones, which is the consequence of the PLAXIS calculation procedure.

Details on the PLAXIS calculation procedure:

The constant settlements when reducing the piles stiffness are due to the fact that PLAXIS does not start the calculation procedure unless there is disequilibrium. By looking at the stress state in the  $p'$ - $q$ -plane, this can be explained more clearly: In Figure 23, the original failure line (1) and the original stress state of a stress point is given, whereas the stress state lies within the elastic region. When reducing the strength, as illustrated with line (2), disequilibrium arises, as the stress state is beyond the yield surface. As such a state is inadmissible, the unbalanced forces – meaning the difference between the nodal forces before strength reduction and the nodal forces which are in equilibrium with the current yield stresses – acting on the corresponding element nodes have to be redistributed to adjacent elements, until the system is balanced. On the other hand, a reduction of stiffness during a PLAXIS-calculation in general does not cause an imbalance, because the stress state of stress points is not changed. Hence, no further settlements occur.

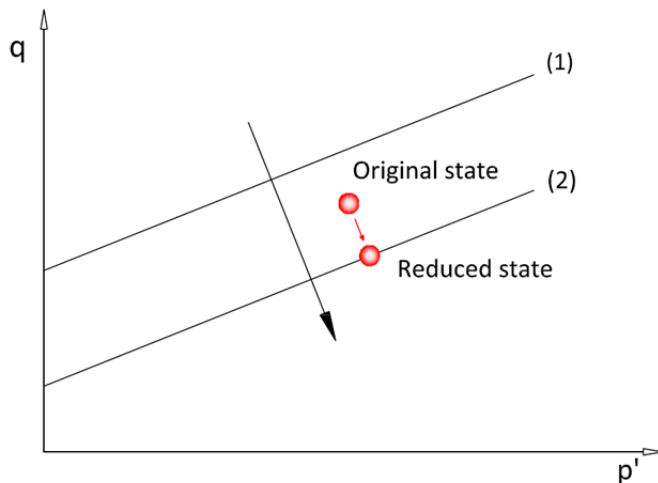


Figure 23: Change of stress state due to strength reduction

In conclusion, this phenomenon is the result of a numeric calculation and is not realistic, as the stress state would actually change if the elastic modulus was modified. Besides, when reducing both parameters, the modified stiffness actually slightly influences the results. However, this is not apparent in above results as the settlements for a reduction of the cohesion and of both parameters do not differ from each other.

Reduction of stiffness and strength

In Figure 24, the relative proportion of load transferred by the pile head ( $N_{Top}$ ) and by the raft ( $R_{Raft}$ ) is shown with respect to the degradation steps. As the pile is much stiffer (and has a greater strength) at the beginning, about 93% of the total load is transferred to the pile head. With on-going decay of the pile, which implies a reduction of cohesion and elastic modulus, the load carried by the raft is increasing.

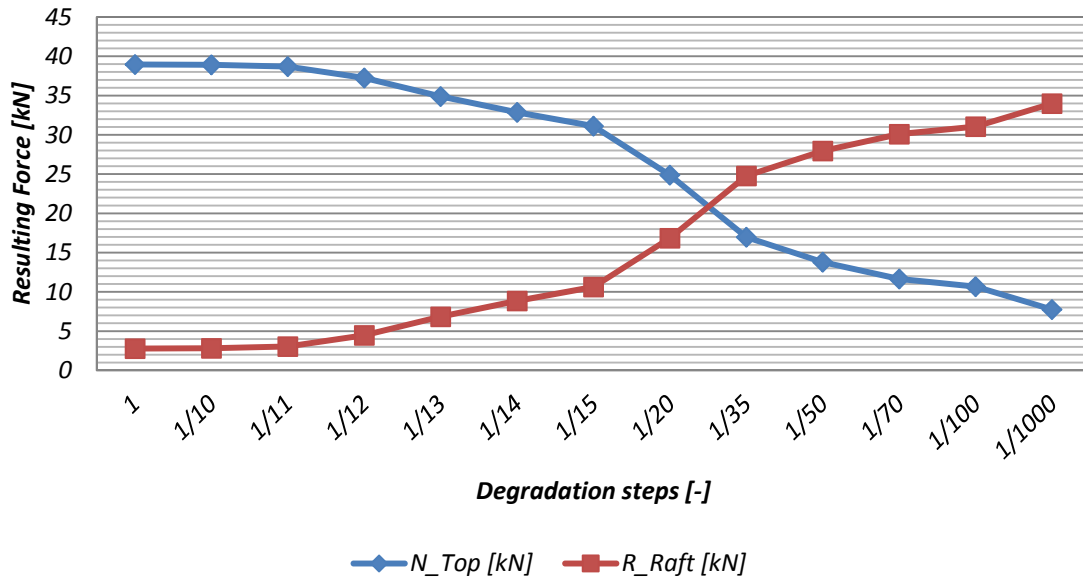
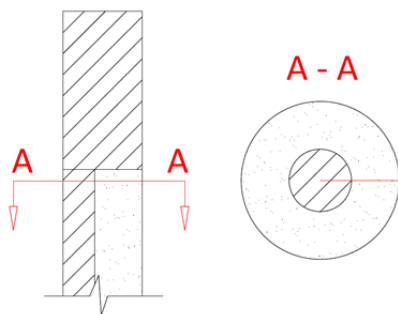


Figure 24: Load transfer, Soil 1 – Gradual reduction of stiffness and strength



The resulting normal force in the pile head (also called pile head resistance in this work), and the resulting force transferred by the raft to the soil (also called resistance of the raft), are obtained by integrating the stresses directly under the foundation slab with respect to the pile area respectively to the circumferential soil area, as illustrated in Figure 25.

Figure 25:  
Cross-section below foundation slab

As it is shown in Figure 24, with progressive decay of the pile the load is redistributed until the raft bears more in terms of forces. Actually, it is more interesting to observe the stress-redistribution during decay. For this purpose, the total normal stresses of different degradation steps are visualized by ‘cutting’ 5 cm below the foundation slab. The cross-sections are shown in Figure 26: If the initial parameters are reduced to a hundredth, the pile is still stiffer with a relative stiffness  $K$  of 2.3. This is reflected in the fact that the stress in the pile is considerably higher than it is in the soil. By reducing the parameters further to 1/233, corresponding to a relative stiffness of 1, the stress distribution is not uniform against one’s expectations. Even at a reduction to a thousandth of the initial parameters,

with the relative stiffness being less than 1, the stress in the pile is still higher than it is in the soil. The reason can be found in the pile’s history and is further discussed on page 58.

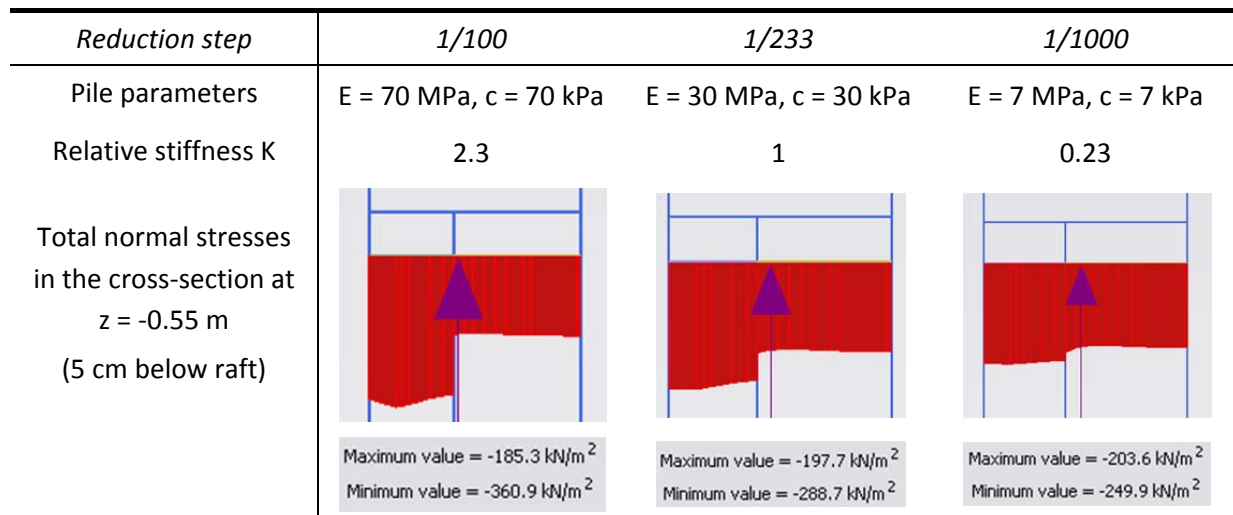


Figure 26: Distribution of total normal stresses, Soil 1 – Gradual reduction of stiffness and strength

Beside the change of load transferred by the pile respectively by the raft, also the bearing capacity of the pile is analyzed. The bearing capacity, in the following called pile resistance, consists of base and skin resistance. These are obtained by integrating the total normal stresses  $\sigma_N$  in the lower interface with respect to the pile foot area respectively the shear stress  $\tau_1$  in the interface along the pile shaft with respect to the pile skin surface. Their values are plotted Figure 27.

Initially, the base and skin resistance are of the same magnitude. Starting from a reduction of the initial parameters to 1/11, the skin resistance is diminishing, until it reaches a final value of about 1.6 at a reduction to 1/35. The base resistance, however, remains constant until a reduction to 1/20 and is then getting smaller.

Compared to the skin resistance of a free-standing pile, which in general is considerably higher than its base resistance, in this case the skin resistance is at maximum equal to the base resistance. This is due to the small distance of 0.3 m from pile to pile, by which the pile’s load-bearing behaviour is completely changed, and behaves like a centre pile of a pile group: The pile and the surrounding soil settle rather uniformly, therefore the mobilized skin resistance is strongly reduced.

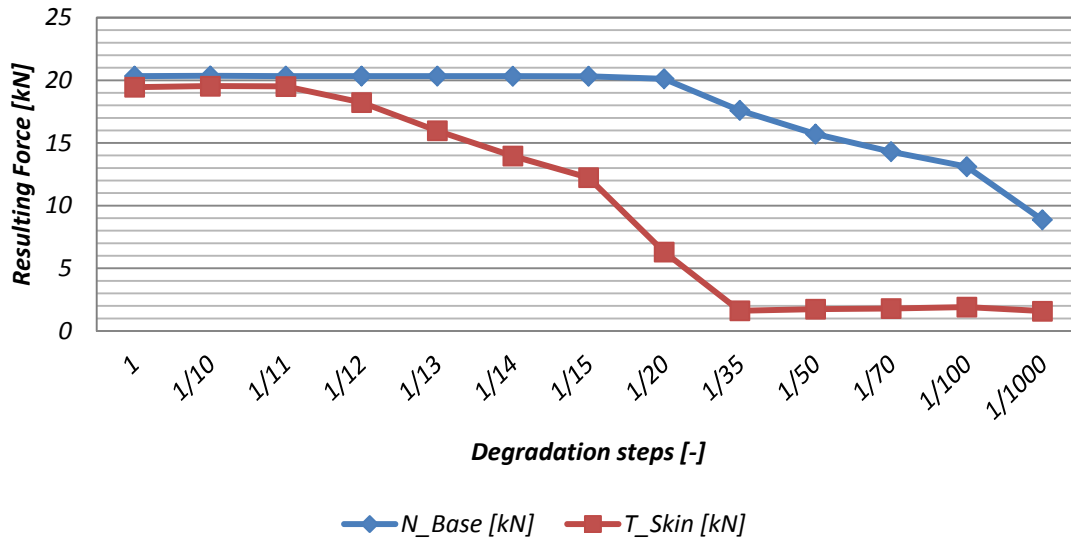


Figure 27: Development of base and skin resistance, Soil 1 – Gradual reduction of stiffness and strength

In Figure 28 the Resistance-settlement curve is plotted, which shows the pile-head settlements and the pile resistance with on-going decay of the pile. Like in the graph before, one can see that the skin resistance starts to reduce earlier than the base resistance does.

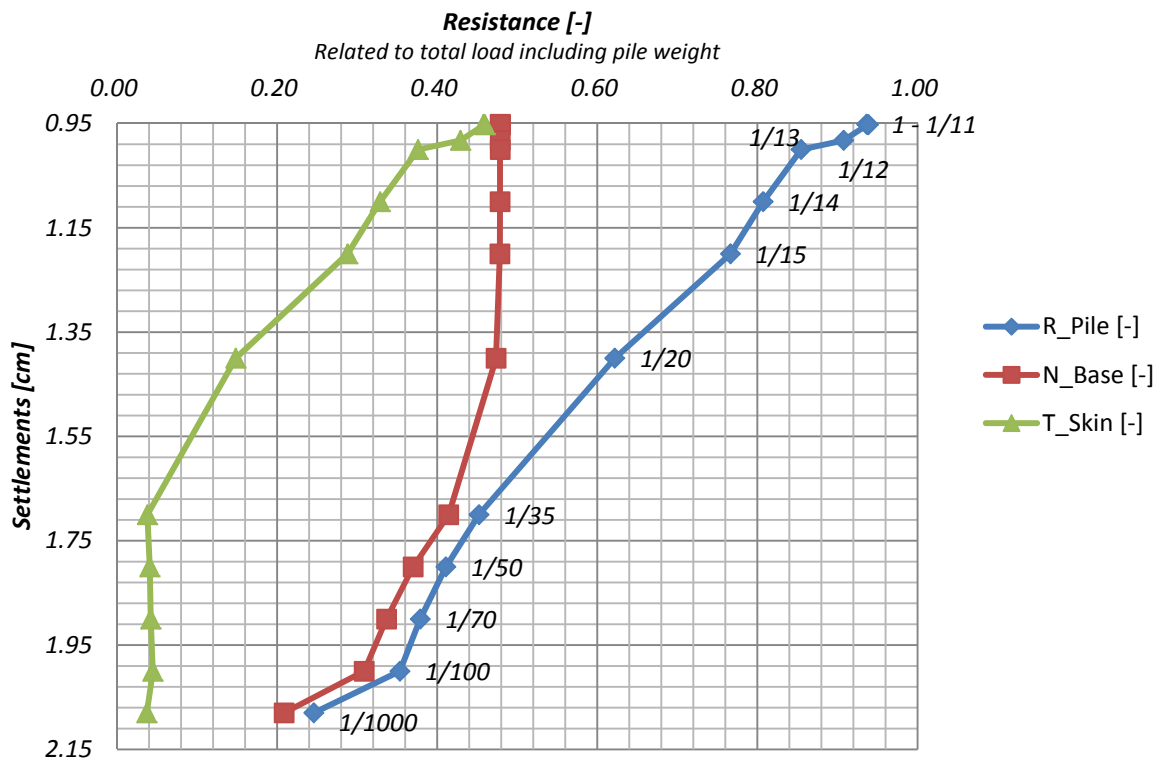


Figure 28: Resistance-settlement curve, Soil 1 – Gradual reduction of stiffness and strength

In this graph, skin ( $T_{skin}$ ) and base resistance ( $N_{base}$ ) of the pile as well as their sum, the total pile resistance ( $R_{pile}$ ), are related to the total load plus the pile's self-weight. The total load is equal to the load applied at the top edge of the foundation slab including the self-weight of the slab:

$$\begin{aligned}
 Total\ Load &= p \times A_{slab} + \gamma_{concrete} \times d_{slab} \times A_{slab} \\
 &= (200 + 25 \times 0.5) \times r^2 \pi = 41.7 [kN]
 \end{aligned}
 \tag{5.4}$$

Adding the self-weight of the pile of 0.8 kN, the total load is equal to 42.5 kN.

Reduction of stiffness

As it was already discussed on page 37, a reduction of the stiffness does not provoke a change in stress state during a PLAXIS-calculation, which is reflected in the steady distribution of total normal stresses, illustrated in Figure 29.

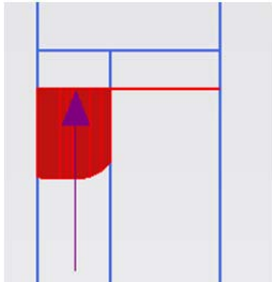
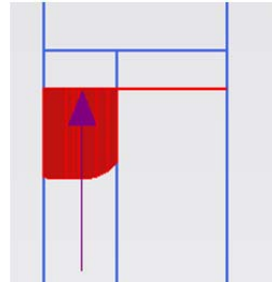
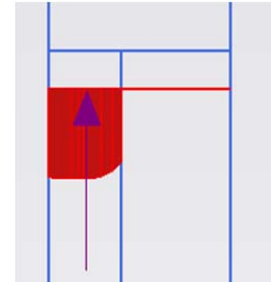
Reduction step	1/100	1/233	1/1000
Pile parameters	E = 70 MPa c = c <sub>0</sub> = 7000 kPa	E = 30 MPa c = c <sub>0</sub> = 7000 kPa	E = 7 MPa c = c <sub>0</sub> = 7000 kPa
Relative stiffness K	2.3	1	0.23
Total normal stresses in the cross-section at z = -0.55 m (5 cm below raft)	 <p>Maximum value = -22.49 kN/m<sup>2</sup> Minimum value = -1257 kN/m<sup>2</sup></p>	 <p>Maximum value = -22.49 kN/m<sup>2</sup> Minimum value = -1257 kN/m<sup>2</sup></p>	 <p>Maximum value = -22.49 kN/m<sup>2</sup> Minimum value = -1257 kN/m<sup>2</sup></p>

Figure 29: Distribution of total normal stresses, Soil 1 – Gradual reduction of stiffness

#### 5.4.1.4 SOIL 1 – RESULTS OF SINGLE ANALYSES

The objective of this analyzing method is to quantify the influence of the pile's history during the gradual analysis. By the term 'history' is meant that the pile has had a higher stiffness and strength in the past compared to its respective degradation state. This is realized by performing the single analyses, which do not imply a continuous, stepwise degradation. Rather, the pile is installed directly with decreased mechanical properties, omitting in this way the influence of the pile's history. A detailed explanation on the procedure is given in Table 13 on page 34 .

In the following, the results are compared with those of the gradual analysis.

#### Settlements

Table 15: Settlements, Soil 1 – Single analyses

Multiplier	K	c	E	$u_y$	K	c	$u_y$	K	E	$u_y$
	[-]	[kPa]	[kPa]	[cm]	[-]	[kPa]	[cm]	[-]	[kPa]	[cm]
1	233	7000	$7 \cdot 10^6$	1.0	233	7000	1.0	233	$7 \cdot 10^6$	1.0
1/10	23	700	$7 \cdot 10^5$	1.2	233	700	1.0	23	$7 \cdot 10^5$	1.2
1/100	2.3	70	$7 \cdot 10^4$	2.1	233	70	2.0	2.3	$7 \cdot 10^4$	1.9
1/1000	0.23	7	$7 \cdot 10^3$	2.5	233	7	2.2	0.23	$7 \cdot 10^3$	2.4

The arrangement of the table is the same as in Table 14 on page 35. The settlements are also referred to the centre of the pile head.

In general, there is no big difference in settlement behaviour between the three types of analysis. As expected, the settlements are slightly higher when reducing both parameters E and c. When looking at the results of a reduced cohesion (in the middle), one can note once again the influence of strength on settlement behaviour. On the right hand side, the settlements due to the reduced pile stiffness are actually increasing in contrast to the results of the gradual analysis.

By comparing these results with those obtained from the gradual reduction (compare Table 14 on page 35), the effect of the pile's history on settlement behaviour is best visible at the degradation step of 1/1000: When the pile has experienced a higher stiffness and/or strength in the past, the resulting settlements of the pile head are in general smaller (2.1 cm) compared to the settlements when the pile is installed directly with minor properties (2.5 cm respectively 2.2 cm).

In Figure 30, the development of settlements is illustrated for both types of analysis for the simultaneous reduction of strength and stiffness. Independent of the type of analysis, at the beginning an elevated stress is transferred from the pile to the soil underneath, as the pile bears most of the applied load. This causes a distinct pressure bulb under the pile foot (compare Figure 33) and elevated strains in this area. As a result, the pile moves downwards as a whole and forces also the foundation slab to settle.

As it can be seen from Table 15, the settlement of the pile head is already higher at the degradation step of 1/10 during Method B (1.2 cm) compared to Method A (1.0 cm). The fact that the pile head

---

settles more during Method B, although the normal force in the pile-head is lower (compare normal forces for both reduction methods on page 45) at first seems paradoxical. This fact, however, can be explained through the system behaviour: When performing a single analysis at the step of 1/10, the resistance of the raft is increased, which means that a higher load is transferred from the raft to the soil underneath. Consequently, beside the pile-head also the adjacent soil settles, what can be seen from Figure 30. The foundation slab moves down quite uniformly, especially at the reduction steps of 1/100 and 1/1000. In these stages, the settlement behaviour actually is the one of a shallow foundation.

When reducing the parameters gradually to 1/10, the settlements do not change, as in this case still the same load is carried by the pile. At the further examined degradation steps, the settlement of the pile head increases, since the resulting force transferred by the raft gets significantly higher. In this way, the whole pile head area is able to settle, comparable with the behaviour described for Method B. Nevertheless, the settlements of the pile head remain smaller during the gradual degradation.

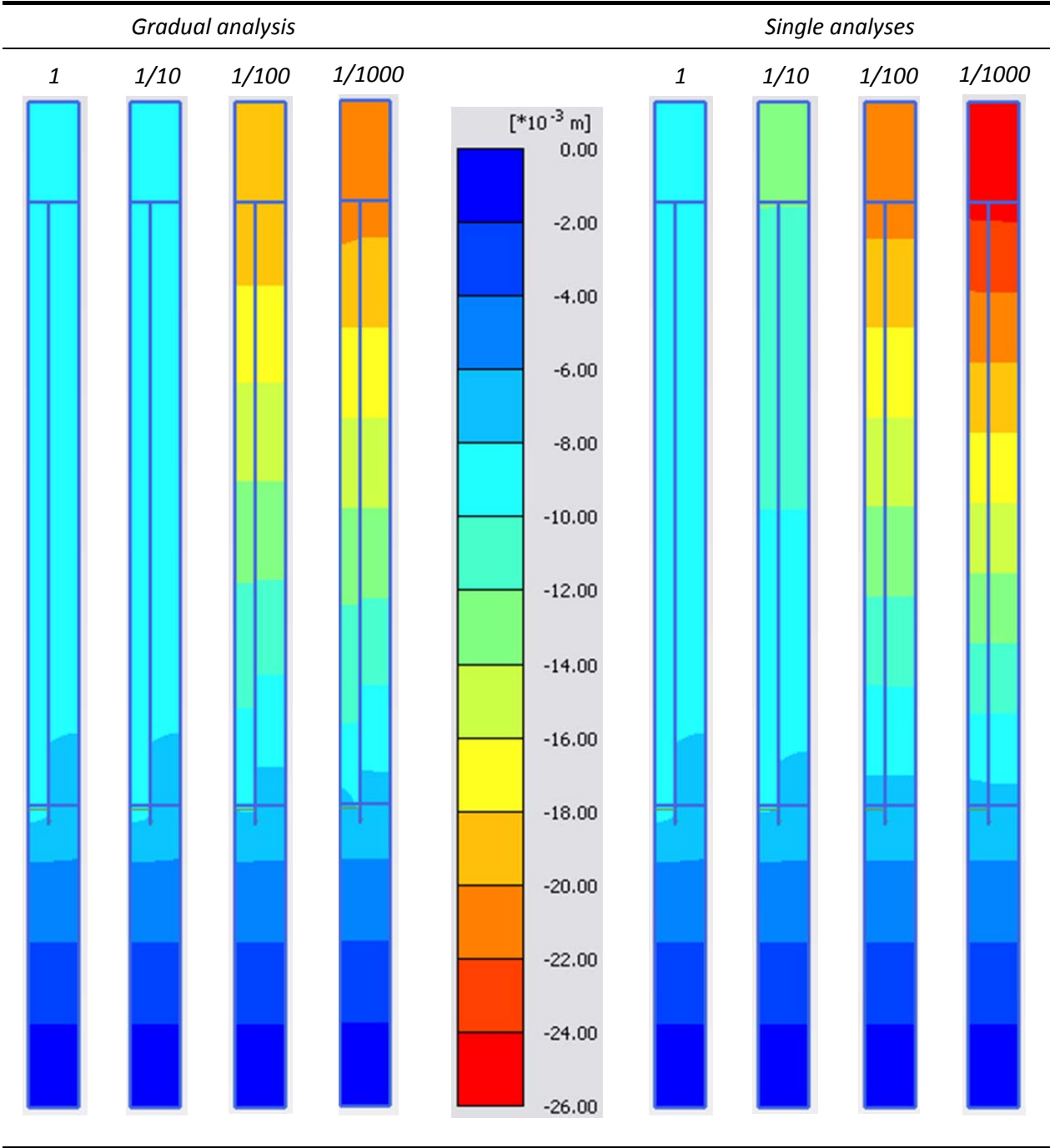


Figure 30: Total displacements  $u_y$  for Method A and B, Soil 1 – Reduction of stiffness and strength

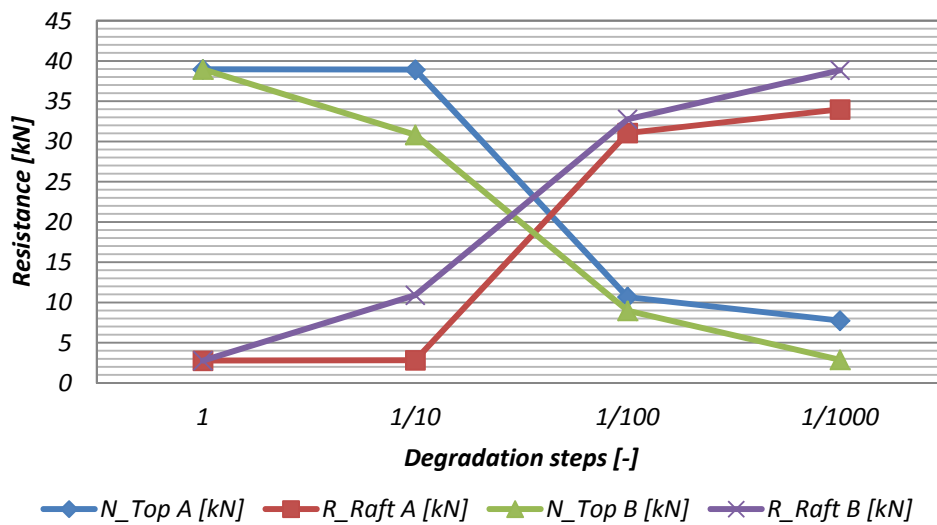
Reduction of stiffness and strength

Figure 31: Load transfer for Method A and B, Soil1 – Reduction of stiffness and strength

In Figure 31 the results of the reduction of stiffness and strength from the gradual analysis are repeated, and compared with those from the single analyses (the latter with identification B for Method B). One can note that during the gradual analysis, the normal force in the pile head is generally higher, and remains even constant when reducing the pile's parameters from 1 to 1/10. This can also be seen from the distribution of total stresses  $\sigma_{yy}$ , illustrated in Figure 32 on the left side: The stress distribution from 1 to 1/10 does not change, as the strength of the pile still allows bearing the nodal forces generated in the previous phase. By further reducing the parameters to 1/100, the yield criterion is reached in stress points all along the pile shaft (compare relative shear stress of 1 in Figure 33, on the left). Hence, the unbalanced forces have to be redistributed, which leads to higher stresses and consequently a higher resulting force transferred by the raft.

When the pile is installed directly with minor properties, evidently the stresses do not have to be redistributed, but are transferred either by the pile or the raft according to the relative stiffness and strength between pile and surrounding soil, which is illustrated in Figure 34 by means of the direction of total principal stresses  $\sigma_1$ . The stresses in the pile then are lower when compared to the results of the gradual analysis (see again Figure 32). The increased stress level in the soil can be seen from Figure 33.

By looking at the normal stresses, the differences in load transfer may become even clearer: Figure 35 shows the development of total normal stresses when gradually reducing the parameters, which was already described on page 39; Figure 36 shows the same for the single analyses. The latter illustrates lower total normal stresses in the pile head, corresponding to the smaller normal force shown in above diagram. Particularly noticeable is the non-uniform distribution of stresses for the relative stiffness of 1.

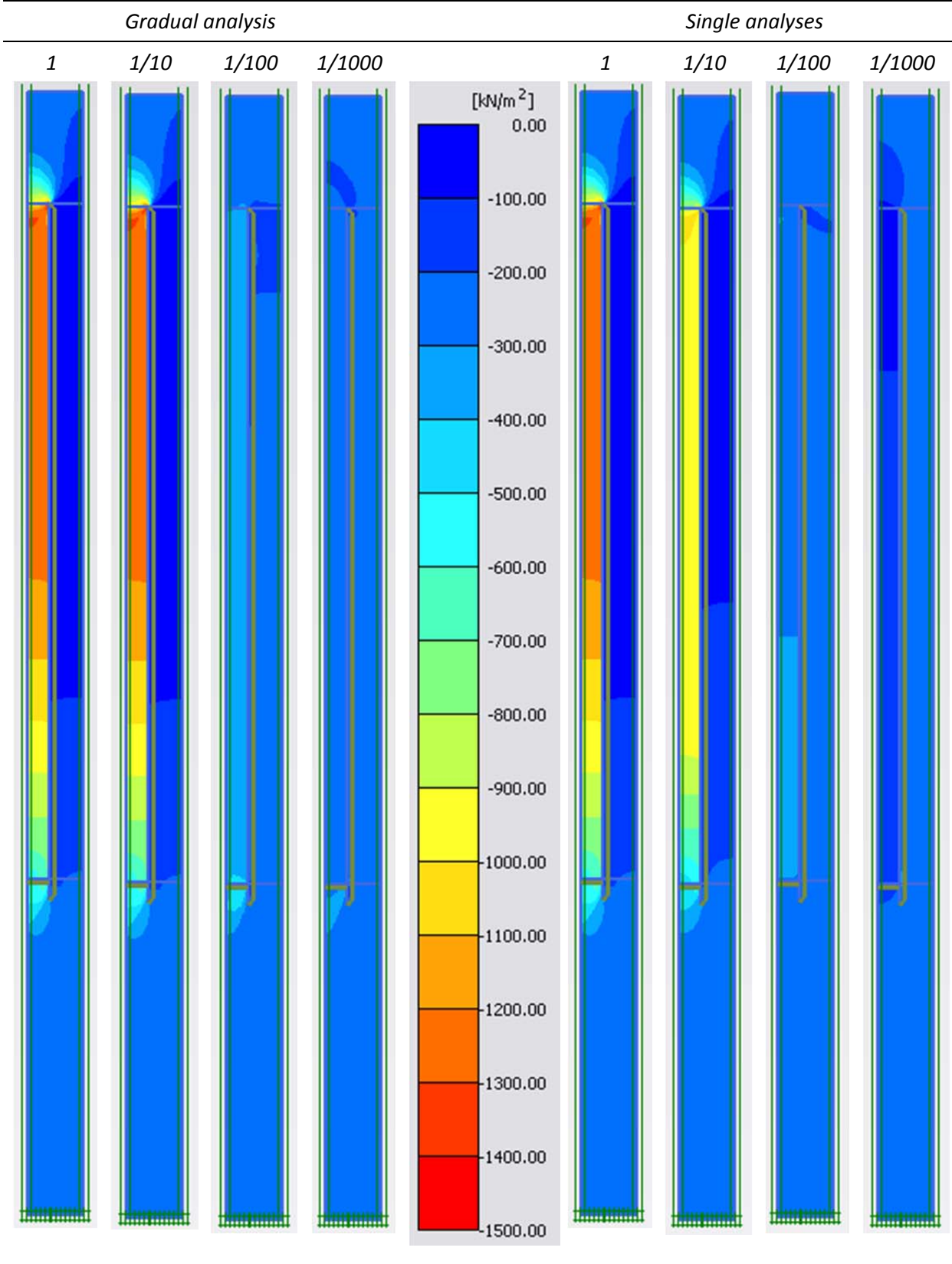


Figure 32: Cartesian total stresses  $\sigma_{yy}$  for Method A and B, Soil1 – Reduction of stiffness and strength

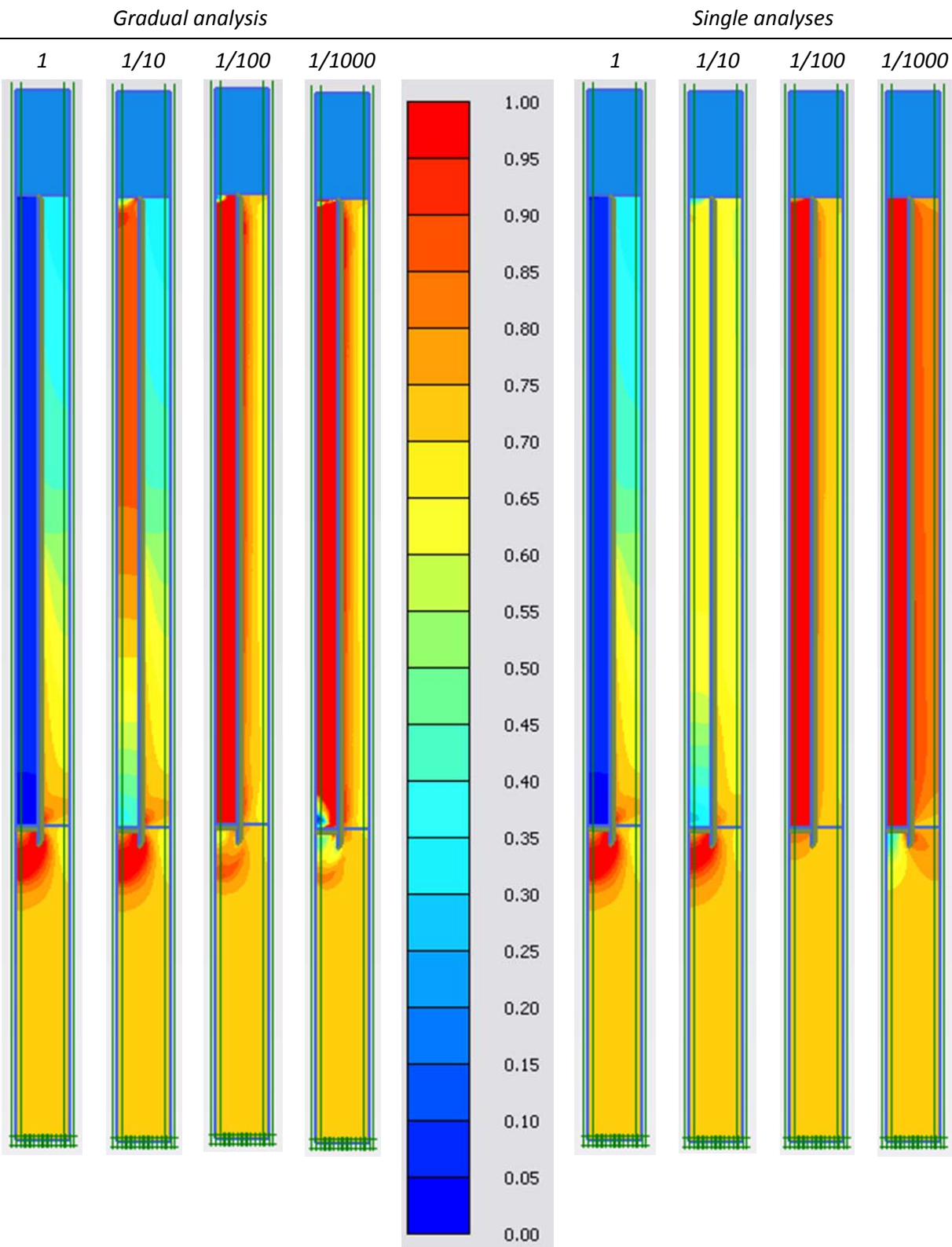


Figure 33: Relative shear stresses for Method A and B, Soil1 – Reduction of stiffness and strength

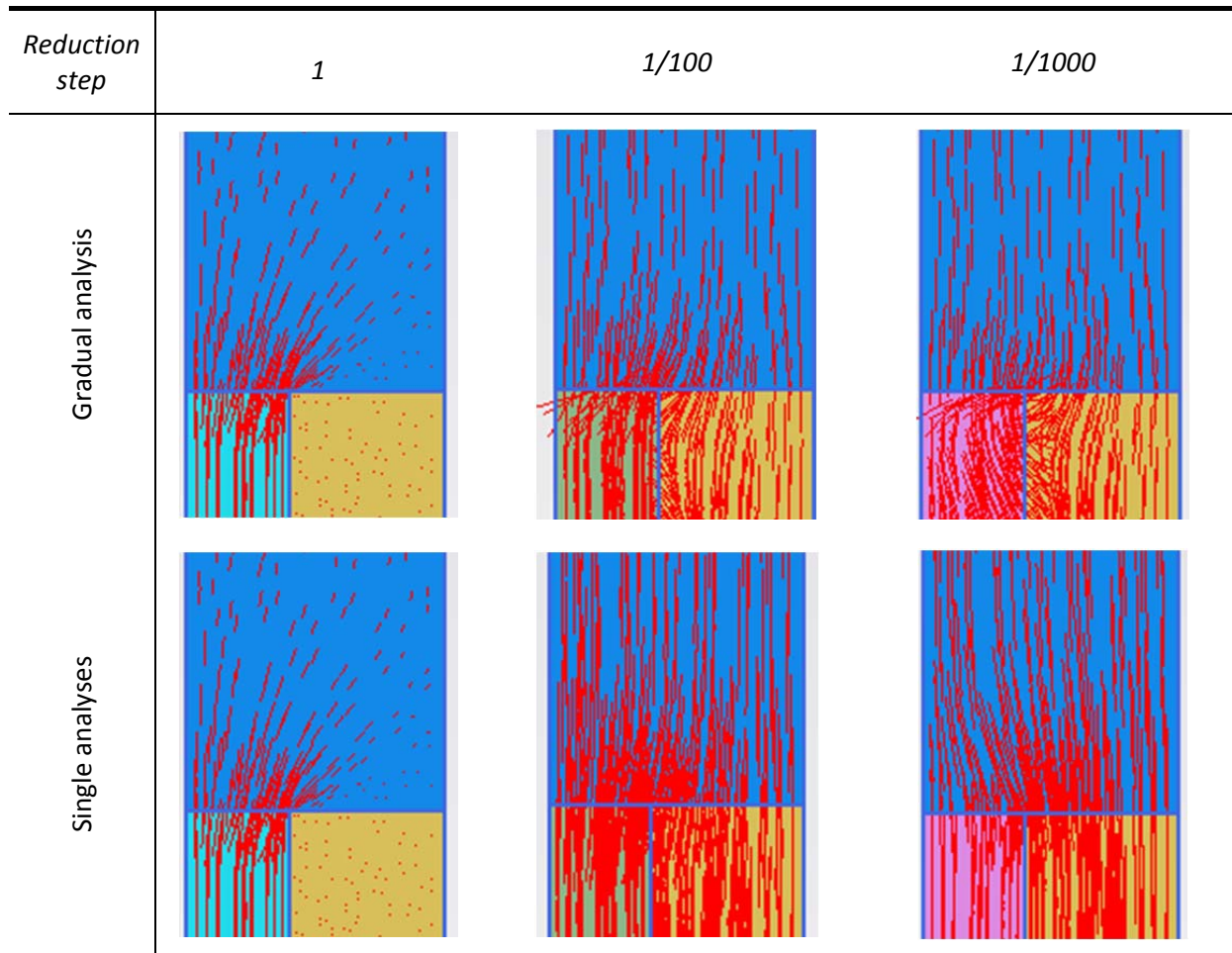


Figure 34: Direction of total principal stresses  $\sigma_1$  for Method A and B, Soil1 – Reduction of stiffness and strength

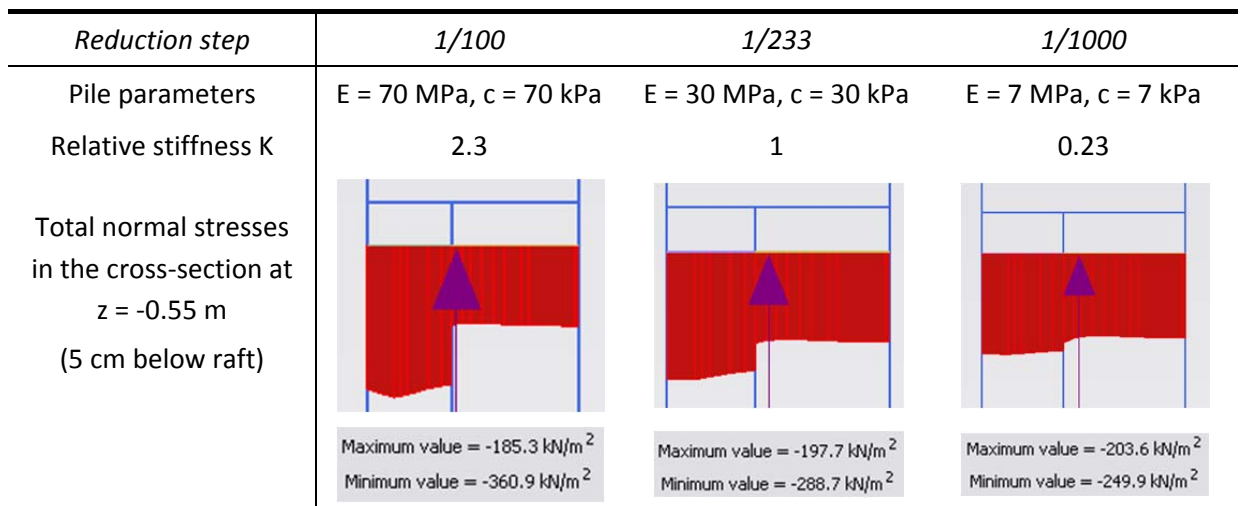


Figure 35: Distribution of total normal stresses for Method A, Soil 1 – Reduction of stiffness and strength (repetition)

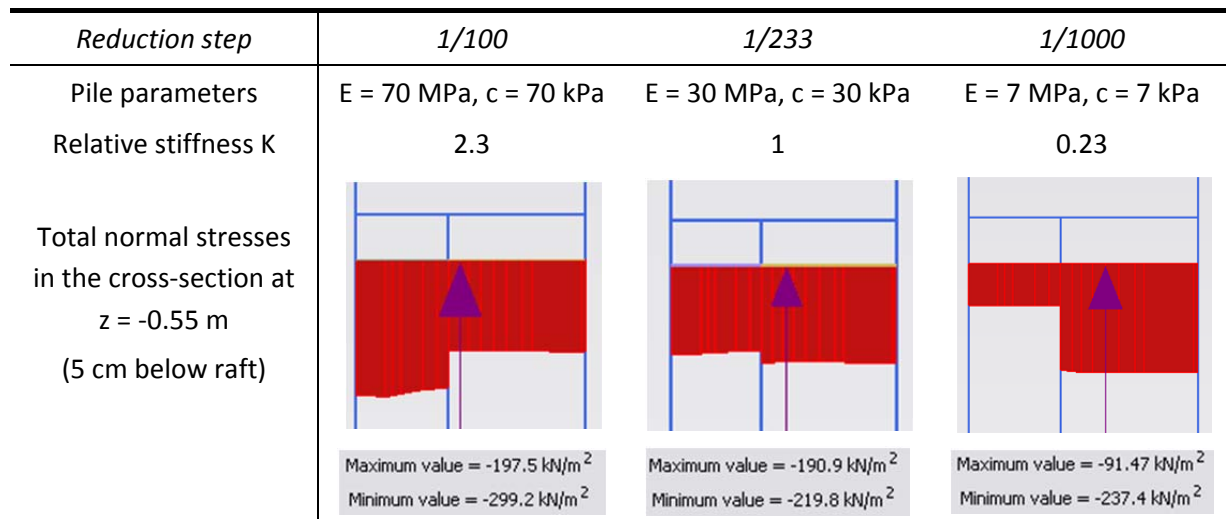


Figure 36: Distribution of total normal stresses for Method B, Soil 1 – Reduction of stiffness and strength

Reduction of stiffness

Comparing the development of stress distribution for a parallel reduction of stiffness and strength from Figure 36 with the reduction of stiffness from Figure 37, one can see that the resulting average stress in the pile is higher when its cohesion remains unaltered at a value of 7 MPa, especially at the reduction step of 1/100. Obviously, the strength of the pile has an influence on stress distribution.

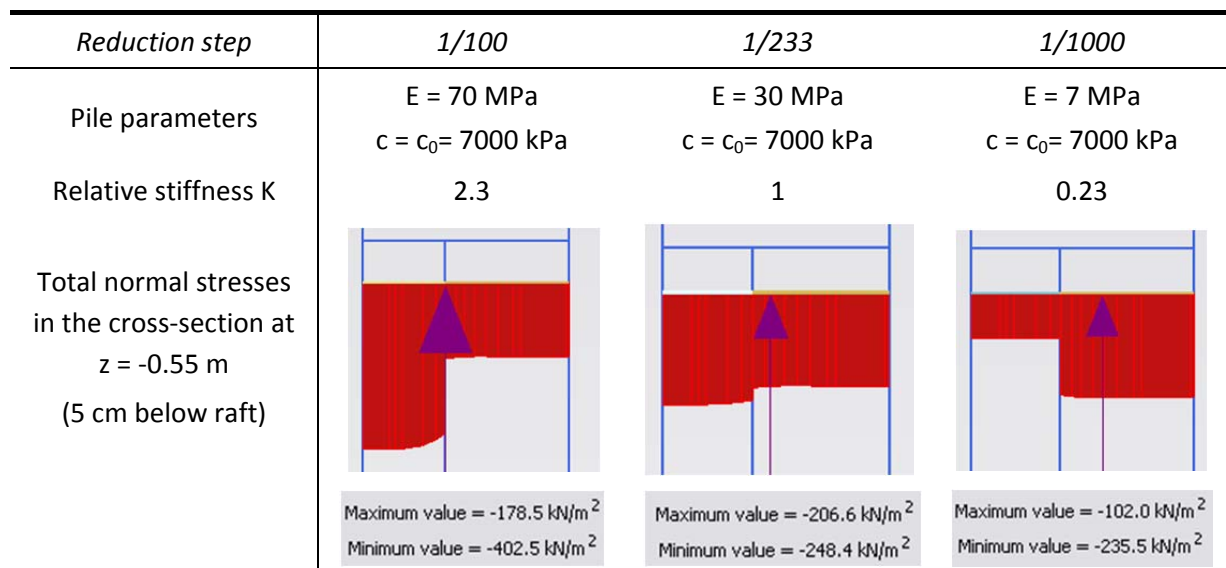


Figure 37: Distribution of total normal stresses for Method B, Soil 1 – Reduction of stiffness

**5.4.1.5 DEPENDENCE OF STRESS DISTRIBUTION ON DIFFERENT PARAMETERS**

If the pile and the surrounding soil had the same stiffness, one would expect a uniform distribution of stresses over the cross-section in case of the single analysis, as the influence of the pile’s history does not exist. However, when comparing the results for a relative stiffness of 1 of the two settings in Figure 36 and Figure 37, it becomes evident that the stress distribution is not only dominated by the relative stiffness. Actually, the strength of the pile respectively the difference in strength between pile and soil seems to be an influencing factor.

In order to investigate this observation, single parameters of the pile are equalized with those of the soil. These are cohesion, friction angle and Poisson’s ratio. The resulting stress distributions for a

relative stiffness of 1, corresponding to a stiffness of 30 MPa for both soil and pile in case of Soil 1, are shown in Figure 38 (a) to (e): In (a) the pile has its initial parameters apart of the reduced stiffness, which are repeated on the right hand side. The stress level is higher in the pile head than in the soil. By assigning to the pile the cohesion of the soil, which is illustrated in (b), the pile's strength is reduced at such a rate that the stresses relocate towards the soil. In a further step, additionally to the cohesion, also the soil's friction angle is applied to the pile. As a consequence, the pile attracts higher stresses, which can be seen from (c). At this stage, the stiffness as well as the strength is the same for pile and soil. Nevertheless, the stress distribution is still not uniform, but is the same as in (a). Instead of the friction angle, in (d) the Poisson's ratio is changed in addition to the cohesion, which again leads to higher stresses in the soil. In (e), finally, the friction angle as well as the Poisson's ratio is adopted from the soil. The resulting distribution can be regarded as uniform. Summing up, the investigation shows that the non-uniform stress distribution despite a relative stiffness of 1 is due to the difference in strength between pile and soil and in their Poisson's ratios.

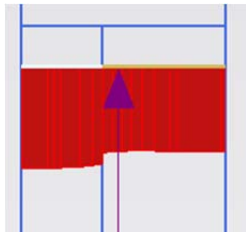
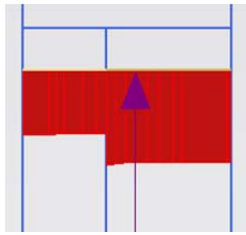
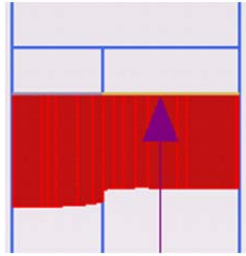
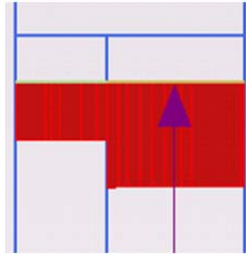
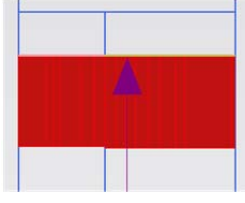
$E = 30 \text{ MPa}$	(a)	(b)	
Pile parameters	$c = c_0 = 7000 \text{ kPa}$	$c = c_{\text{Soil1}} = 7 \text{ kPa}$	Initial pile parameters
Total normal stresses in the cross-section at $z = -0.55 \text{ m}$ (5 cm below raft)	 Maximum value = $-206.6 \text{ kN/m}^2$ Minimum value = $-248.4 \text{ kN/m}^2$	 Maximum value = $-153.8 \text{ kN/m}^2$ Minimum value = $-230.8 \text{ kN/m}^2$	$E_0 = 7\,000 \text{ MPa}$ $c_0 = 7\,000 \text{ kPa}$ $\varphi_0 = 0^\circ$ $\nu_0 = 0.4$
$E = 30 \text{ MPa}$	(c)	(d)	(e)
Pile parameters	$c = c_{\text{Soil1}} = 7 \text{ kPa}$ $\varphi = \varphi_{\text{Soil1}} = 30^\circ$	$c = c_{\text{Soil1}} = 7 \text{ kPa}$ $\nu = \nu_{\text{Soil1}} = 0.3$	$c = c_{\text{Soil1}} = 7 \text{ kPa}$ $\varphi = \varphi_{\text{Soil1}} = 30^\circ$ $\nu = \nu_{\text{Soil1}} = 0.3$
Total normal stresses in the cross-section at $z = -0.55 \text{ m}$ (5 cm below raft)	 Maximum value = $-206.6 \text{ kN/m}^2$ Minimum value = $-248.4 \text{ kN/m}^2$	 Maximum value = $-126.9 \text{ kN/m}^2$ Minimum value = $-231.4 \text{ kN/m}^2$	 Maximum value = $-209.5 \text{ kN/m}^2$ Minimum value = $-214.2 \text{ kN/m}^2$

Figure 38: Stress distributions for soil and pile having the same stiffness of 30 MPa ( $K=1$ )

### 5.4.1.6 SOIL 2 – GRADUAL ANALYSIS

In the following, the results of the gradual analysis of Soil 2 are presented and directly compared with those of Soil 1.

#### Settlements

Soil 2 represents the weaker and softer soil, which causes settlements in the order of ten times higher in comparison to Soil 1. Besides, also in this case reducing both stiffness and strength or just strength gives the same results for settlements, and the settlements for a modified stiffness do not change, as it is explained on page 37.

Table 16: Settlements of the pile head, Soil 2, Gradual analysis

Multiplier	K	c	E	u <sub>y</sub>	K	c	u <sub>y</sub>	K	E	u <sub>y</sub>
	[-]	[kPa]	[kPa]	[cm]	[-]	[kPa]	[cm]	[-]	[kPa]	[cm]
1	2333	7000	7*10 <sup>6</sup>	10.9	2333	7000	10.9	2333	7*10 <sup>6</sup>	10.9
1/10	233	700	7*10 <sup>5</sup>	10.9	2333	700	10.9	233	7*10 <sup>5</sup>	10.9
1/100	23	70	7*10 <sup>4</sup>	20.6	2333	70	20.7	23	7*10 <sup>4</sup>	10.9
1/1000	2.3	7	7*10 <sup>3</sup>	22.1	2333	7	22.1	2.3	7*10 <sup>3</sup>	10.9

#### Reduction of stiffness and strength

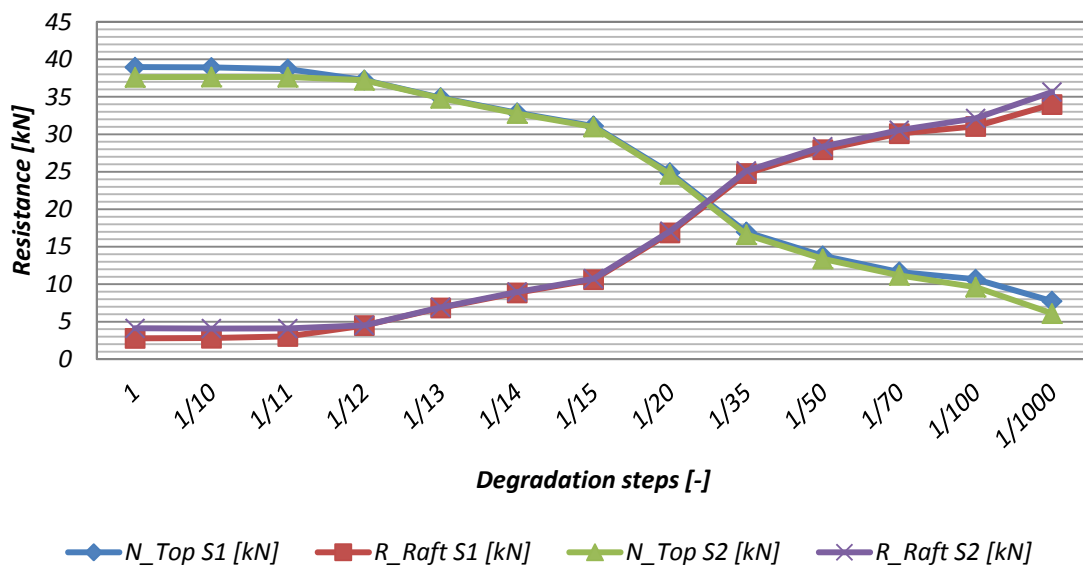


Figure 39: Load transfer, Soil 1 & 2 – Gradual reduction of stiffness and strength

In Figure 39, the graphs of the two soils show a very similar development of load transfer of pile and raft, which implies that the system behaviour is independent of the type of soil. By going into detail, one can note a slightly higher normal force in the pile head at the beginning and the end of the observation in case of Soil 1, with a corresponding lower resistance of the raft. The reason for this may be seen from Figure 40, which shows the development of skin and base resistance during

degradation: In accordance with the higher pile head resistance, more skin friction is mobilized in case of Soil 1, as the interface strength is directly coupled with the ‘better’ material properties of Soil 1.

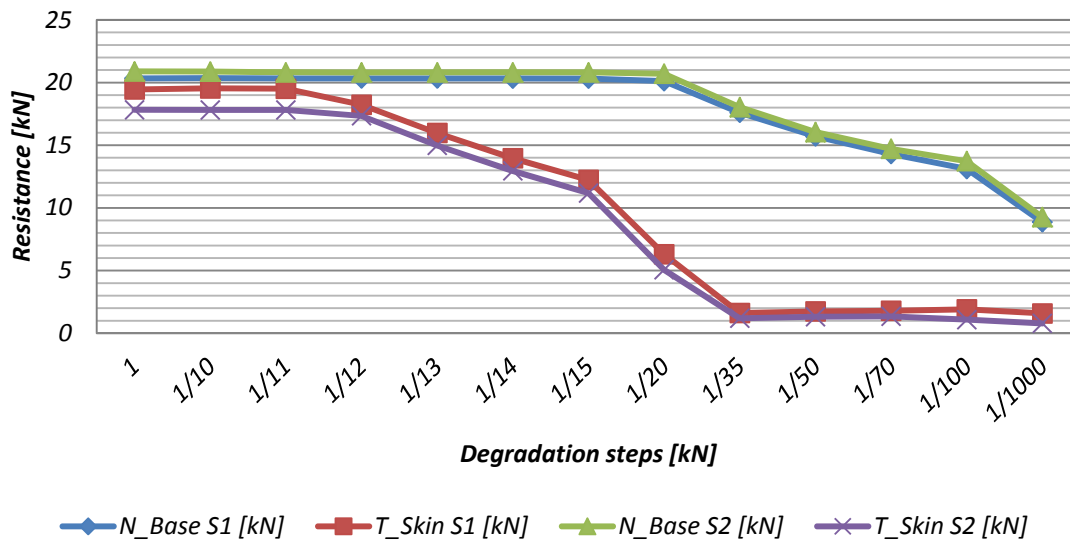


Figure 40: Development of base and skin resistance, Soil 1 & 2 – Gradual reduction of stiffness and strength

In the first stages, the skin friction is at maximum for both soils. According to that, plastic points are located in the interface, which can be seen from Figure 41 and Figure 42. Plastic points can also be found in the pile foot area, in particular in case of Soil 2 since its strength is much lower.

At a further degradation of the pile (to 1/12), the pressure bulb and the number of corresponding plastic points in the soil is diminishing, while the pile-head starts to plastify. This goes along with a decrease in skin resistance (and consequently in total resistance), which finally reaches its minimum at the degradation step of 1/35. At this stage, plastic points actually occur in the whole pile, independently of the type of soil.

In case of Soil 1, the extension of plastic points is limited to the pile and the interface, which means that the soil's behaviour is linear elastic. During the calculation with Soil 2, however, the plastic points are spread in the soil all along the pile shaft, and also in the contact area between raft and soil. Consequently, the soil shows plastic, non-linear behaviour, which in combination with the low stiffness in the elastic region results in settlements ten times higher than with Soil 1.

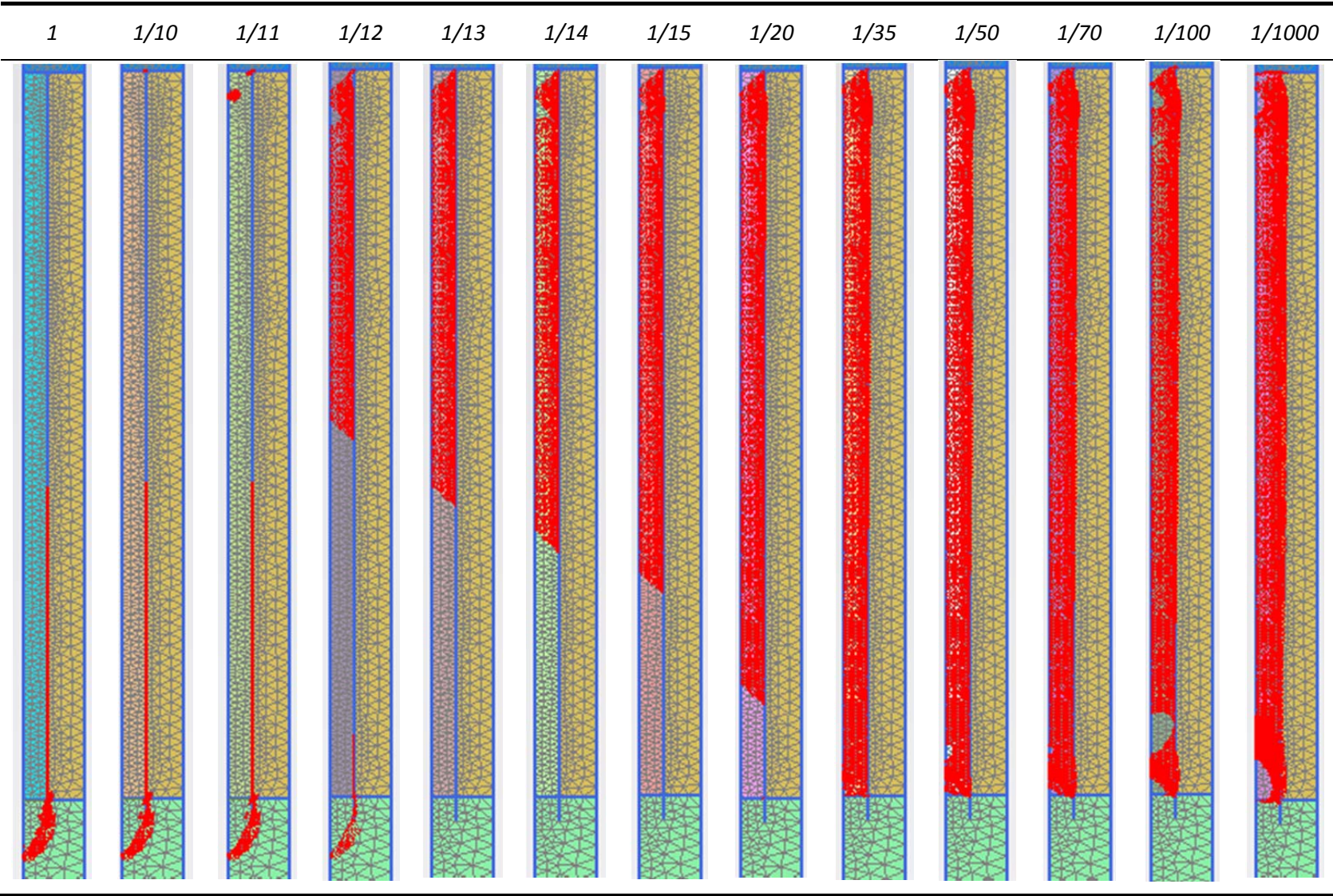


Figure 41: Development of plastic points, Soil 1, Gradual analysis

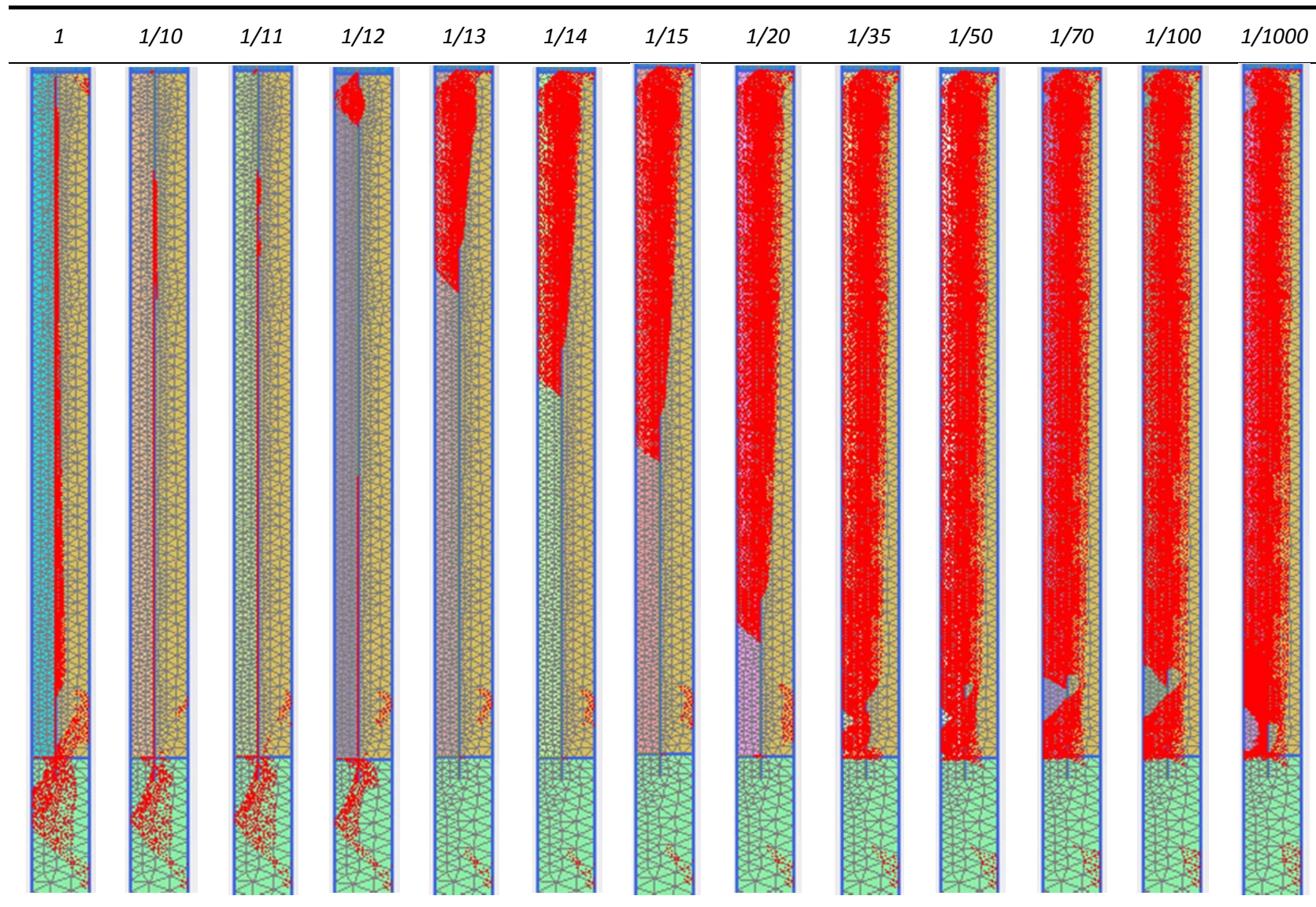


Figure 42: Development of plastic points, Soil 2, Gradual analysis

Finally, the Resistance-settlement curve is plotted in Figure 43.

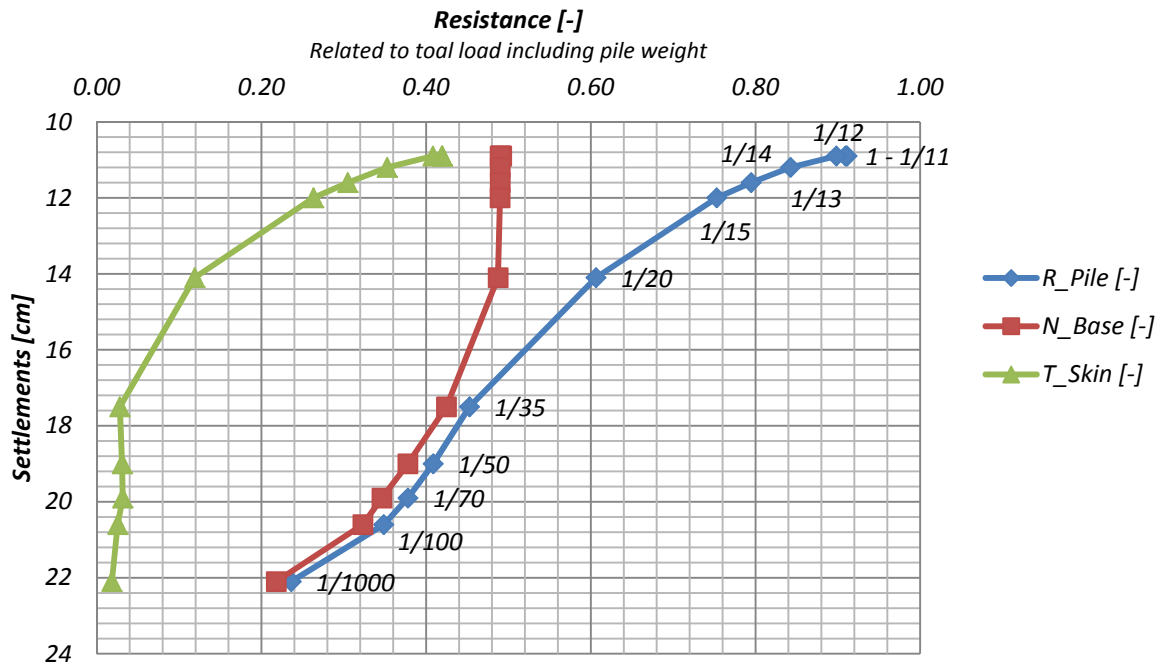


Figure 43: Resistance-settlement curve, Soil 2 – Gradual reduction of stiffness and strength

Detail on formation of plastic points, using the example of Soil 1

When the loading of a pile causes a pressure bulb, plastic points in general develop directly under the pile foot, starting from the corner. More precisely, the main direction of plastic points passing through the corner and the horizontal draw an angle of  $(45 + \varphi/2)$ , which is  $60^\circ$  for Soil 1. However, the main direction of plastic points in the pile foot area in case of Soil 1, illustrated in Figure 41 and repeated in Figure 44 (a) in detail, seems to be shifted downwards, passing through the end point of the geometry line, and from that point progressing towards the pile's corner. It shall be investigated if this formation of plastic points is due to the placing of the geometry line, or instead represents the 'natural' mechanism.

For this purpose, different scenarios are studied: In (b), no interface extension is considered at all, in (c) the extension is 20 cm, and in (d) beside the extension of 10 cm also a horizontal geometry line is provided. Through the supplemental vertical geometry line, more plastic points appear along this line due to the corresponding mesh refinement. Nevertheless, the rough shape of the formation is the same for all cases and is therefore independent of the placement or extension of the geometry line. However, there is a lack of clarity concerning the reason why the formation of plastic points differs from the expected one.

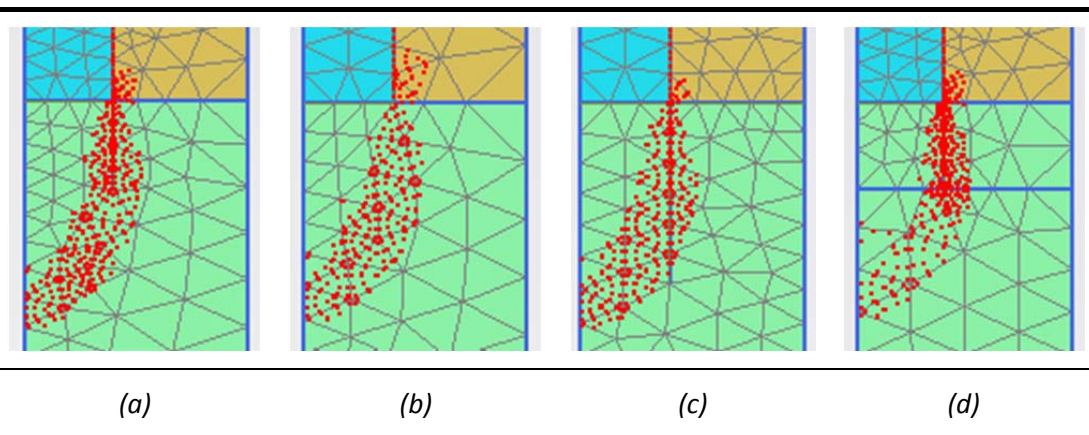


Figure 44: Formation of plastic points in dependence of placing of geometry lines, for interface extension of (a) 10 cm, (b) 0 cm, (c) 20 cm and (d) 10 cm with additional horizontal geometry line

### 5.4.1.7 SOIL 2 – SINGLE ANALYSES

#### Settlements

In Table 17, the settlements of the Single analyses with Soil 2 are provided.

Table 17: Settlements, Soil 2 – Single analyses

Multiplier	K	c	E	u <sub>y</sub>	K	c	u <sub>y</sub>	K	E	u <sub>y</sub>
	[-]	[kPa]	[kPa]	[cm]	[-]	[kPa]	[cm]	[-]	[kPa]	[cm]
1	2333	7000	7*10 <sup>6</sup>	10.9	2333	7000	10.9	2333	7*10 <sup>6</sup>	10.9
1/10	233	700	7*10 <sup>5</sup>	11.0	2333	700	10.9	233	7*10 <sup>5</sup>	11.0
1/100	23	70	7*10 <sup>4</sup>	20.5	2333	70	20.5	23	7*10 <sup>4</sup>	12.6
1/1000	2.3	7	7*10 <sup>3</sup>	22.5	2333	7	22.0	2.3	7*10 <sup>3</sup>	19.6

#### Reduction of stiffness and strength

In Figure 45, the load-bearing behaviour of the pile respectively of the raft is shown for Method A and B. The two graphs do not differ from each other, which implies that the pile’s past does not have a major influence on the behaviour. Only in stress distribution, illustrated for Method A and B in Figure 46 and Figure 47, a slight difference can be observed in the respective degradation stages.

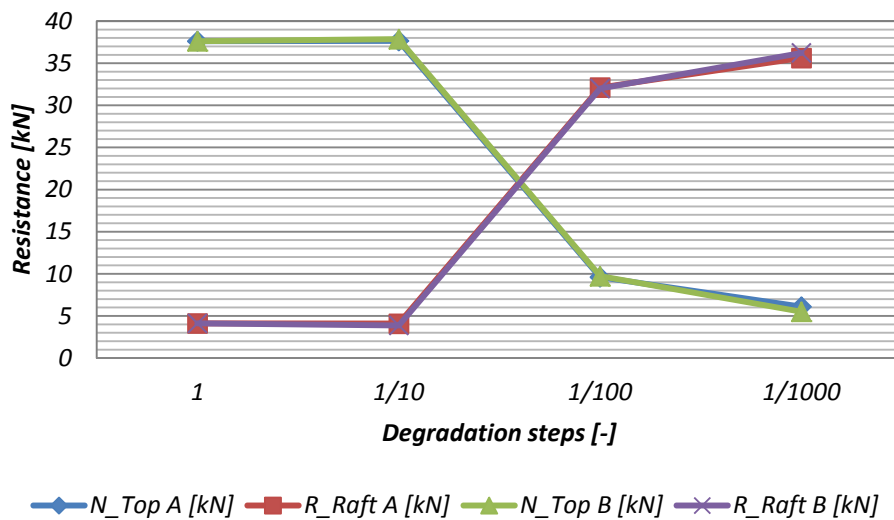


Figure 45: Load transfer for Method A and B, Soil 2 – Reduction of stiffness and strength

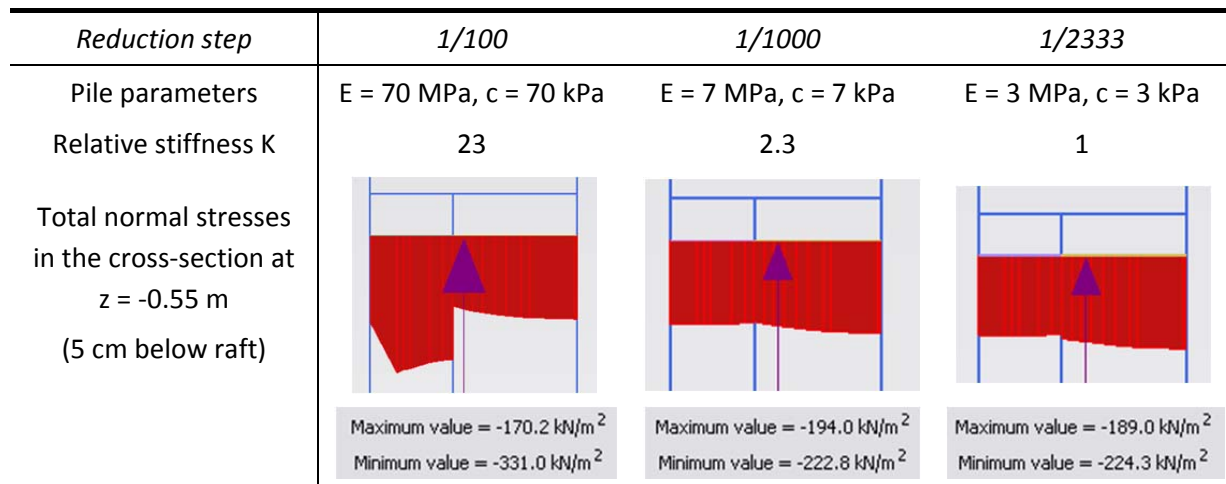


Figure 46: Stress distributions for Method A, Soil 2 – Reduction of stiffness and strength

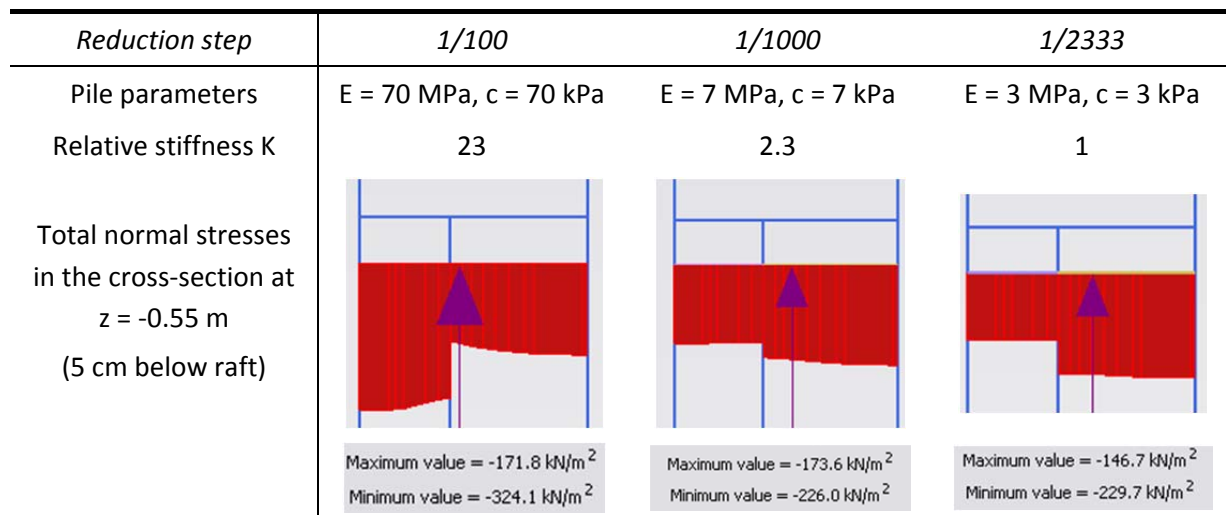


Figure 47: Stress distributions for Method B, Soil 2 – Reduction of stiffness and strength

### 5.4.1.8 HISTORY EFFECT – DIFFERENCES IN SOIL 1 AND SOIL 2

When comparing Figure 45 with the results of Soil 1, the question arises why the effect of the pile’s history is so different for the two soils. For answering to this question, the results for reducing the two parameters simultaneously and separately are summarized.

Figure 48 repeats the results of Method A and Method B for Soil 1. The history effect is obvious, since the normal force in the pile head for Method A is higher for all three degradation steps. In the following figures, the results of reducing either the cohesion [Figure 49 (a)] or the elastic modulus (Figure 49 (b)) with reduction-method B are presented. When reducing the cohesion to 1/10, no change in forces can be observed. When reducing the elastic modulus to 1/10 (corresponding to K = 23), however, the normal force in the pile head is decreasing significantly. Also from the reduction step of 1/1000, the normal force in the pile head results lower than it does for the reduction of c. Finally, the influence of the stiffness reduction can then clearly be seen when reducing both parameters E and c simultaneously (with Method B), whereas the largest differences between Method A and B actually can be found at the degradation steps of 1/10 and 1/1000.

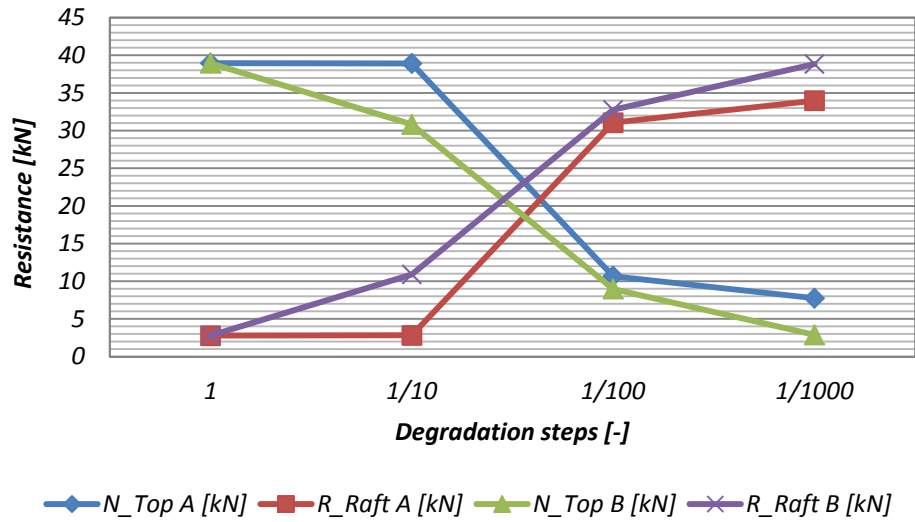


Figure 48: Load transfer for Method A and B, Soil 1 – Reduction of stiffness and strength (repetition)

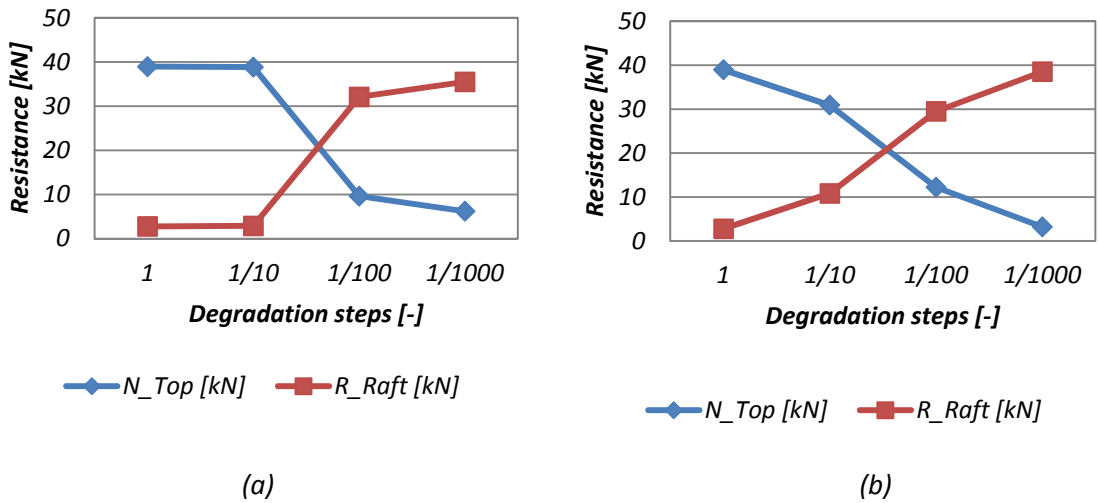


Figure 49: Load transfer for Method B, Soil 1 – Reduction of strength (a) and of stiffness (b)

In Figure 50 the results of Method A and Method B for Soil 2 are repeated, and Figure 51 shows the results for reducing the cohesion (a) and the stiffness (b) respectively with Method B. The graph for a reduced cohesion is practically the same compared to the one of Soil 1. When reducing the stiffness, on the other hand, at the step of 1/10 the normal force in the pile head has still the initial value. This is due to the fact that the Relative stiffness between pile and soil in this case is still high enough ( $K = 233$ ) to enable the pile bearing most of the load. Indeed, at this stage the relative stiffness has the same value as it does at the initial stage in case of Soil 1, since the stiffness of Soil 2 is 1/10 of the one of Soil 1. When reducing the stiffness further to 1/100, the value of the normal force in the pile head actually is the same as in case of Soil 1 at the degradation step of 1/10 (about 30 kPa). This, however, does not become significant when reducing both parameters, since the strength reduction leads to a much lower normal force in the pile head. From this we can draw the final conclusion that the difference in the effect of history is due to the different relative stiffness parameters for Soil 1 and Soil 2 at a particular degradation stage.

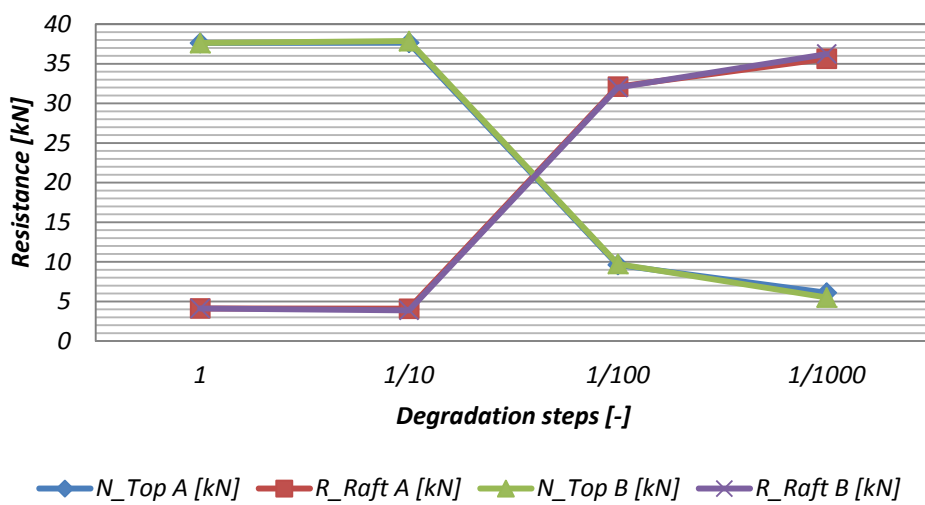


Figure 50: Load transfer for Method A and B, Soil 2 – Reduction of stiffness and strength (repetition)

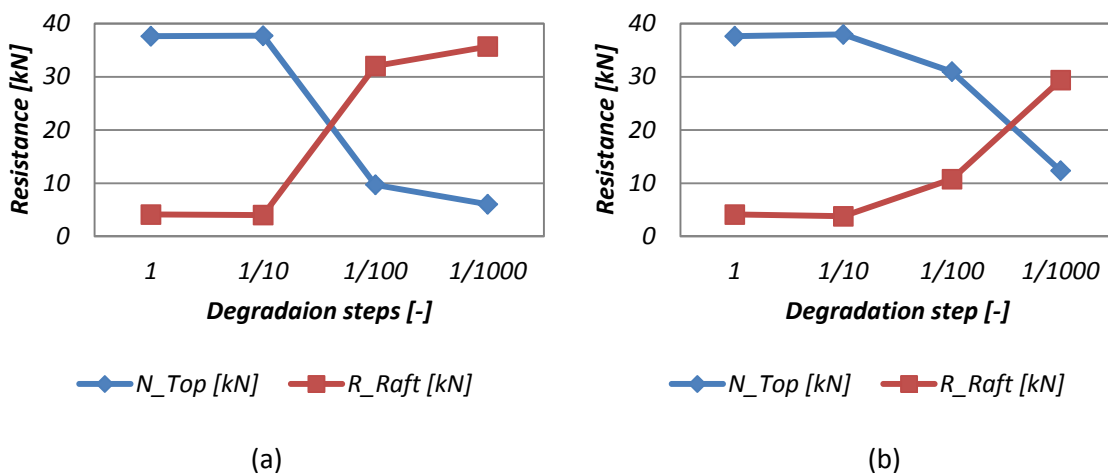


Figure 51: Load transfer for Method B, Soil 2 – Reduction of strength (a) and of stiffness (b)

Furthermore, the observation is made that, when both parameters are reduced with Method B, the normal force in the pile head is guided by either the stiffness or the strength, depending on which

parameter gives the lower value for this normal force, what can be seen from the separate reductions.

When reducing the parameters simultaneously with Method A, however, the influence of the cohesion is predominant. This is confirmed by the fact that, when diminishing the cohesion gradually (not illustrated), the development of the normal force in the pile head is practically the same as when reducing both parameters. Consequently, the relative stiffness  $K$  has, apart from the initial stage, only a marginal influence on the general load-bearing behaviour, which explains also the large difference for Method A and B in case of Soil 1.

#### **5.4.1.9 DIFFERENCES IN STRESS DISTRIBUTION AND REDISTRIBUTION FOR SOIL 1 AND SOIL 2**

In general, the system behaviour is very similar for both soils when the pile is degraded gradually. Differences, however, can be detected on a small scale. In Figure 52, the total normal stresses for both soils are summarized and compared. Due to the observations made, the difference in the behaviour of the two soils can be explained by the lower 'effect of history' in case of Soil 2, and the influence of the strength ratio between pile and soil.

In contrast to Soil 1, the stresses in Soil 2 are already higher at a relative stiffness of 2.3, which seems to be inconsistent. When looking at the stress distributions for a relative stiffness of 2.3 or 1, the stresses in Soil 2 are higher since the cohesion of the pile is just one tenth compared to the pile's cohesion in case of Soil 1. Moreover, the cohesion in (e) and (f) is reduced at such a rate that the strength of Soil 2 (with  $c=7$  kPa,  $\phi = 30^\circ$ ) results higher as the one of the pile, leading to higher stresses in the soil than in the pile. In case of (e), the soil's strength obviously has a bigger influence on stress distribution than the pile's stiffness does.

By comparing the stresses for a reduction step of 1/1000, the fact that the pile in (c) bears more than the one in (e) also seems contradictory, as in the first case the relative stiffness is smaller. Again, beside the relative stiffness also the strength of the soils has to be taken into account: As Soil 1 represents the 'stronger' material, a higher pile resistance is mobilized, and consequently the stresses in the pile head are higher. Definitely, the effect of the pile's history amplifies the stress level in the pile.

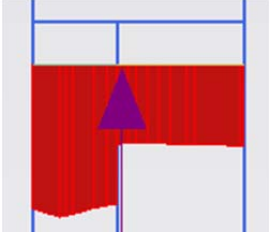
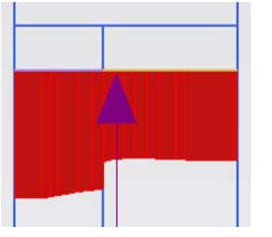
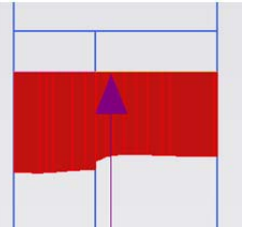
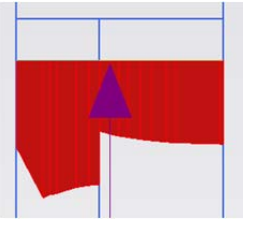
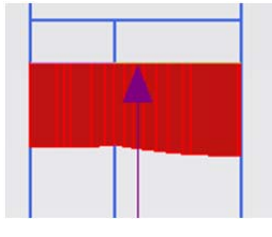
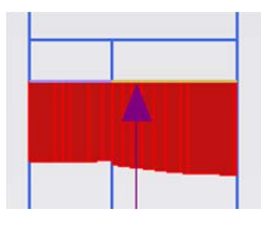
Soil 1	(a)	(b)	(c)
Reduction step	1/100	1/233	1/1000
Pile parameters	$E = 70 \text{ MPa}, c = 70 \text{ kPa}$	$E = 30 \text{ MPa}, c = 30 \text{ kPa}$	$E = 7 \text{ MPa}, c = 7 \text{ kPa}$
Relative stiffness K	2.3	1	0.23
Total normal stresses in the cross-section at $z = -0.55 \text{ m}$ (5 cm below raft)	 <p>Maximum value = <math>-185.3 \text{ kN/m}^2</math> Minimum value = <math>-360.9 \text{ kN/m}^2</math></p>	 <p>Maximum value = <math>-197.7 \text{ kN/m}^2</math> Minimum value = <math>-288.7 \text{ kN/m}^2</math></p>	 <p>Maximum value = <math>-203.6 \text{ kN/m}^2</math> Minimum value = <math>-249.9 \text{ kN/m}^2</math></p>
Soil 2	(d)	(e)	(f)
Reduction step	1/100	1/1000	1/2333
Pile parameters	$E = 70 \text{ MPa}, c = 70 \text{ kPa}$	$E = 7 \text{ MPa}, c = 7 \text{ kPa}$	$E = 3 \text{ MPa}, c = 3 \text{ kPa}$
Relative stiffness K	23	2.3	1
Total normal stresses in the cross-section at $z = -0.55 \text{ m}$ (5 cm below raft)	 <p>Maximum value = <math>-170.2 \text{ kN/m}^2</math> Minimum value = <math>-331.0 \text{ kN/m}^2</math></p>	 <p>Maximum value = <math>-194.0 \text{ kN/m}^2</math> Minimum value = <math>-222.8 \text{ kN/m}^2</math></p>	 <p>Maximum value = <math>-189.0 \text{ kN/m}^2</math> Minimum value = <math>-224.3 \text{ kN/m}^2</math></p>

Figure 52: Stress distributions for Method A, Soil 1 and 2 – Reduction of stiffness and strength (repetition)

#### 5.4.1.10 SUMMARY OF RESULTS AND DISCUSSION

During the pile-degradation analysis, the behaviour of the load-bearing system, composed of raft and pile, was studied in detail. Two different types of analysis were carried out, namely the gradual analysis (Method A) and the single analyses (Method B).

It was shown that, when the pile is loaded, a distinct pressure bulb is formed under the pile foot. By reducing the pile parameters gradually with Method A, the stresses are redistributed from the pile head towards the soil under the raft. The effect of redistribution of stresses, often referred to as 'history effect' in this work, causes that the stresses in the pile are higher than with Method B, and therefore also the pressure bulb is more pronounced during gradual degradation.

The differences in results for Method A and B were considerable for Soil 1, whereas in case of Soil 2 the history effect is very small. The reason for this was found in the different values of the relative stiffness parameter  $K$ , which are  $K = 233$  for Soil 1 and  $K = 2333$  for Soil 2 in non-degraded state of the pile. Due to the good mechanical properties of Soil 1, during Method B the stresses transferred to the pile head are already significantly reduced at the degradation step of  $1/10$ , which basically could be traced back to the relative stiffness of  $K = 23$  at this stage.

Despite these differences concerning the history effect, one could observe that for the two soils the system virtually shows the same behaviour during gradual degradation. This is due to the fact that with Method A the modification of the relative stiffness does not have a big influence on the outcome. Of major importance is the strength of the pile, which is the criterion for stress-redistribution.

However, the way how the stresses are distributed over the cross-section turned out to depend on several factors. First of all, the initial relative stiffness has a fundamental influence on stress distribution. Moreover, it was found out that also the relative strength between pile and soil plays a decisive role. This aspect was proven during the examination of stress distributions resulting from Method B for a relative stiffness of 1. Thus, the history effect and also the influence of different stiffness parameters could be eliminated. In the course of this investigation it became clear too that for finally obtaining a uniform distribution of stresses, the strength of the pile and the one of the soil have to range in the same order of magnitude and that also the Poisson's ratio has to be adapted.

## 5.4.2 INTERFACE DEGRADATION

### 5.4.2.1 PARAMETER REDUCTION

The gradual reduction of interface parameters is a possibility to simulate the diminishing contact properties between the wooden pile and the soil due to the decay of the pile. This represents a quite realistic scenario, as the outer part of the pile's cross section, the so-called sapwood, is more delicate and has a strong influence on the contact-behaviour between pile and soil.

The soil models used are Soil 1 and 2 (both MC) of the previous study, and also the stratigraphy of the Frari site (SSC and HSS). For the interface properties own parameter sets are defined, which defer from the presented soil materials just by reduced strength properties. The reduction is done according to Equation 5.5 and 5.6, whereas for every degradation step the parameters are multiplied by the same percentage, using the *multiplier* of Table 18 as follows:

$$c_{Interface} = x * c_{Soil} \quad (5.5)$$

$$\tan \varphi_{Interface} = x * \tan \varphi_{Soil} \quad (5.6)$$

This means that the interface is not coupled with the surrounding soil and the interface parameter  $R_{inter}$  is 1 during the whole calculation. The strength parameters are summarized in Table 18 and Table 19.

It is worth noticing that the reduction of the initial parameters is done simply mathematically in order to get an idea of the general load-bearing behaviour. Further, the degradation of the interface is carried out to its complete degradation. Actually, it is not known how the condition of the interface develops with time and in which order of magnitude the properties range in the relative degradation stages. Of course, these properties also vary between different piles. Therefore, the worst case is assumed.

Table 18: Reduced interface parameters of Soil 1 and Soil 2

Parameter	Unit	Value		Multiplier
		Soil 1	Soil 2	
$\varphi$	[°]	30	22	1
c	[kN/m <sup>2</sup> ]	7.0	0	1
$\varphi$	[°]	22	15.8	0.7
c	[kN/m <sup>2</sup> ]	4.9	0	0.7
$\varphi$	[°]	16.1	11.4	0.5
c	[kN/m <sup>2</sup> ]	3.5	0	0.5
$\varphi$	[°]	9.8	6.9	0.3
c	[kN/m <sup>2</sup> ]	2.1	0	0.3
$\varphi$	[°]	3.3	2.3	0.1
c	[kN/m <sup>2</sup> ]	0.7	0	0.1
$\varphi$	[°]	0.33	0.23	0.01

c	[kN/m <sup>2</sup> ]	0.07	0	0.01
φ	[°]	0.033	0.023	0.001
c	[kN/m <sup>2</sup> ]	0.007	0	0.001
φ	[°]	0	0	0
c	[kN/m <sup>2</sup> ]	0	0	0

Table 19: Reduced interface parameters of soil of Frari site

<i>Time [years]</i>	<i>Cumul. time [years]</i>	<i>Friction angle [°]</i>	<i>Multiplier</i>
50	50	32.9	1
50	100	24.4	0.7
50	150	17.9	0.5
50	200	11	0.3
50	250	3.7	0.1
200	450	0.37	0.01
70	520	0.037	0.001
130	650	0	0

By using the stratigraphy of the Frari site, also the effect of creep has to be taken into account. For roughly estimating the settlements, time periods for every degradation phase are chosen arbitrarily. The total period is 650 years. See Table 19.

#### 5.4.2.2 CALCULATION PHASES

The calculations are carried out according to the gradual analysis of the previous chapter, the relative calculation phases are listed in Table 20. The indicated time periods are needed for the calculation with the soil of the Frari site.

Table 20: Calculation phases for gradual interface degradation

<i>Identification</i>	<i>Phase no.</i>	<i>Start from Phase no.</i>	<i>Explanation</i>
Initial phase	0	N/A	K0-procedure
Pile & slab activation	1	0	Activation of pile and slab, the interface has the properties of the adjacent soil (10 days)
Load	2	1	Application of 200 kPa at the top edge of the slab (50 years)
Interface degradation 0.7	3	2	Change of the interface material such that the initial strength parameters are reduced to 70% of their initial values, the interface starts degrading

---

Interface degradation 0.5 - 0	4-9	3-8	Further degradation of the interface material by reducing the initial strength parameters from 70% to 50%, 30% etc.
----------------------------------	-----	-----	---

---

### 5.4.2.3 RESULTS OF SOIL 1

Figure 53 presents the transfer of load-bearing from the pile head towards the raft with decay. In contrast to the results obtained from the pile-degradation analysis (see Figure 24 on page 38), this graph does not show a complete change in load-bearing of pile and raft: The normal force in the pile head decreases with decay, but is still larger than the resulting force transferred by the raft at the end of the observation. This is due to the very high stiffness and strength of the pile material in comparison to the soil properties.

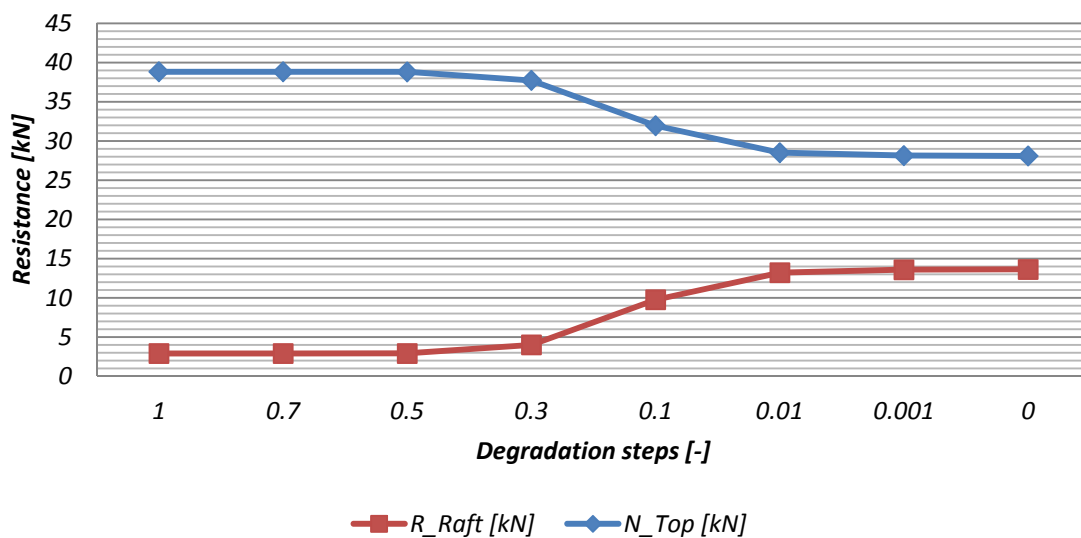


Figure 53: Load transfer, Soil 1 – Interface degradation

Figure 54 illustrates the development of base and skin resistance. The skin resistance is decreasing continuously, as the strength properties of the lateral interface are reduced. Simultaneously, the base resistance is growing, even outweighing the reducing skin resistance until the degradation step of 0.5, whereby the total pile resistance remains the same. Afterwards, the total pile resistance is decreasing, as a growing part of the load is carried by the raft itself.

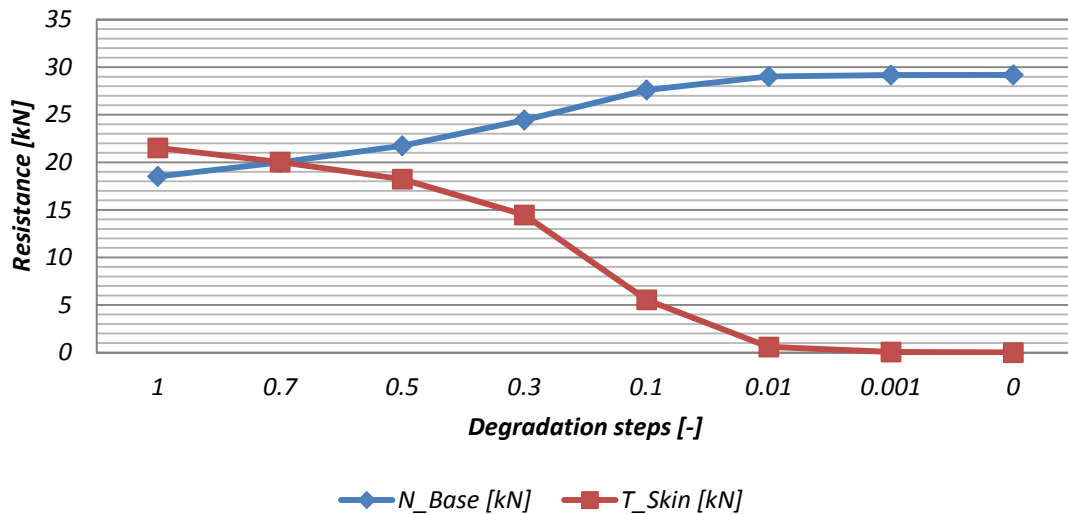


Figure 54: Development of base and skin resistance, Soil 1 – Interface degradation

The total settlement of the pile head is significantly smaller than its settlement during pile degradation (see Figure 28 on page 40): The higher settlement (2.1 cm) towards the end of the pile-degradation analysis is the consequence of strains in the soil and with advancing degradation especially high elasto-plastic strains of the pile. Compared to that, the settlements that occur during the interface-degradation analysis originate from strains in the soil primarily in the pile foot area, whereas the portion of settlements due to the pile’s shortening is very small. With on-going interface degradation, the normal force in the pile foot increases, provoking a further growth of strains in this area. However, the total settlement of the pile head reaches a final value of only 1.2 cm at the complete degradation of the interface. The settlements for the relative degradation steps can be seen from Figure 55.

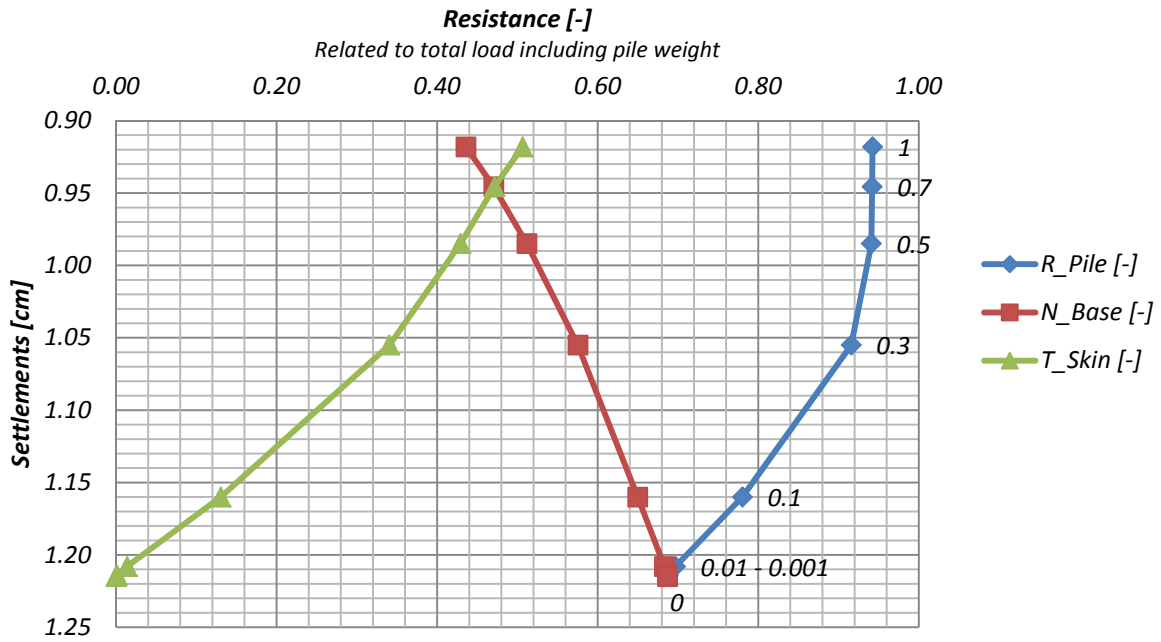


Figure 55: Resistance-settlement curve, Soil 1 - Interface degradation

#### 5.4.2.4 RESULTS OF SOIL 2

##### Standard Model

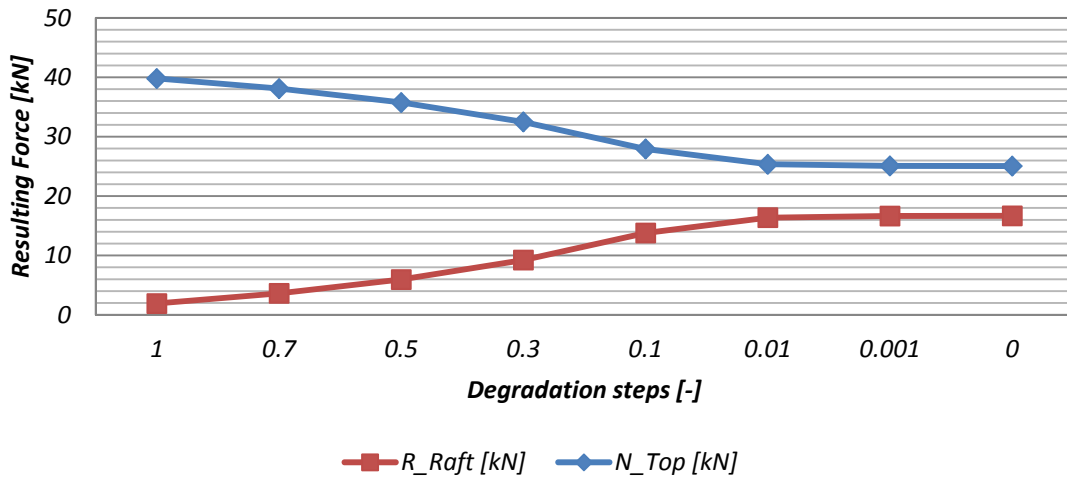


Figure 56: Load transfer, Soil 2 – Interface degradation

In Figure 56, the relative portion of the load carried by the pile respectively by the raft is illustrated. The same tendency as for Soil 1 is observed, whereas in case of Soil 2 the pile-head resistance is diminishing already with the first degradation step. This is due to the fact that also the skin resistance is strongly diminishing from this step, while the base resistance is increasing again (Figure 57). However, the final value of the pile-head resistance is lower than for Soil 1, as the strength of Soil 2 is lower.

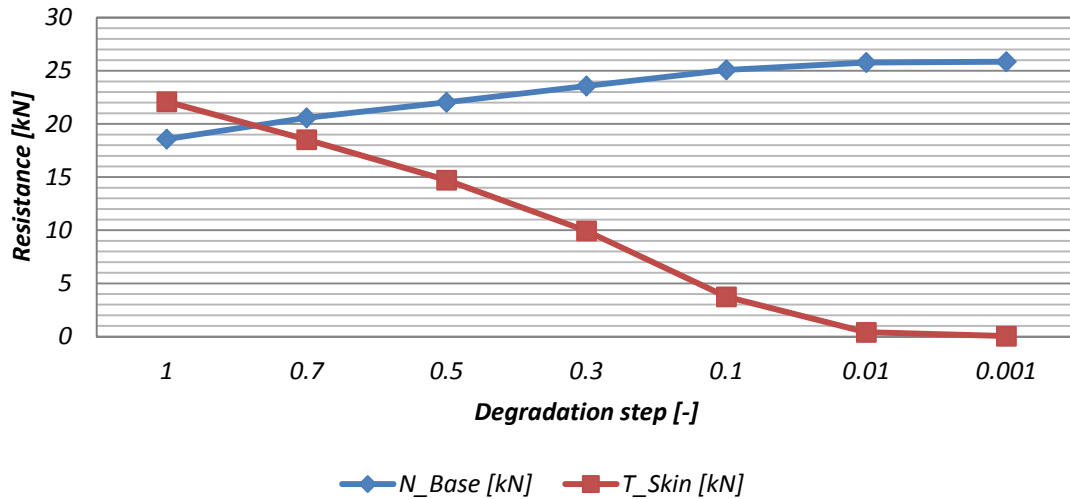


Figure 57: Development of base and skin resistance, Soil 2 – Interface degradation

The fact that Soil 2 is also the softer soil is reflected in settlements 10 times higher than for Soil 1. This is because the pressure bulb under the pile foot provokes much higher strains due to the low stiffness of Soil 2 ( $E = 3 \text{ MPa}$ ). The settlements can be seen from Figure 58.

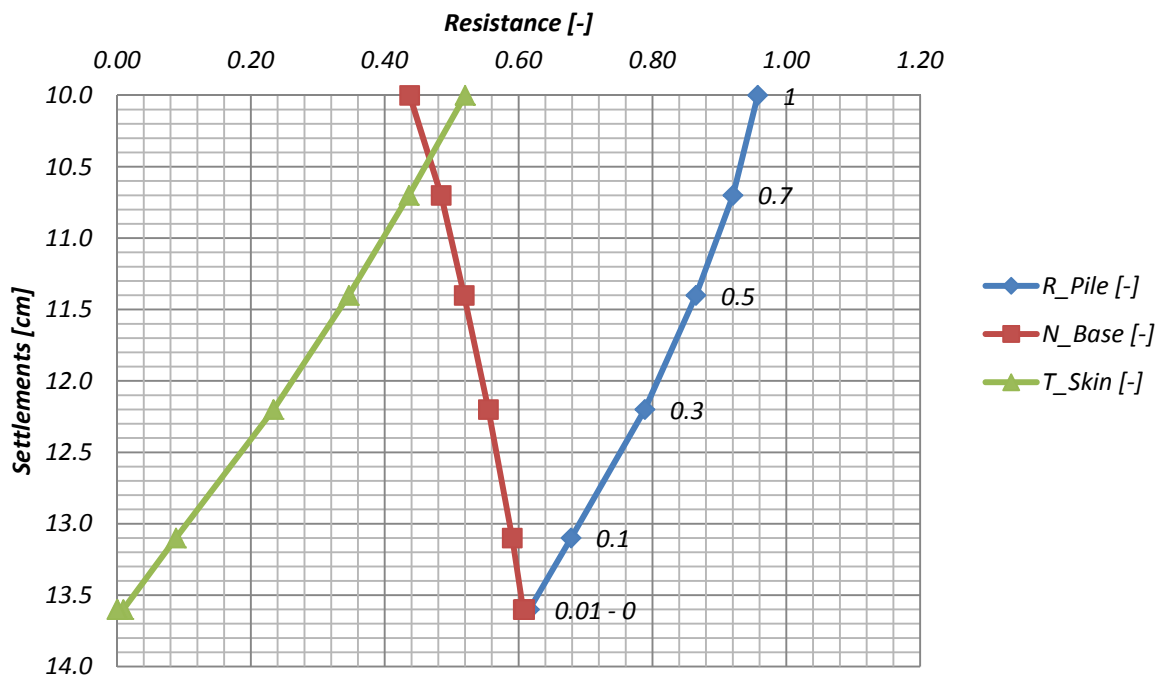


Figure 58: Resistance-settlement curve, Soil 2 – Interface degradation

Influence of stiffness of the raft on bearing behaviour, using the example of Soil 2

The objective of this study is to quantify the influence of the stiffness of the raft on load distribution, or more precisely, on the portion of load transferred by the raft and the pile respectively. This is done by reducing the initial stiffness to a thousandth, to  $E = 3\,000\text{ kPa}$ .

In Figure 59 to Figure 61, the results of the calculation are shown (with indication “R”) and compared to those of the original analysis. Due to the more flexible raft, the normal force in the pile head is reduced only in the first two stages. Hence, the mobilized skin and base resistance at these stages is slightly smaller. Simultaneously, the increased stresses transferred from the raft to the soil cause much higher settlements. Afterwards, the settlements exhibit a difference of less than 5%.

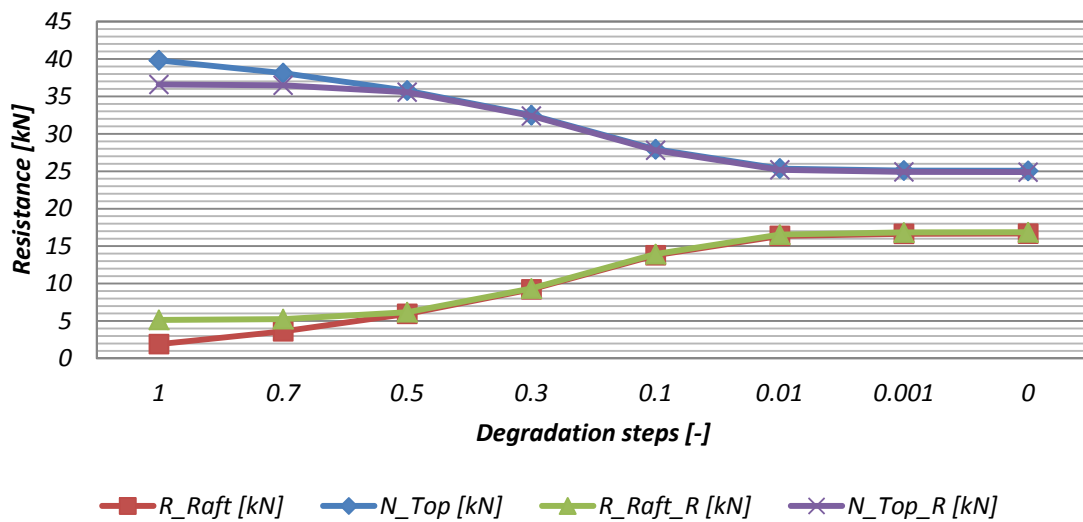


Figure 59: Influence of the raft's stiffness on load transfer, Soil 2 – Interface degradation

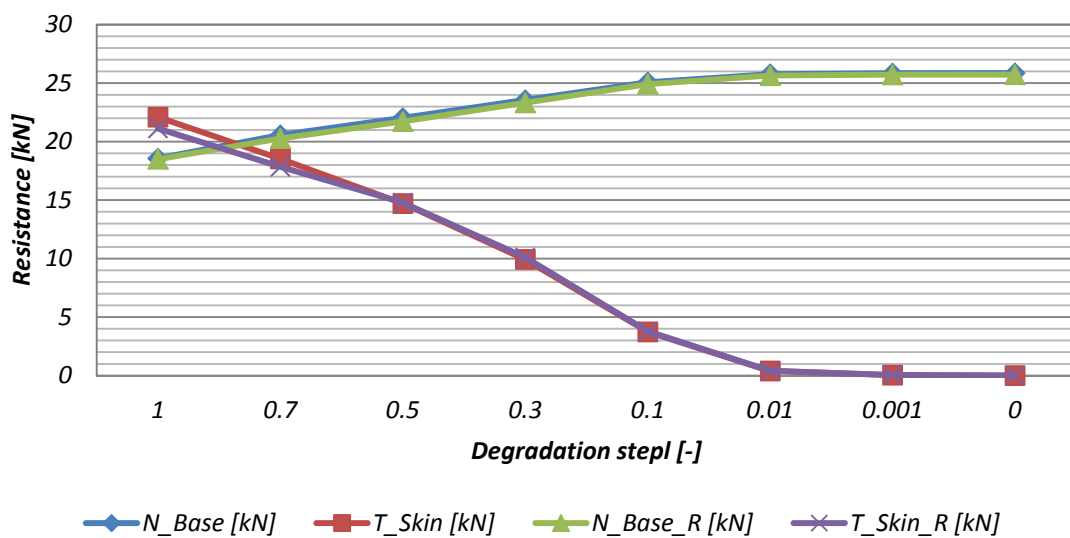


Figure 60: Influence of the raft's stiffness on Pile resistance, Soil 2 – Interface degradation

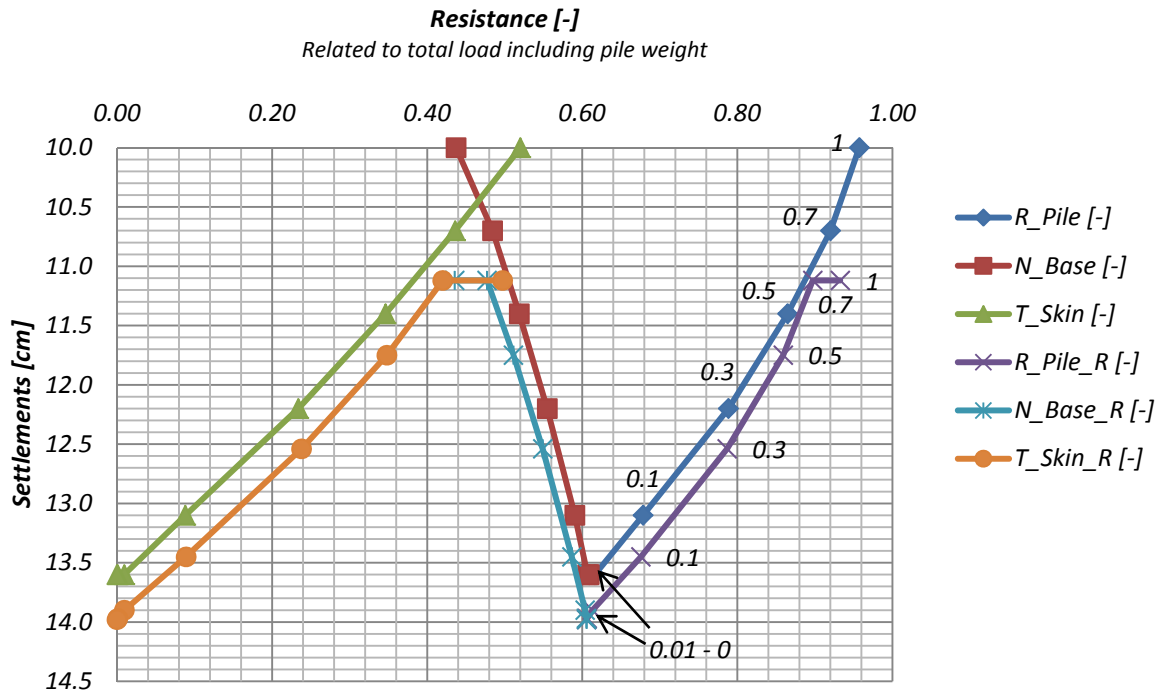


Figure 61: Influence of the raft's stiffness on Resistance-settlement curve, Soil 2 – Interface degradation

The low influence of the reduced stiffness of the raft might be based on the small pile-to-pile distance (0.3 m) in combination with a relatively thick raft (0.5 m).

Influence of the model size, using the example of Soil 2

A further analysis is carried out to see if a larger model would actually change the general load-bearing behaviour. To this end, the standard model is enlarged from a height of 5 m to one of 10 m.

In Figure 62 to Figure 64, the results of the standard model and those of the larger model (with indication “L”) are illustrated. No significant differences in the load-bearing behaviour can be observed. However, the model size has a strong influence on the magnitude of settlements; the settlements of the larger model are about 3 to 3.5 times higher throughout the observation.

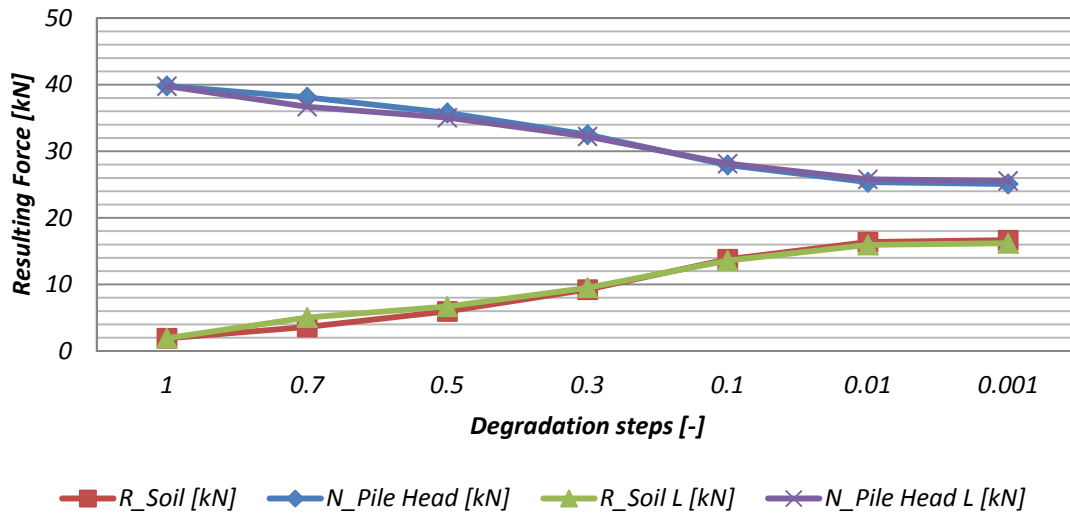


Figure 62: Influence of the model size on load transfer, Soil 2 – Interface degradation

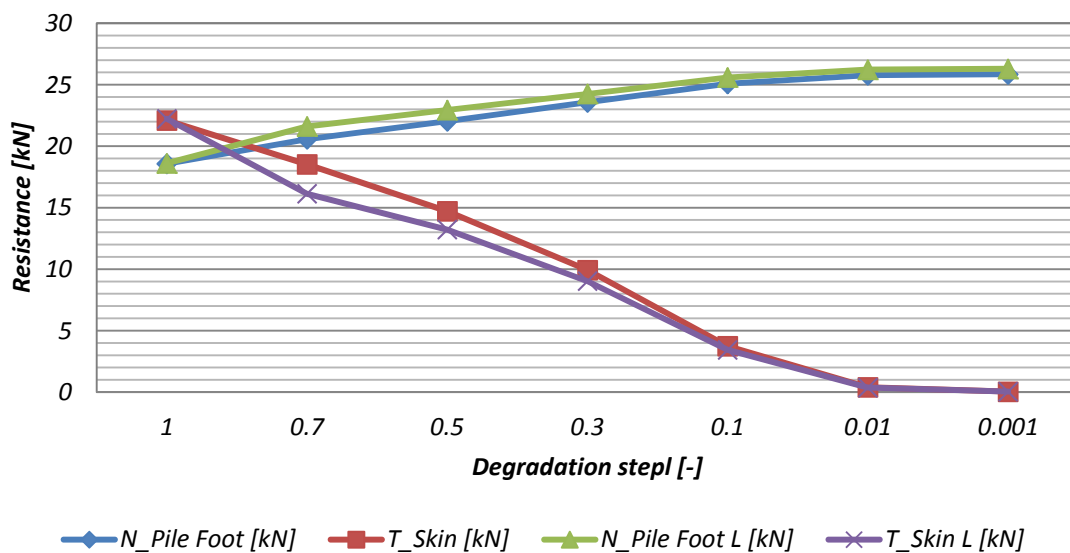


Figure 63: Influence of the model size on load transfer, Soil 2 – Interface degradation

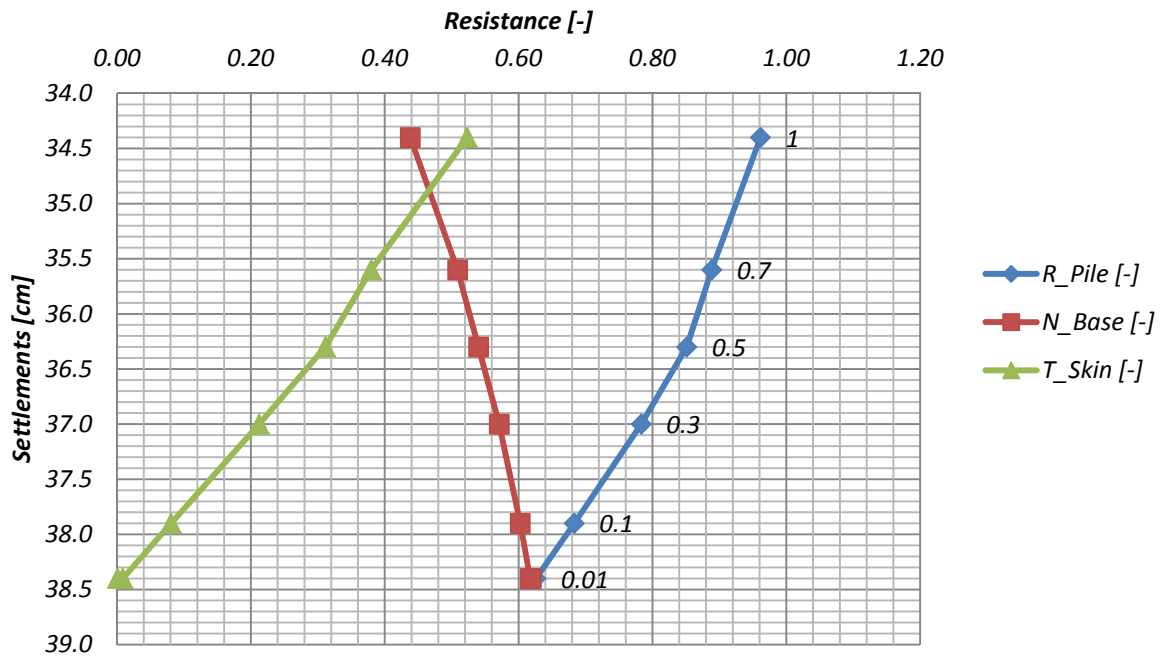


Figure 64: Influence of the model size on load transfer, Soil 2 – Interface degradation

### 5.4.2.5 RESULTS OF THE FRARI SOIL

The same study is performed with the stratigraphy of the Frari site. As the parameters given in Table 6 on page 24 are estimated, the stiffness parameters are slightly modified within a reasonable range. The original parameters (for  $e_{init} = 0.9$ ) and their modifications are listed in Table 21.

Table 21: Variation of initial pore ratio and stiffness parameters

$e_{init}$	$\lambda^*$	$\kappa^*$	$\mu^*$
0.9	0.06316	0.01053	0.00347
1.3	0.075	0.0123	0.0041
0.5	0.053	0.0083	0.0029

The results are summarized in Figure 65 to Figure 67. First of all, no difference in load-bearing behaviour can be observed. The relative portion of load transferred by the raft and by the pile is the same for all 3 parameter sets throughout the degradation procedure.

Furthermore, the degradation of the interface does not have a significant influence on the behaviour. The fact that the normal force in the pile head has a value of about 40 kPa over the whole calculation is particularly interesting, as for Soil 1 and 2 this value is reduced to 28 kPa respectively 25 kPa at the end of the calculation. The difference is that in case of the Frari site, the portion of load which is at first transferred by means of the pile shaft is then almost entirely transferred by the pile foot, whereas at the beginning the mobilized skin resistance is more than 10 kPa lower and the base resistance more than 10 kPa higher compared to the results of Soil 1 and 2.

The high stress level in the pile foot area in combination with the low stiffness of the soil provokes relatively high settlements. When reducing the parameters of the interface from '0.1' to '0.01', only a slight reduction of the normal force in the pile head can be noticed. Nevertheless, this causes a significant increase of settlements of more than 40%, which is illustrated in Figure 67. The diagram shows the increase of settlements when decreasing the stiffness parameters. This can also be seen from the Time-settlement curve in Figure 68, where the settlements for the 3 parameter sets are shown with respect to the time intervals.

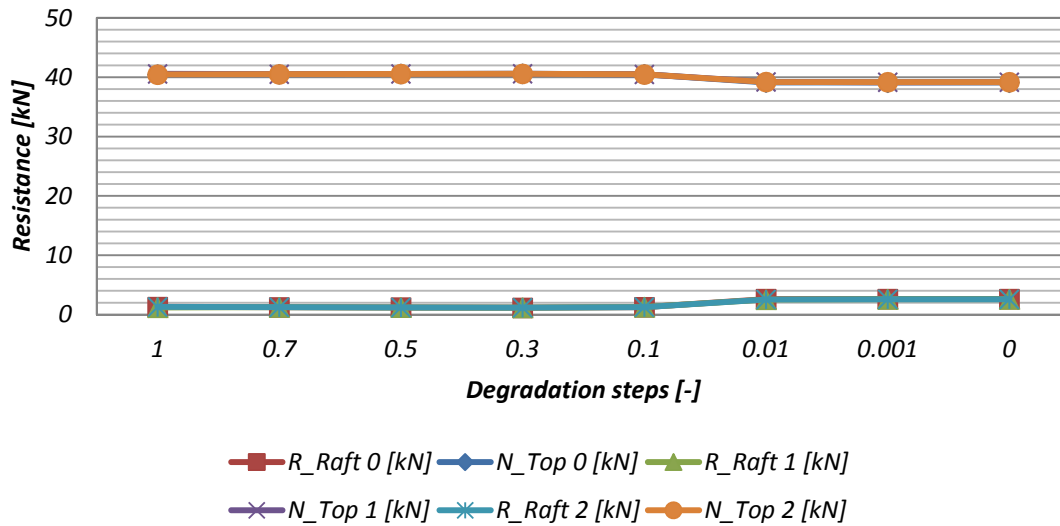


Figure 65: Load transfer, Frari soil - SSC model

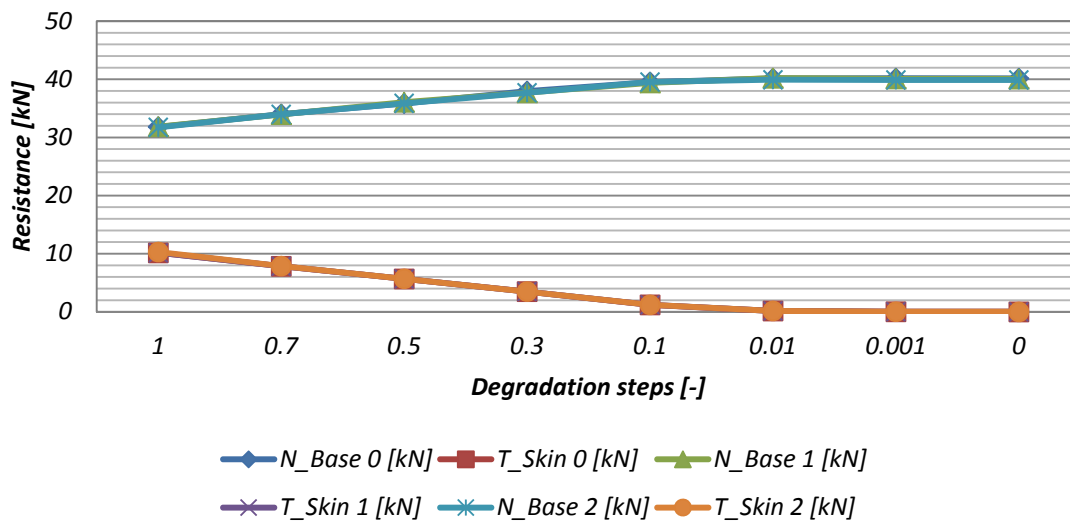


Figure 66: Development of base and skin resistance, Frari soil - SSC model

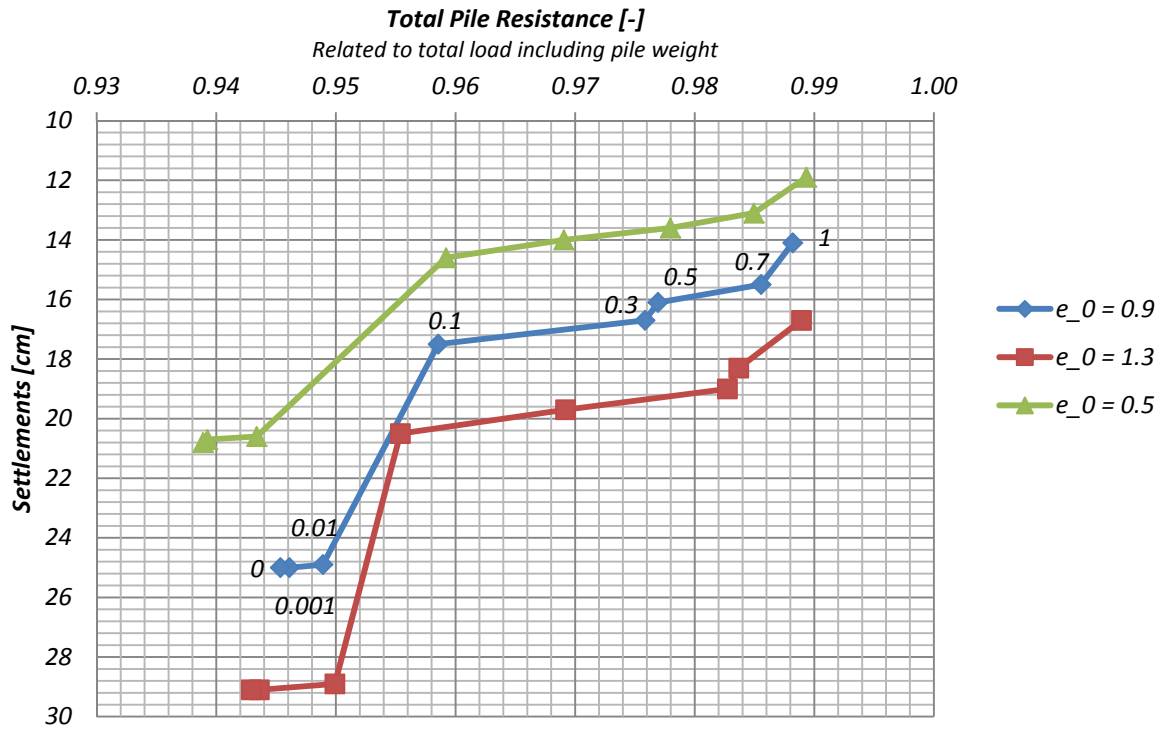


Figure 67: Resistance-settlement curve, Frari soil – SSC model

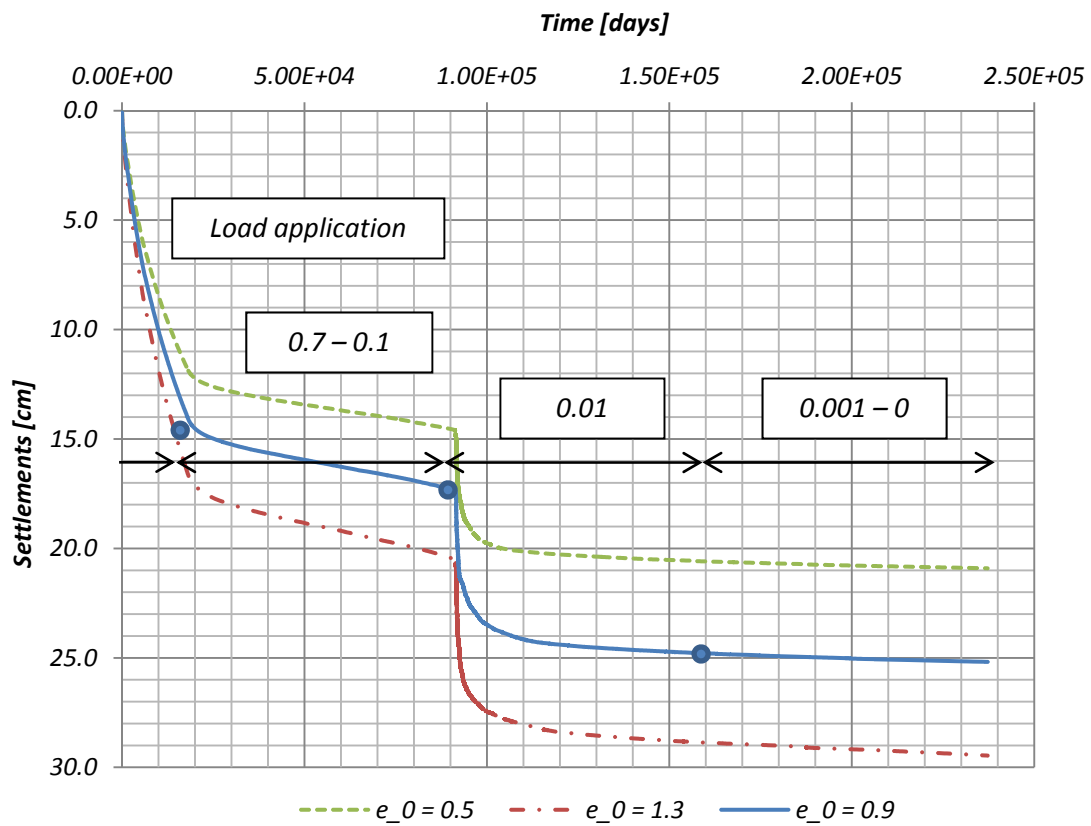


Figure 68: Time-settlement curve, Frari soil – SSC model

SSC with vs. without degradation of the interface

In order to quantify the settlements due to degradation, a comparative calculation is carried out, which basically consists of a pure creep analysis after the application of the full load. For this purpose, the pile’s interface is not subjected to any degradation, but the soil is left for creeping for a period of 600 years after load application. In Figure 69, the difference in settlement behaviour can be observed. When the load is fully applied after 50 years, the settlements reach a value of about 14.5 cm. After the total time period of 650 years, the settlements are increased for 2.5 cm due to the visco-plasticity of the soil (see pure creep). Through the interface degradation, however, 10.5 cm are added forming a total of 25 cm, whereas the biggest growth in settlements can be found when reducing the interface to ‘0.01’. From the degradation phases of ‘0.7’ to ‘0.1’, only a slight divergence from the results of pure creep can be observed.

Summing up, the impact of the interface degradation turns out to be predominant in respect of the impact of the soil’s visco-plasticity, as the difference in final settlement of pure creep and the one of creep in combination with interface degradation amounts to 9 cm.

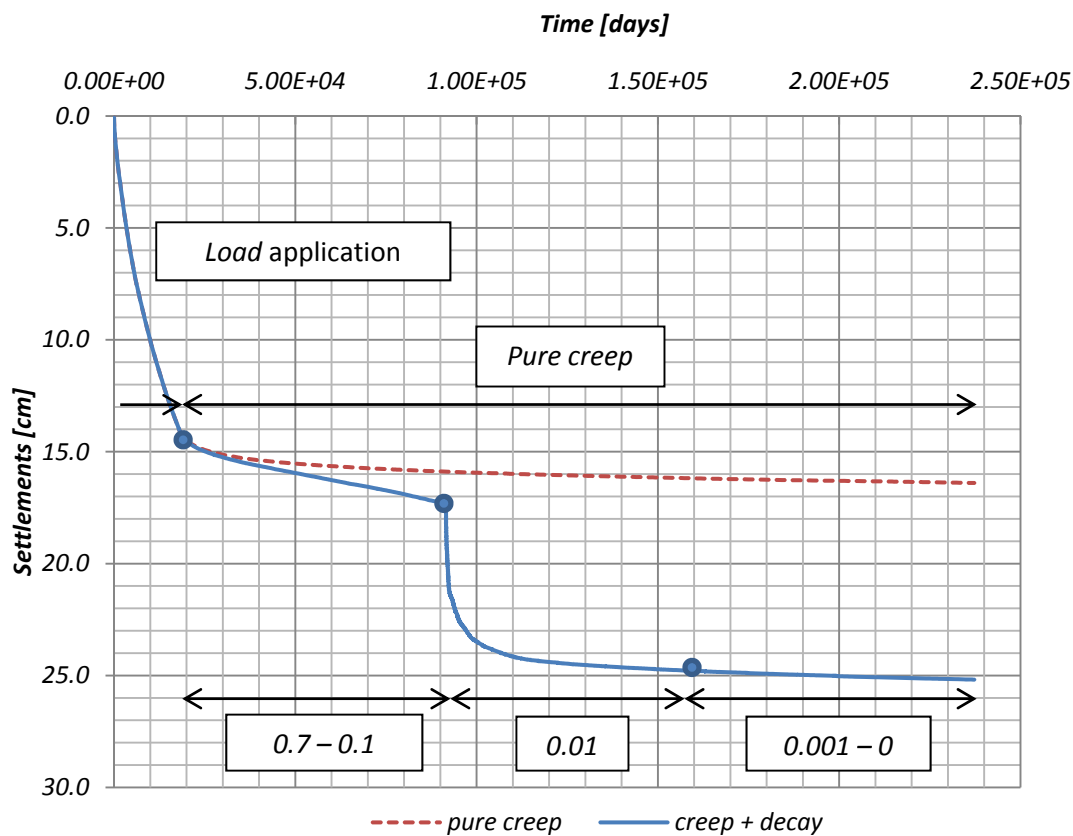


Figure 69: Time-settlement curve with and without interface degradation, Frari soil – SSC model

Comparative calculation with SS model

The objective of this calculation is to quantify the influence of the soil’s visco-plasticity on settlements and load-bearing behaviour. For this purpose, the results obtained from the Soft Soil Creep analysis are compared with those of a simple Soft Soil analysis. During the analysis with the Soft Soil Model, the parameters of Table 6 on page 24 are used, whereas the Modified Creep Index is omitted.

As it is shown in Figure 70, the relative portion of load carried by the raft and by the pile does not change during the decay of the pile, independently of the soil model in use. By looking at Figure 71, one can note an increase in pile base resistance due to the viscous behaviour of the soil in the SS Creep model, with corresponding lower skin resistance. Therefore, the settlements of the SS analysis result in general smaller, with a value of 13.6 cm after the final phase for the SS model, and 25.0 cm for the SSC model.

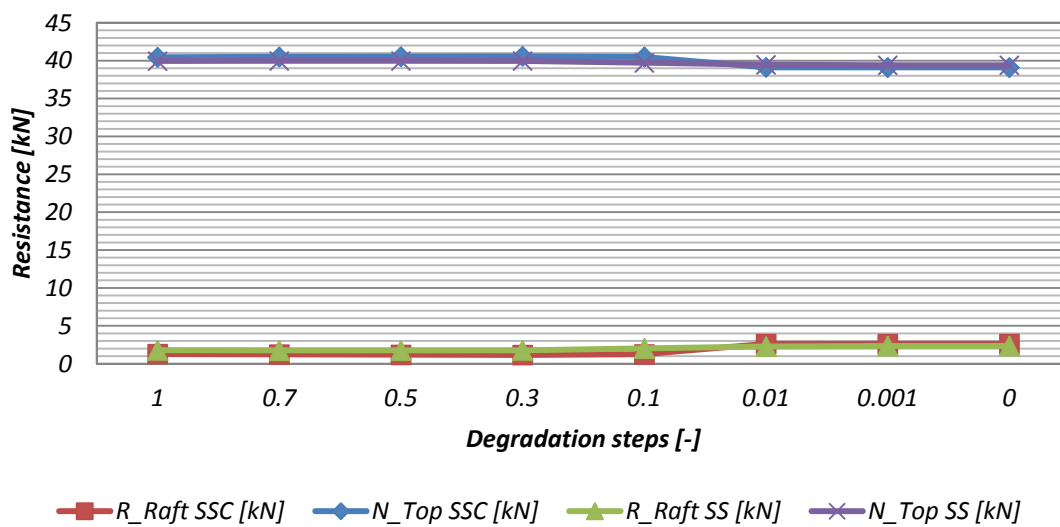


Figure 70: Load transfer, Frari soil – SSC vs. SS model

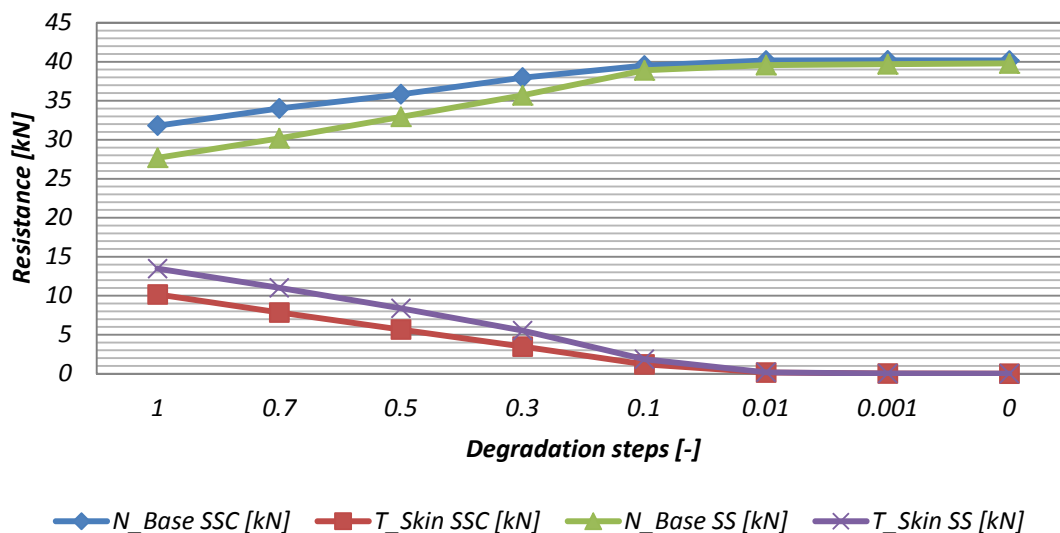


Figure 71: Development of base and skin resistance, Frari soil – SSC vs. SS model

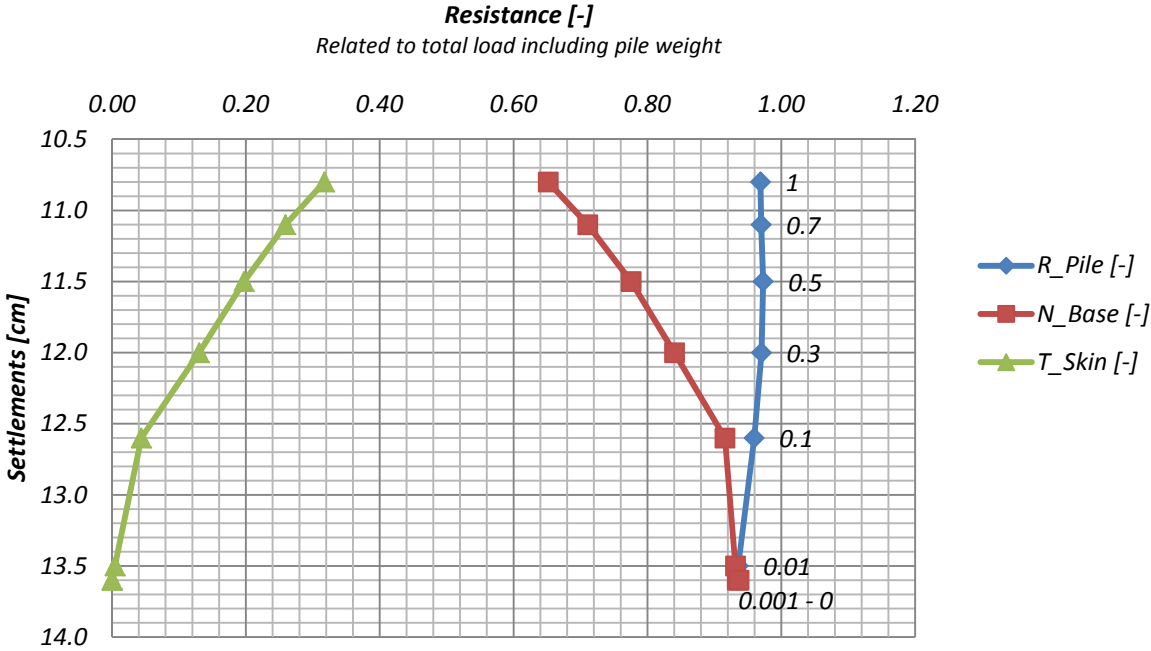


Figure 72: Resistance-settlement curve, Frari soil – SS model

### Comparative calculation with HS model

From the variation of the initial pore ratio it is learned that on the whole the relative portion of the load transferred by the raft or by the pile respectively does not change during degradation. Therefore, this study is performed to see whether the outcome is a result of the used soil model rather than of the type of soil per se. For this purpose, SS parameters given in Table 6 on page 24 are transformed to HS parameters with Equations 5.7 and 5.8:

$$E_{oed}^{ref} = \frac{p^{ref}}{\lambda^*} \quad (5.7)$$

$$E_{ur}^{ref} \approx \frac{2p^{ref}}{\kappa^*} \quad (5.8)$$

These equations have to be applied together with an  $m$  of 1.

In Table 22, the resulting stiffness parameters  $E_{oed}^{ref}$  and  $E_{ur}^{ref}$  of the Hardening Soil model are compared with the original SS parameters for compression  $\lambda^*$  and swelling  $\kappa^*$ .

Table 22: Stiffness parameters for SS model and HS model

$e_{init}$	$\lambda^*$	$\kappa^*$	$E_{oed}^{ref}$	$E_{ur}^{ref}$
[-]	[-]	[-]	[kN]	[kN]
0.9	0.06316	0.01053	1 583	18 993

For the use in PLAXIS, the obtained HS parameters have to be modified. The modifications for  $E_{ur}^{ref}$  and  $m$  are needed for reducing the friction angle at least to the degradation step of '0.1', otherwise the reduction would not be accepted by the calculation program. The used parameters are listed in Table 23.

Table 23: Soil parameters of the HS model

Parameter	Unit	Explanation	Value
<i>Standard Parameters for Hardening-Soil Model</i>			
$\gamma_{unsat} = \gamma_{sat}$	[kN/m <sup>3</sup> ]	Unit weight (unsaturated, saturated)	19
$\varphi'$	[°]	Friction angle (Mohr-Coulomb)	32.9
$c'$	[kN/m <sup>2</sup> ]	Cohesion (Mohr-Coulomb)	0
$\psi$	[°]	Dilatancy angle	0
$\nu_{ur}$	[-]	Poisson's ratio for unloading-reloading	0.2
$E_{50}^{ref}$	[kPa]	Secant modulus for un- and reloading	2 000
$E_{oed}^{ref}$	[kPa]	Tangent modulus for oedometric loading	1 600
$E_{ur}^{ref}$	[kPa]	Secant modulus for un- and reloading	16 000
$m$	[-]	Exponent of the Ohde/Janbu law	0.7
$p_{ref}$	[kPa]	Reference stress for the stiffness parameters	100

$K_0^{nc}$	[-]	Coefficient of earth pressure at rest (NC)	$1-\sin(\varphi')$
$R_f$	[-]	Failure ratio	0.90
$\sigma_{Tension}$	[kPa]	Tensile strength	0

In Figure 73 and Figure 74, the results of the SS analysis are compared with those of the HS analysis. One can see that the relative portion of load transferred to the pile head is practically the same for both constitutive models except for the last phase. Because of the increasing base resistance, however, also with the HS model a significant reduction of the normal force in the pile head is expected if the interface is further degraded. From this it can be concluded that the proportion of load transferred by the raft or the pile respectively is independent from the used constitutive model. On the other hand, it is noticeable that the portion of base and skin resistance is actually dependent on the used model, as their values are similar to the ones in case of Soil 1 or 2. This, however, might be influenced by the necessary change of HS model parameters described above.

Finally, the settlements when using the HS model are in general higher, with final settlement of about 16.5 cm compared to 12.6 cm in case of the SS model. See Figure 75.

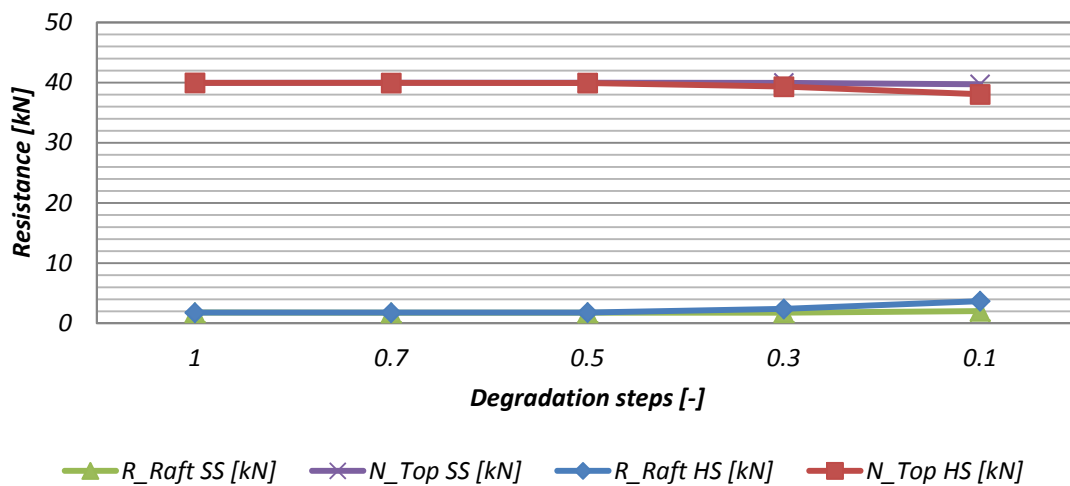


Figure 73: Load transfer, Frari soil – SS vs. HS model

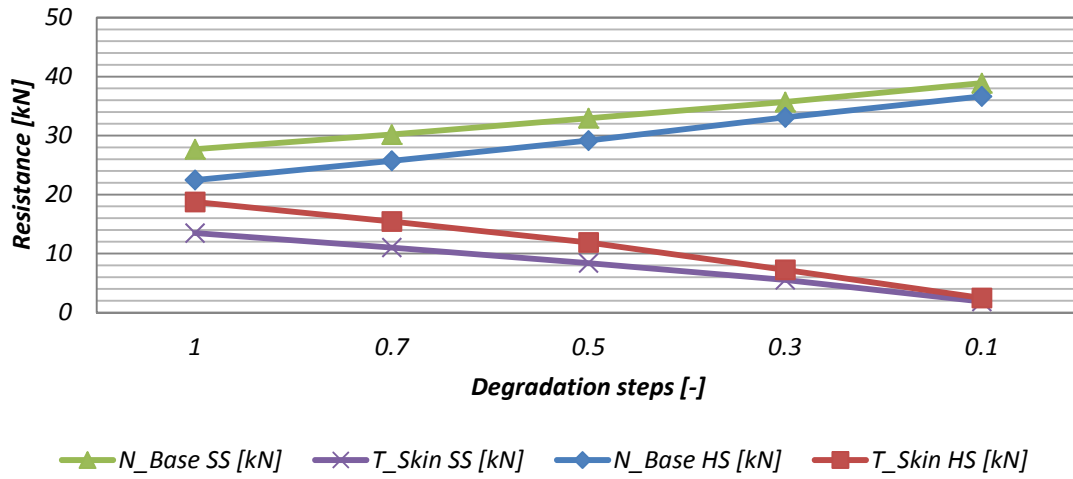


Figure 74: Development of base and skin resistance, Frari soil – SS vs. HS model



Figure 75: Resistance-settlement curve, Frari soil – HS model

#### 5.4.2.6 SUMMARY OF RESULTS AND DISCUSSION

The response of the load-bearing system to the interface degradation was studied. For this purpose, the strength of the pile's interface was reduced gradually. Hence, this procedure is comparable with Method A of the pile-degradation analysis.

The comparison of the two degradation methods showed a very different behaviour: During pile degradation, the pile is weakened uniformly over the cross-section, so that the skin and base resistance of the pile decrease whereas the raft resistance increases. This leads to an inversion in load-bearing behaviour, which means that at the end of the observation the raft transmits the major portion of the load. During the interface degradation, however, the base resistance of the pile is increasing and therefore the bearing-capacity of the pile remains predominant compared to the one of the raft till the last degradation step.

The different behaviour patterns can also be observed with the development of settlements: At the beginning of the pile-degradation analysis, the settlements of the pile head are due to elevated strains in the pile foot area. With advancing decay of the pile, the strain level in the soil near the pile head and in the pile itself is growing; simultaneously, the strains in the pile foot area get smaller. The settlements of the pile head at the end of the observation are then primarily due to the elastic and plastic shortening of the pile, and just to a small part due to the strains in the pressure bulb at the pile foot. In case of the interface degradation, however, the initial strains in the pressure bulb are growing, as the stress level in this area is increasing with the decay of the interface.

During interface degradation, the stress level in the pile foot area and consequently the pile base resistance is increasing in a similar way for both soils. Furthermore, one can note that for Soil 1 and Soil 2 the curves for pile head resistance and for the resistance of the raft show the same tendency. In case of Soil 2, though, the pile's resistance is diminishing earlier due to the earlier decrease in skin resistance. This is contrasting with the results of the pile-degradation analysis, where the skin resistances for Soil 1 and 2 practically describe the same curve. A similarity to pile degradation is found in the fact that also during interface degradation the settlements are in the order of 10 times higher for Soil 2 compared to Soil 1.

Due to the similar results obtained for the two soils, it was questioned if the outcome is influenced by the model size, as the size originally was assessed too small for not having an effect on the results. The analysis with the enlarged model was conducted using the example of Soil 2, and showed that the influence of the size on load-bearing behaviour is actually negligibly small. However, the settlements exhibit a notable increase.

Within the analyses with the interface-degradation method, also the influence of the stiffness of the raft on load transfer was studied. It turned out that, in this specific model, a change of the stiffness to 1/1000 does not provoke another reaction of the bearing system. Therefore, the use of the chosen Elastic modulus is justified.

Finally, the interface-degradation analysis was performed with the soil of the Frari site, using the same single-pile model. As it was mentioned before, there is uncertainty about the mechanical behaviour of the sand and clay layers in-situ, which is especially significant for the clay. Therefore, the parameters given in Table 6, namely the 3 stiffness parameters, were modified according to the initial pore ratio. All three variations provoked the same system response, which practically remained constant until the complete degradation of the pile. Again, just the settlements differed due to the different stiffness parameters. However, independently of the used parameter set, the settlements

---

after the application of the full load are controlled by the effect of interface degradation rather than by the soil's visco-plasticity. This was shown exemplarily in Figure 48 with the Time-settlement curve, using the original set of  $e_{init} = 0.9$ .

In order to study the influence of the inherent property of creeping in the SSC model, and to clarify if the steady system response is actually based on the use of this model, analyses with different material models were carried out. These are the SS and the HS model. In the course of these analyses, it was shown that the relative proportion of base and skin resistance in the first degradation stages is changed; for the SS model, the skin resistance experienced just a small increase (with simultaneous decrease in base resistance) compared to the SSC model, whereas for the HS model the proportion of skin and base resistance was similar to the one of Soil 1 and 2. However, with both models the pile base resistance reaches the same final value as within the SSC model. Consequently, the pile-head and raft resistance did not experience a significant change.

Hence, further investigations have been conducted, which are not presented in this work. These include the increasing of the stiffness parameters, the lowering of the strength and also the replacement of the sand layer with clay. However, there is still a need for clarification as none of these modifications gave a satisfying answer.

### 5.4.3 CONCLUSION

Finally, it can be stated that the single-pile model illustrates how a single pile works in the middle of a pile-group. Through the small radius of the model, representing a reduced pile-to-pile distance, it was possible to simulate the typical behaviour of a group pile, intending the minor relative settlements between pile and soil and corresponding lower mobilized skin friction compared to a free-standing pile, not being affected by the pile-group.

The conclusion is drawn that the reduction of the interface parameters represents the more suitable method for modelling degradation in the early stages, as the outer part of the wooden pile is already from the beginning more vulnerable and is also the first to be under attack of bacteria. By the time, however, also inner parts of the section will be affected, whereas the attack will then not spread uniformly from the outside to the inside. Furthermore, it is unlikely that the whole cross-section is ever completely damaged. To simplify matters, the degradation is smeared over the whole cross-section of the pile, which calls for the presented pile-degradation method.

A possible combination of interface and pile degradation is presented in the following for concluding this chapter. After the complete degradation of the interface, the pile parameters are reduced to 1/35 of their initial values. During the pile-degradation analysis it was shown that at least this degradation stage is needed so that the pile-skin resistance can be neglected. The relative calculation steps are illustrated in Table 24. In Figure 76 to Figure 78, the results of the combined degradation are presented.

Table 24: Calculation steps for a combined interface and pile degradation analysis

<i>Time [years]</i>	<i>Cumul. Time [years]</i>	<i>Friction angle [°]</i>	<i>Multiplier</i>
50	50	32.9	1
50	100	24.4	0.7
50	150	17.9	0.5
50	200	11	0.3
50	250	3.7	0.1
200	450	0.37	0.01
70	520	0.037	0.001
10	530	0	0
120	650	0	0 (1/35)

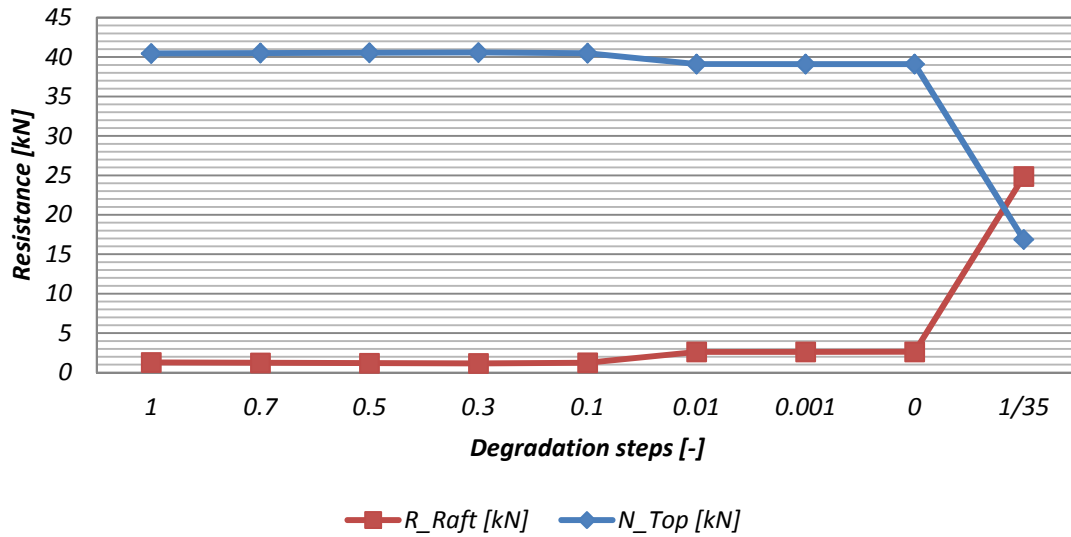


Figure 76: Load transfer, Frari soil – Combined analysis

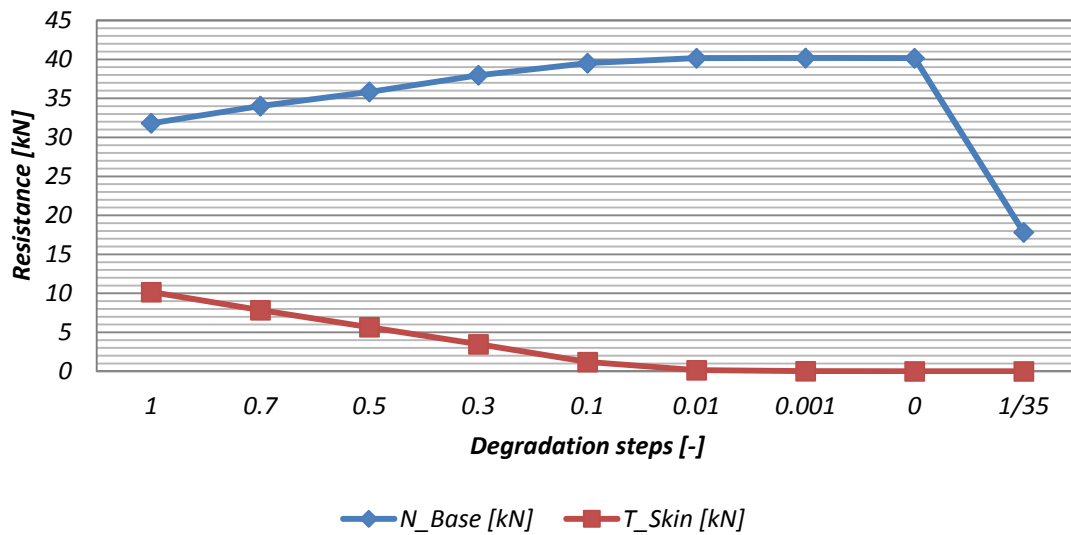


Figure 77: Development of base and skin resistance, Frari soil – Combined analysis

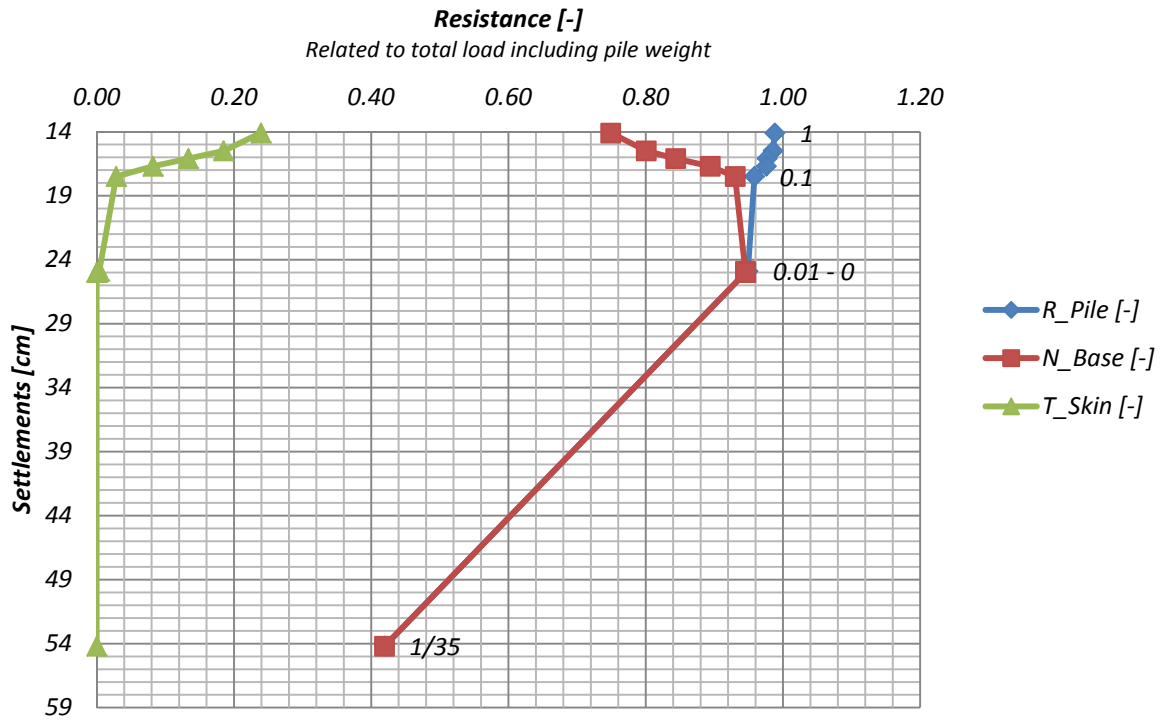


Figure 78: Resistance-settlement curve, Frari soil – Combined analysis

The conclusions made from the single-pile model are used in the frame of a real-size problem, namely are applied to the foundation of the Frari bell tower.

## 6 NUMERICAL ANALYSIS OF THE FOUNDATION OF THE FRARI BELL TOWER

### 6.1 INTRODUCTION

The foundation of the bell tower of the basilica *Santa Maria Gloriosa dei Frari* consists of a massive masonry footing of stone blocks, wooden planking and wooden piles. From the stone masonry, the load of the superstructure is transferred to several layers of wooden planks acting as stiff elements, which distribute the load more uniformly to the pile heads and soil in between the piles. As the piles are very close to each other, single piles are not used during the finite element analysis. Rather, the piles and soil between the same are summed up to a block with smeared parameters. Detailed information on the original geometry of the foundation is given in Chapter 2 on page 7. In the following, the geometry as it is used within the numerical model is explained.

### 6.2 GEOMETRY AND INPUT IN PLAXIS 3D FOUNDATION

The raft of wooden planks is assumed to be quadratic in plan, with a side length of 11.0 m, and to be 0.5 m thick. The block representing the piles as well as the stone masonry, which is resting on the raft, have the same dimensions in plan. The pile-block has a 'length' of 2 m and a quadratic opening in the centre, with a side length of 1.5 m. The opening of the raft and the masonry is neglected. In the model, the upper edge of the masonry coincides with ground level. The water level is assumed 1 m below ground level. The geometry and its dimensions are visualized in Figure 79 and Figure 80.

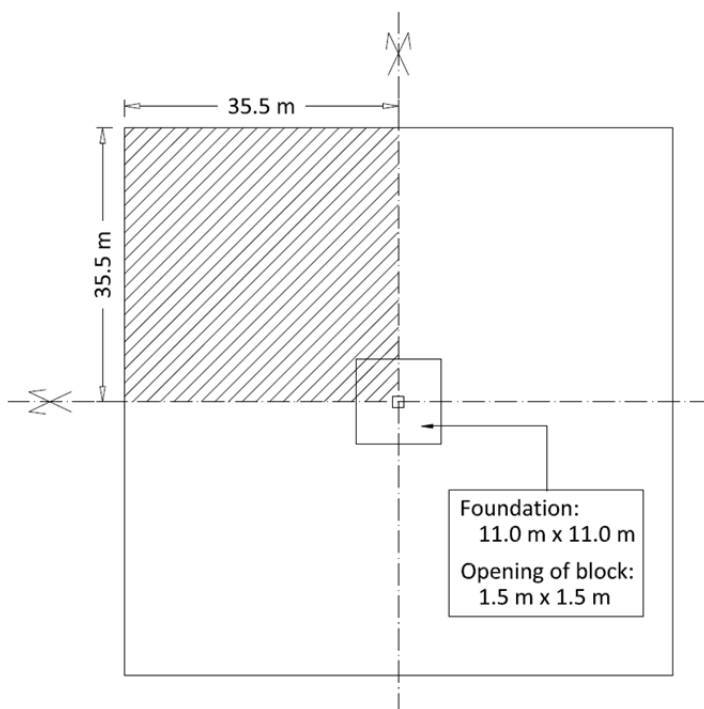


Figure 79: Top view of the geometry

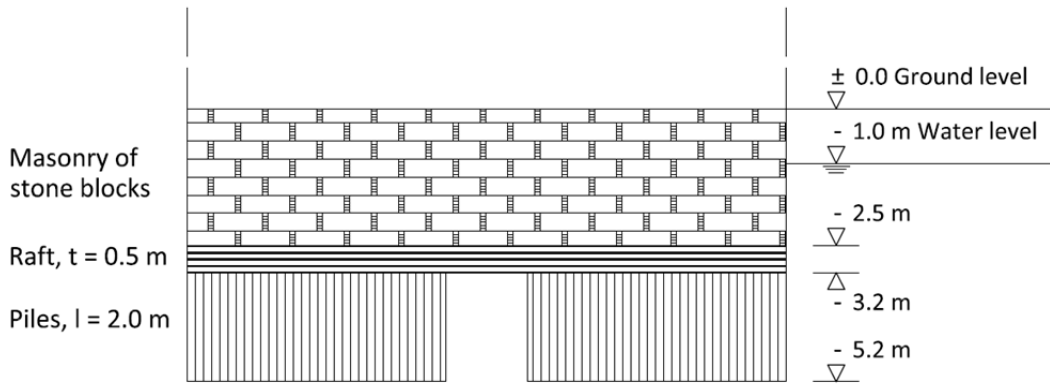


Figure 80: Section of the geometry, situated in symmetry axis

In order to reduce the model size, the advantage of double symmetry is taken. As it is shown in Figure 79 by means of the shading, the model dimensions are then 35.5 m per 35.5 m in plan, and 38 m in depth. The 3D model including the generated mesh is shown in Figure 81.

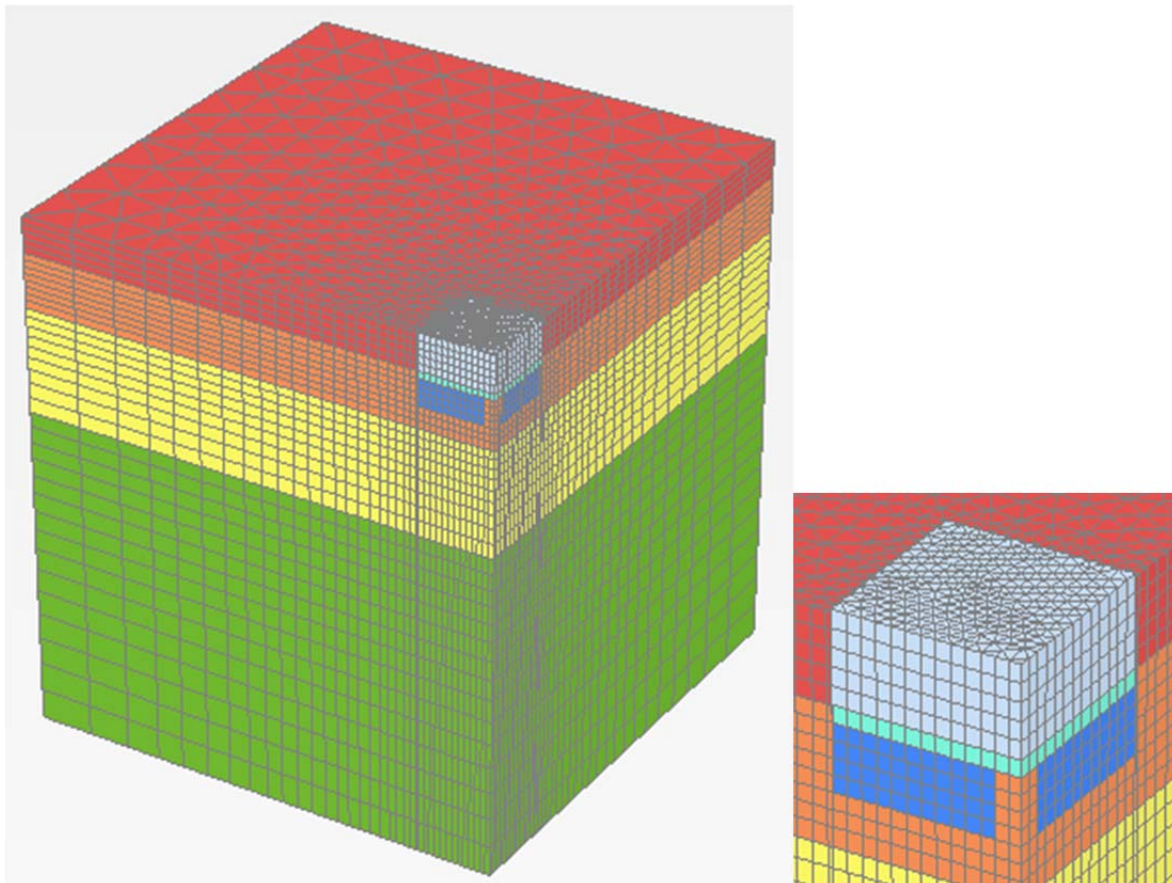


Figure 81: Three-dimensional view of the model including detail on foundation

As it is seen from above figure, apart from the soil itself also the block (of piles) and the raft are modelled with 3D-elements. The mesh is refined horizontally and vertically towards the foundation and consists of 44 622 elements with 120 790 nodes. The refinements are depicted in top view in Figure 82 and in front view in Figure 83.

The contact behaviour between masonry and soil is simulated by utilizing the interface of the plate element, which is installed during the construction phase (see calculation phases in Table 31 on page 94). In this regard, the interface parameter  $R_{inter}$  is set to 0.5. In Figure 81, both red layers represent clay; to the first layer, the  $R_{inter}$  of 0.5 is assigned, whereas for the  $R_{inter}$  of the second layer the default value of 1.0 is kept. The interface properties in the area of the raft and the pile-block are therefore those of the surrounding soil, which implies a very good bond between soil and wooden structure.

For simulating the contact behaviour between the soil and the piles *with time*, the interface is simulated in another way. This is necessary, as through the  $R_{inter}$  only one parameter set can be assigned to the plate's interface. Further, it is not possible to manually assign parameter sets to this interface, as it is done in the 2D model. During the degradation analysis, however, different degradation stages have to be investigated, which demands different parameter sets. Hence, a narrow element cluster is created around the foundation, as it is illustrated in Figure 82. See section 6.4.1.2 on page 100 for details on the degradation procedure.

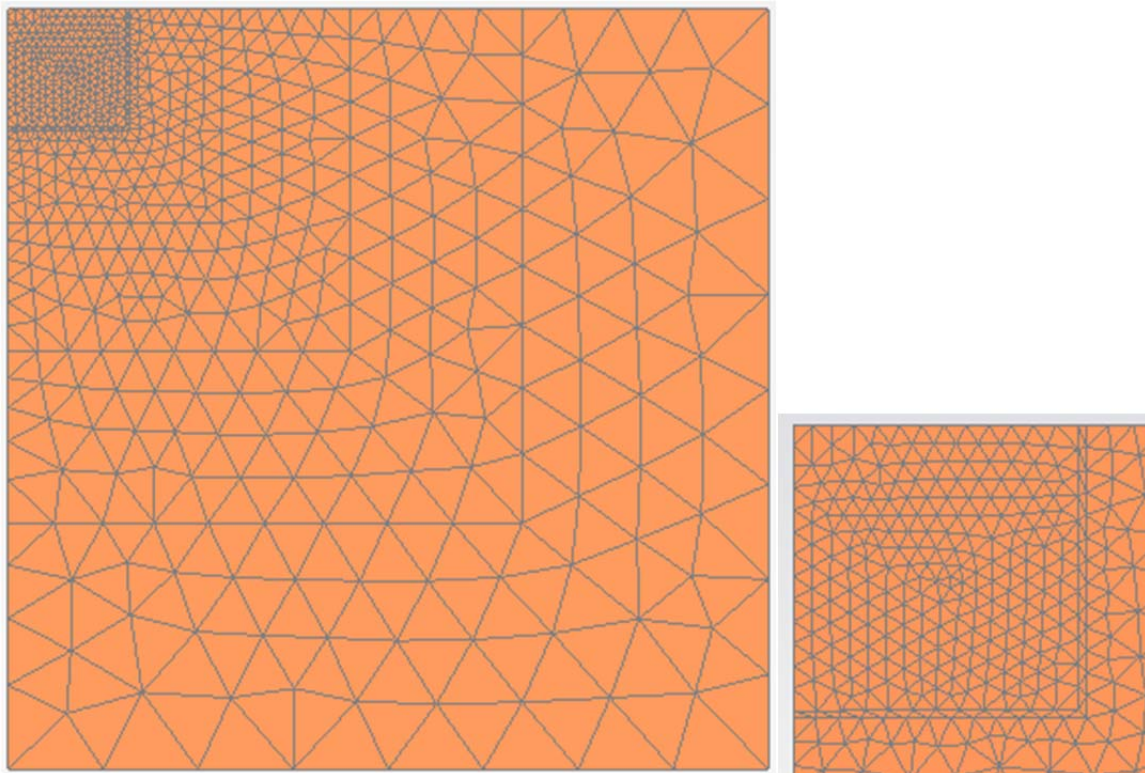


Figure 82: Top view of the mesh with detail on narrow element-cluster representing the interface

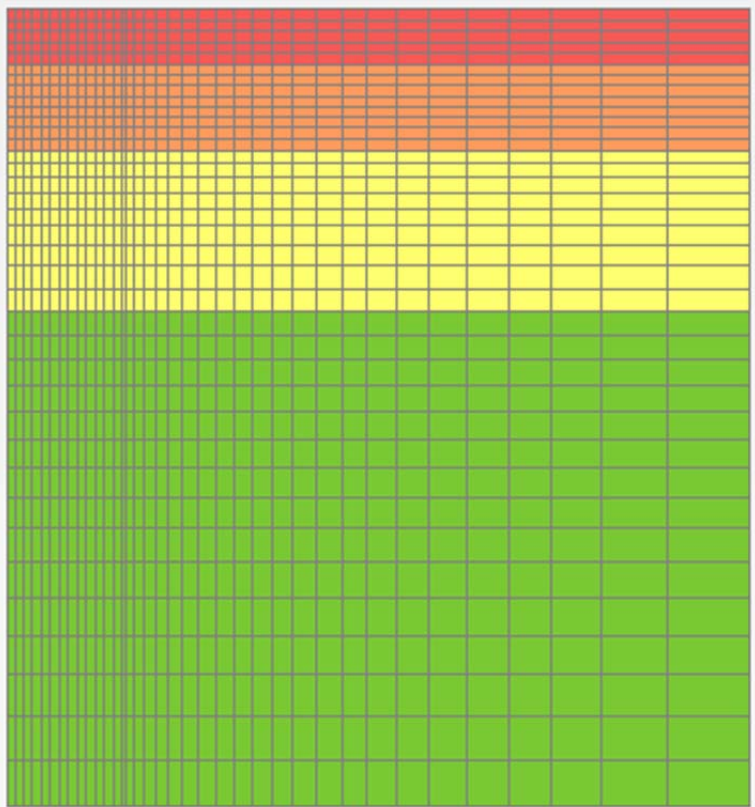


Figure 83: Front view of the mesh

## 6.3 MATERIAL PARAMETERS

### 6.3.1 SOIL

#### 6.3.1.1 INTRODUCTION

The layering of the model is based on the stratigraphy of the Frari site, given in Chapter 3 on page 9. To simplify matters, the set of parameters of the clay layer is also assigned to the upper layer of filling material.

Table 25: Stratigraphy of the Frari site

<i>Soil Layer</i>	<i>Depth [m]</i>	<i>Details</i>
Clay	$\pm 0.0 \text{ m} \div -3.2 \text{ m}$	Filling material and clay layer
Sand	$-3.2 \text{ m} \div -6.8 \text{ m}$	
Alternating strata	$-6.8 \text{ m} \div -38.2 \text{ m}$ (coinciding with the lower model boundary)	Several layers of clay and sand summarized in one set of parameters

The water table is chosen in a depth of -1.0 m below ground level.

#### 6.3.1.2 SOIL PARAMETERS

For the upper clay and sand layers, the same parameters and constitutive models (SSC respectively HSS model) as in the Frari single-pile analysis are used (see Table 6 on page 24 and Table 7 on page 25). The alternating strata below the sand layer are summarized to one with smeared parameters, which are listed in Table 26. For describing the behaviour of this layer, the HSS model is chosen.

Table 26: Soil parameters for layer representing alternating strata (Frari bell tower)

<i>Parameter</i>	<i>Unit</i>	<i>Explanation</i>	<i>Value</i>
<i>Standard Parameters for Hardening-Soil Model</i>			
$\gamma_{\text{unsat}} = \gamma_{\text{sat}}$	[kN/m <sup>3</sup> ]	Unit weight (unsaturated, saturated)	19
$\varphi'$	[°]	Friction angle (Mohr-Coulomb)	34
$c'$	[kN/m <sup>2</sup> ]	Cohesion (Mohr-Coulomb)	0.1
$\psi$	[°]	Dilatancy angle	0
$\nu_{\text{ur}}$	[-]	Poisson's ratio for unloading-reloading	0.2
$E_{50}^{\text{ref}}$	[kPa]	Secant modulus for un- and reloading	23 000
$E_{\text{oed}}^{\text{ref}}$	[kPa]	Tangent modulus for oedometric loading	23 000
$E_{\text{ur}}^{\text{ref}}$	[kPa]	Secant modulus for un- and reloading	69 000
$m$	[-]	Exponent of the Ohde/Janbu law	0.6
$p_{\text{ref}}$	[kPa]	Reference stress for the stiffness parameters	100
$K_0^{\text{nc}}$	[-]	Coefficient of earth pressure at rest (NC)	0.441

$R_f$	[-]	Failure ratio	0.90
$\sigma_{\text{Tension}}$	[kPa]	Tensile strength	0
<i>Supplemental parameters for Small strain stiffness</i>			
$G_0^{\text{ref}}$	[kPa]	Initial or very small strain shear modulus	90 000
$\gamma_{0,7}$	[kN/m <sup>3</sup> ]	Reference shear strain where $G_{\text{sec}}=0,7*G_0$	0.00015

### 6.3.2 PILES

In case of the Frari bell tower, the piles were driven into the soil very close to each other. Because of the little intermediate soil mass (speaking of several cm of soil between two piles), it is assumed that inner piles can mobilize only relatively small skin resistance, compared to the resistance mobilized by a free-standing (single) pile. This assumption is based on the results obtained in the single-pile analysis, which showed strongly reduced skin resistance and small relative settlements between pile and soil already at a mutual distance of the piles of 30 cm. Therefore, the piles and the soil in between are modelled as a block with smeared parameters, summarized in Table 27. Further, the block is assumed to be non-porous.

Table 27: Parameters of the block representing the piles (Frari bell tower)

<i>Parameter</i>	<i>Unit</i>	<i>Explanation</i>	<i>Value</i>
$\gamma$	[kN/m <sup>3</sup> ]	Unit weight	19
$\varphi'$	[°]	Friction angle	0
$c_0'$	[kN/m <sup>2</sup> ]	Initial cohesion	5 500
$\psi$	[°]	Dilatancy angle	0
$\nu$	[-]	Poisson's ratio	0.3
$E_0'$	[MN/m <sup>2</sup> ]	Initial elastic modulus	5 500

The used constitutive model is the Mohr-Coulomb model. The corresponding values for strength and stiffness are based on the pile parameters used during the single-pile analysis (see Table 8 on page 28), and on the clay parameters. Those values are obtained by weighting the strength and stiffness parameters of the two components with respect to their *equivalent area*. For the pile, the equivalent area is given in Equation 6.1:

$$\frac{A_P}{A_{GEO}} = \frac{r^2 \pi}{(2r)^2} = \frac{\pi}{4} = 0.79 \quad (6.1)$$

However, the skin resistance of piles at the edge respectively the contact behaviour between the entire block and the surrounding soil has to be taken into account in the model. On page 88, it was already explained that this is realized by a narrow element cluster, which represents the interface. In the 3D model, the simulation of decay is for a start restricted to the interface degradation. Therefore, different parameter sets are assigned to the narrow cluster with proceeding degradation. Further steps regarding the degradation procedure are explained in section 6.4.1.2 on page 100.

### 6.3.3 RAFT

During the geotechnical investigation at the Frari bell tower executed in 2003 (compare Chapter 3), the wooden planking still appeared to be in very good condition. Therefore, a decay of the planking is neglected during the analyses. The parameters are summarized in Table 28.

Table 28: Parameters of the planking (Frari bell tower)

<i>Parameter</i>	<i>Unit</i>	<i>Explanation</i>	<i>Value</i>
E	[MN/m <sup>2</sup> ]	Elastic modulus	10 000
$\nu$	[-]	Poisson's ratio	0.2
$\gamma$	[kN/m <sup>3</sup> ]	Unit weight	13

The planking is considered to behave linear elastically and is assumed to be non-porous.

### 6.3.4 MASONRY FOOTING

The masonry footing is assumed to be non-porous; its behaviour is modelled linear elastically. The corresponding parameters are given in Table 29.

Table 29: Parameters of Masonry (Frari bell tower)

<i>Parameter</i>	<i>Unit</i>	<i>Explanation</i>	<i>Value</i>
E	[MN/m <sup>2</sup> ]	Elastic modulus	1 000
$\nu$	[-]	Poisson's ratio	0.2
$\gamma$	[kN/m <sup>3</sup> ]	Unit weight	0

### 6.3.5 TEMPORARY SUPPORT SYSTEM FOR CONSTRUCTION PIT

There is a lack of information concerning the support measures needed during excavation. It is most likely that wooden piles were installed. To simplify matters, in the model the support system during the construction phase is represented by wall elements. To the walls, linear elastic, isotropic material behaviour is assigned. The parameters are listed in Table 30.

Table 30: Wall parameters (Frari bell tower)

<i>Parameter</i>	<i>Unit</i>	<i>Explanation</i>	<i>Value</i>
d	[m]	Thickness	0.6
$\gamma$	[kN/m <sup>3</sup> ]	Unit weight	0
E	[kN/m <sup>2</sup> ]	Young's modulus	$3 \cdot 10^7$
G	[kN/m <sup>2</sup> ]	Shear modulus	$1.25 \cdot 10^7$
$\nu$	[-]	Poisson's ratio	0.2

## 6.4 CALCULATIONS

### 6.4.1 DRAINED ANALYSIS

Initially, the calculation is performed drained, as the focus of the study lies on final settlements. However, it has to be kept in mind that, when combining a drained analysis with a creep analysis, the portion of settlements due to creep might be overestimated. A drained analysis, though, is a reasonable first estimation.

#### 6.4.1.1 PURE CREEP ANALYSIS

In this analysis it is assumed that the properties of the pile respectively of the block remain constant with time. The only time-dependent feature is the visco-plasticity of the soil. Because of the lack of information regarding the construction of the tower's foundation, the construction sequence is set up as follows in Table 31.

Table 31: Calculation phases of pure creep analysis in drained conditions (Frari bell tower)

<i>Identification</i>	<i>Phase no.</i>	<i>Start from Phase no.</i>	<i>Explanation</i>
Initial phase	0	N/A	K0-procedure
Activation of walls	1	0	Installation of support system to a depth of -6.2 m below ground level (1 year)
Groundwater lowering	2	1	Lowering of groundwater to a depth of -3.7 m (1 year)
Excavation	3	2	Excavation to a depth of -3.2 m (1 year)
Activation of block and raft	4	3	Installation of piles (represented by the block) from -3.2 m to -5.2 m and of the raft (1 year)
Deactivation of walls and activation of masonry	5	4	Deactivation of support system and activation of the foundation masonry of the tower with zero weight (1 year)
Rising of groundwater level	6	5	Rising groundwater level to original level of -1.0 m (1 day)
Load	7	6	Application of 480 kPa on the raft, corresponding to the full structural loads (30 years), resetting displacements to zero
Pure creep	8	7	Creep analysis (615 years)

It has to be considered that the execution of the construction works is not realistically represented. This, for example, regards the size of the excavation pit, which in the model has the dimensions of the foundation, and the installation of the temporary support system. The fictitious construction sequence is illustrated in Figure 84. The support system is represented by the blue plate in (a) and (b).

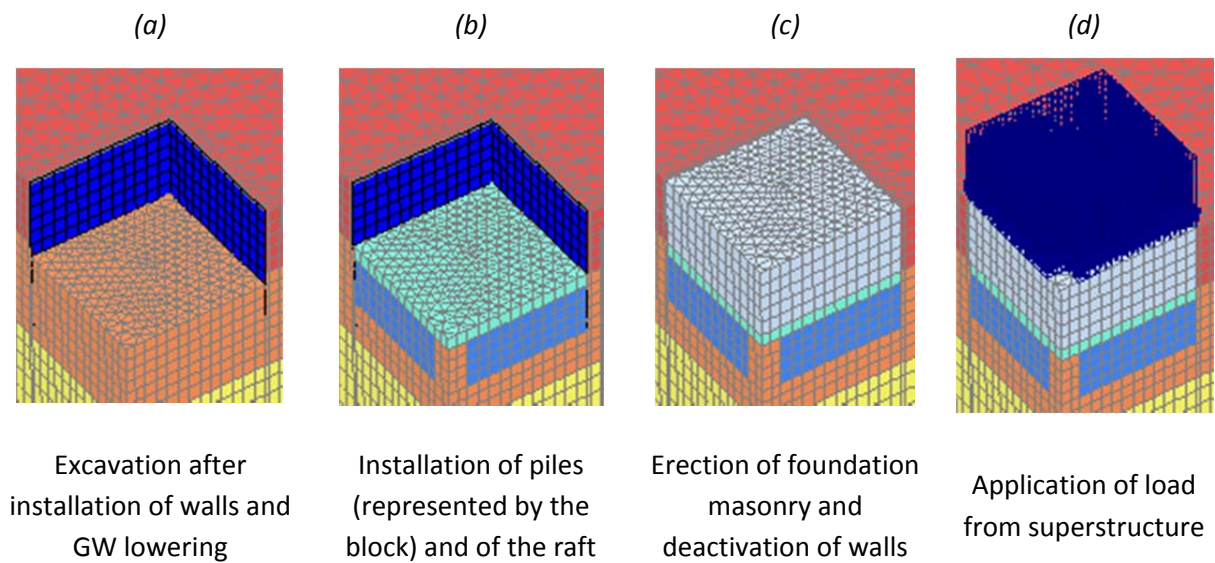


Figure 84: Construction sequence of the Frari bell tower

## Results

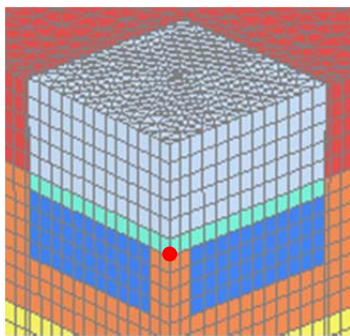


Figure 85: Position of node for displacement curves

The settlements of the foundation for settlement curves are measured in node A, which lies in the centre of the foundation. Its position is marked with a red dot in Figure 85.

The surface settlements after the activation of the plates, corresponding to a time period of 1 year, already amount to 10.2 cm, and are generated in the upper clay layers ( $t = 6.8\text{m}$ ). In order to clarify whether or not these relatively high settlements are due to the use of SSC in the 3D model, comparative calculations are carried out in 3D and 2D. For this purpose, the thickness of the clay layer in the 3D model is adjusted to the one in the 2D model ( $t = 4.1\text{ m}$ ), so that results are comparable. After the k0-procedure, a creep analysis (plastic analysis) is carried out for 1 year without installing any structures. Further, this calculation is performed with an OCR of 1.1 as well of 1.35. The results obtained are summarized in Table 32.

Table 32: Creep-settlements due to self-weight of the soil after 1 year

	OCR = 1.1	OCR = 1.35
3D	6.1 cm	2.1 cm
2D	5.8 cm	2.1 cm

The difference between 3D and 2D results is negligibly small. Therefore, it is assumed that the amount of settlements due to creep, caused solely by the self-weight of the overburden, ranges in a reasonable order of magnitude for these OCRs. Further, the sensitivity of the soil regarding the pre-consolidation becomes obvious, since the values for an OCR of 1.35 are strongly reduced.

In Figure 86, the development of settlements in Node A during the construction period is shown for both OCRs. The difference in results before load application amounts to 4.4 cm.

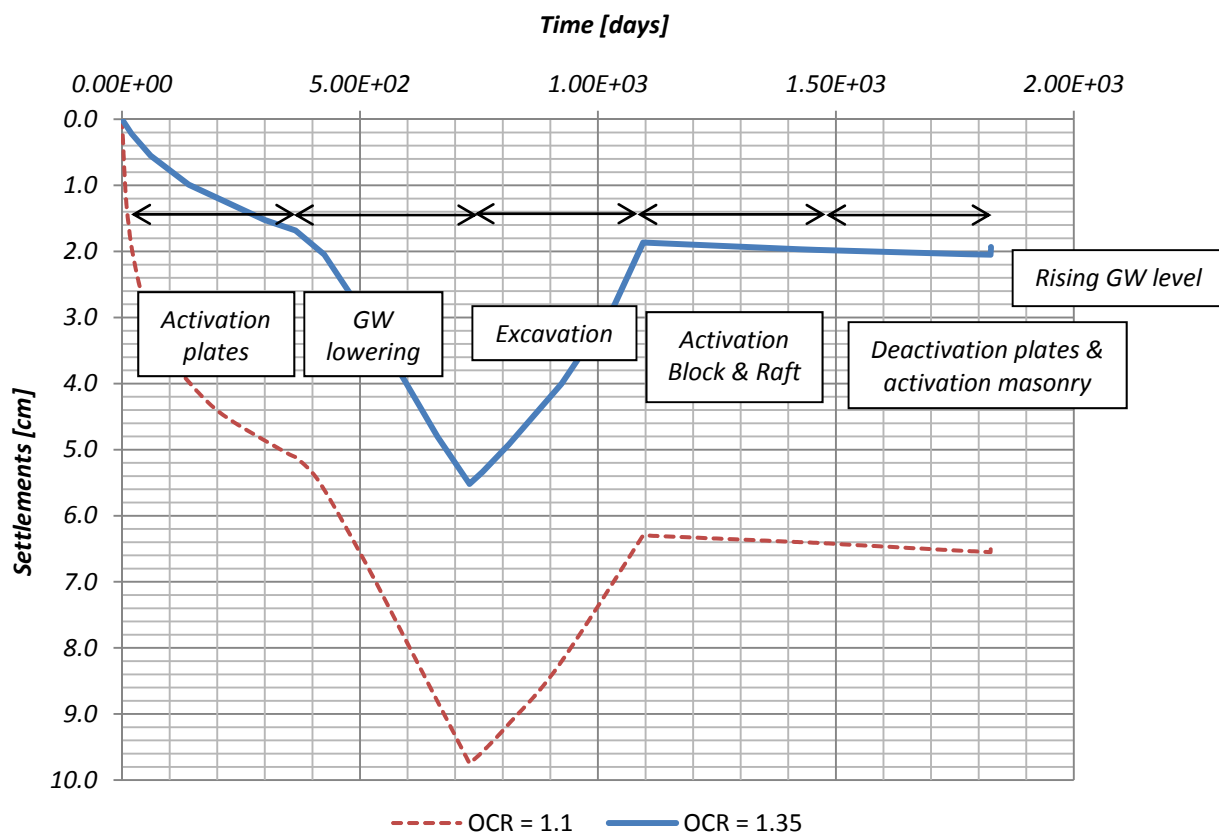


Figure 86: Time-settlement behaviour during construction period

In Figure 87 and Figure 88, the 'load'-displacement curve respectively the time-settlement curve for the phase of load application and for the subsequent creep phase is illustrated. At the end of the observation, the difference in results is in the order of several mm. The portion of settlements from the creep phase amounts to slightly more than 4 cm for both OCRs, compared to a period of 615 years.

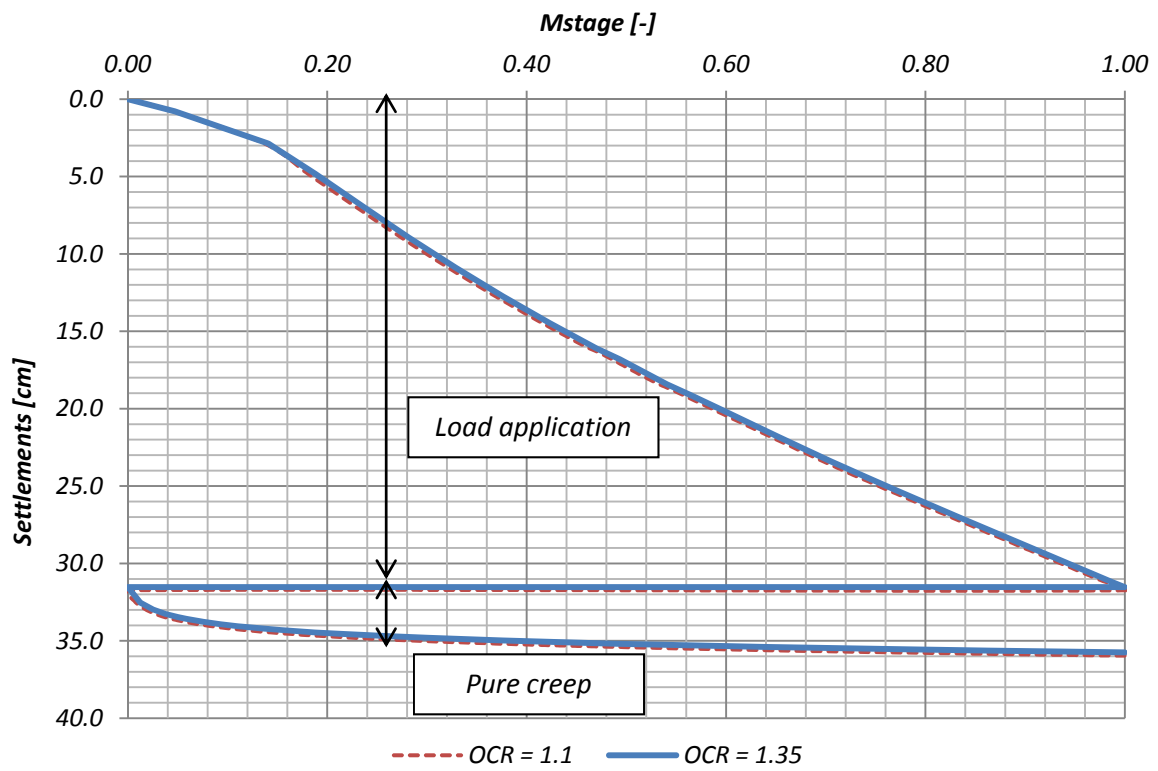


Figure 87: 'Load'-displacement curve for OCR 1.1 and 1.35

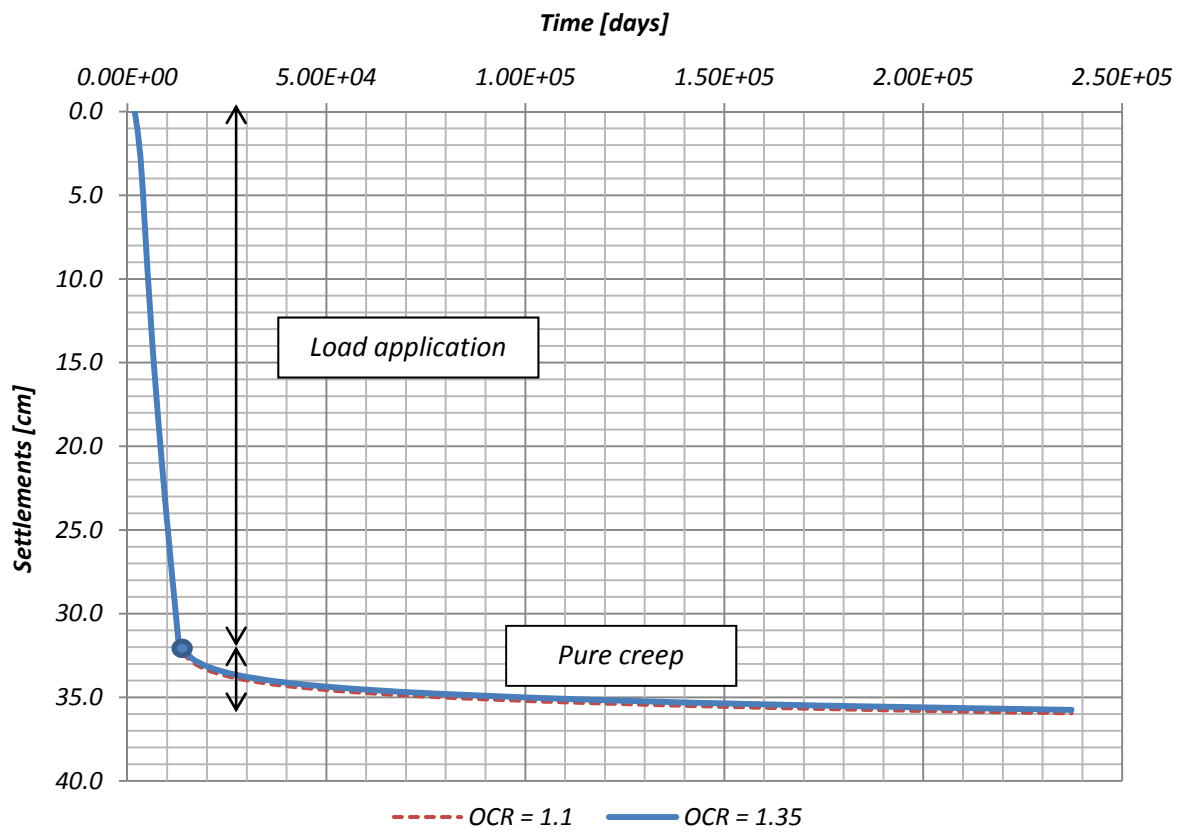


Figure 88: Time-settlement curve for OCR 1.1 and 1.35

The total settlements from the phases of load application and creeping are about 36 cm in Node A. Compared to that, settlements in zones unaffected by the load application amount to about 11.5 cm from these phases, independently from the OCR. These settlements are solely due to the visco-plastic behaviour of the soil. The corresponding deformed mesh and the total settlements at the end of the observation are illustrated in Figure 89 and Figure 91 respectively.

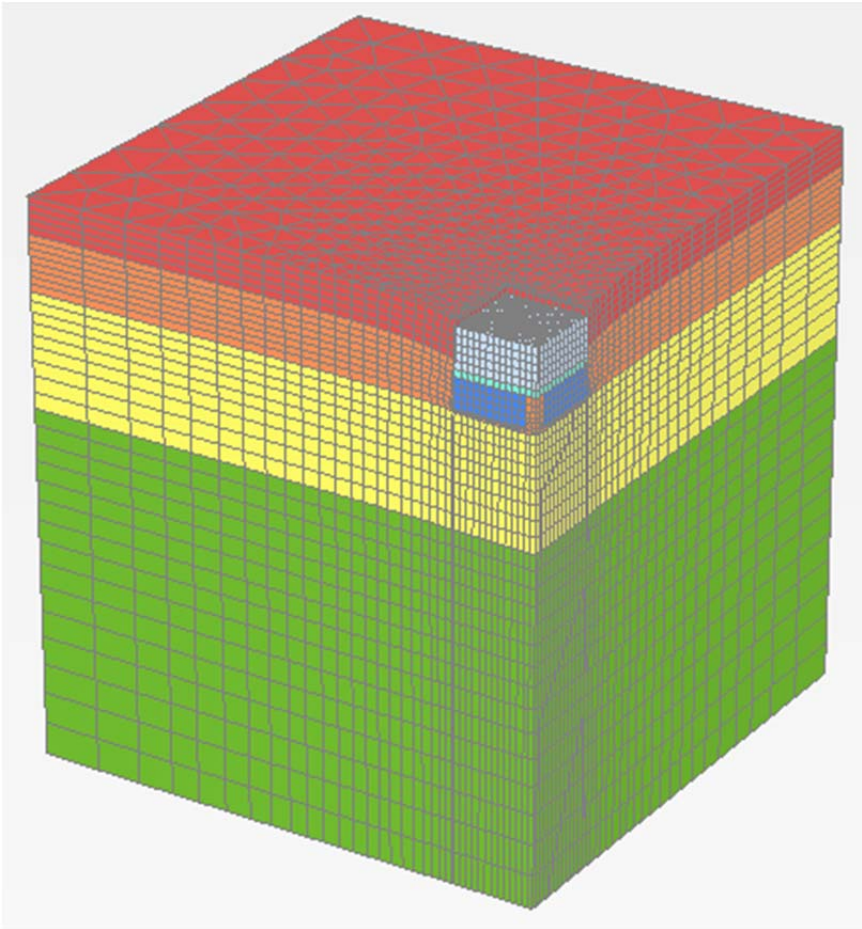


Figure 89: Deformed mesh at the end of the observation (scaled up 5 times)

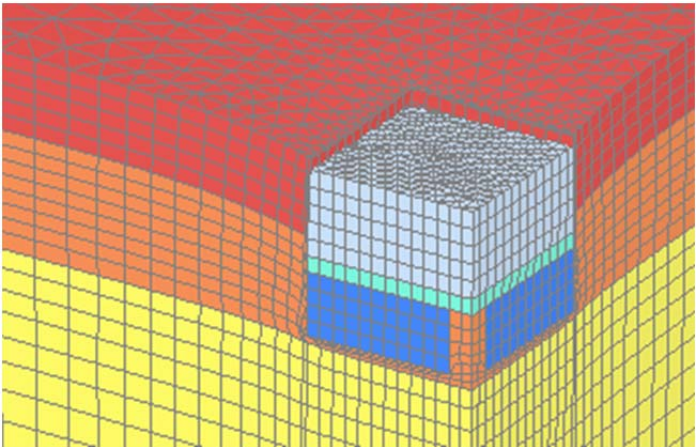
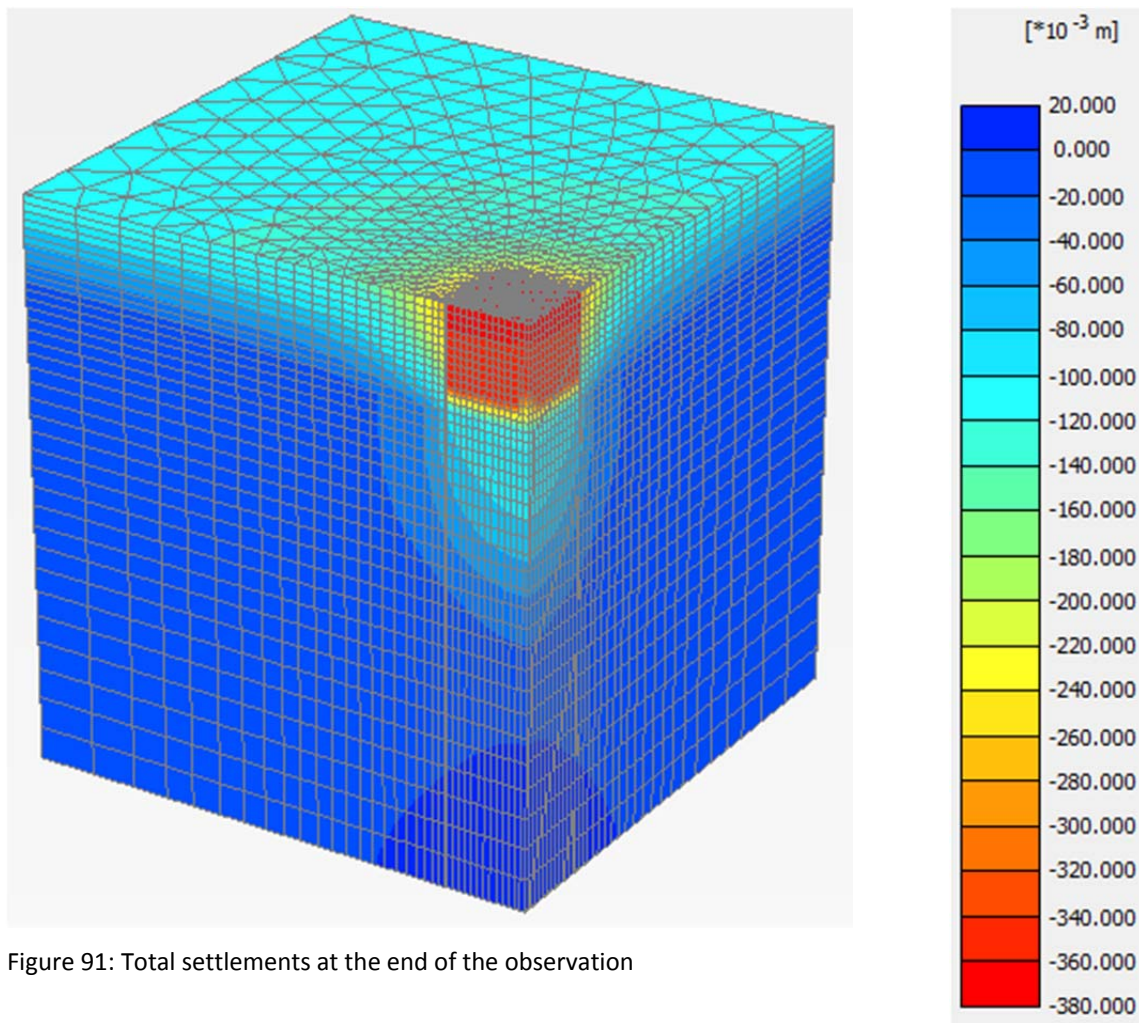


Figure 90: Detail on Figure 89



### Summary of results and discussion

According to the results obtained, the settlements are guided primarily by the application of the load itself; the settlements directly after load application amount to about 32 cm, which under the made assumptions would imply that the raft in any case was dimensioned much too small for sustaining a load of 480 kPa.

It is shown that the choice of the OCR plays a relevant role only for the construction phase; afterwards, however, results are basically the same for both tested OCRs. Further, it is observed that in this phase the settlement rate due to creep is much more significant than in the phases of load application and pure creep, especially in case of a very low OCR. When activating the wall elements, settlements in the order of 10 cm (for OCR = 1.1) result, compared to a period of only 1 year. From the phases of load application and creeping, however, the total creep settlements (at the model borders) are in the order of 11 to 12 cm compared to a period of 645 years.

### 6.4.1.2 COMBINED CREEP AND DEGRADATION ANALYSIS

The objective of this analysis is to quantify the influence of the pile's degradation on settlement behaviour. For this scope, interface degradation - similar to the one of the single-pile analyses - is done, which is a possibility to model the diminishing interface properties. In Table 33, the corresponding calculation phases are listed.

Table 33: Calculation phases for combined creep and degradation analysis

<i>Identification</i>	<i>Phase no.</i>	<i>Start from Phase no.</i>	<i>Explanation</i>
Initial phase	0	N/A	K0-procedure
Activation of wall elements	1	0	Installation of support system to a depth of -6.2 m below ground level (1 year)
Ground-water lowering	2	1	Lowering of ground-water to a depth of -3.7 m (1 year)
Excavation	3	2	Excavation to a depth of -3.2 m (1 year)
Activation of block and raft	4	3	Installation of piles (represented by the block) from -3.2 m to -5.2 m and of the raft (1 year)
Deactivation of walls and activation of masonry	5	4	Deactivation of support system and activation of the foundation masonry of the tower with zero weight (1 year)
Rising of groundwater level	6	5	Rising groundwater level to original level of -1.0 m (1 day)
Load	7	6	Application of 480 kPa on the raft, corresponding to the full structural loads (30 years)
Pure creep	8	7	Creep analysis, 15 years
Interface degradation 0.7 – 0.1	9 - 12	8 - 11	Reduction of interface strength to 70% and further (manual application), 50 years every phase
0.01	13	12	Reduction of interface strength to 1 %, 200 years
0.001	14	13	Reduction of interface strength to 0.1 %, 70 years
Creep analysis	15	14	130 years

The interface degradation is carried out by applying new parameter sets to the narrow element cluster representing the interface between piles and soil, which was introduced on page 89. The parameter sets differ from the original one of the soil only by a reduced friction angle, which is given in Table 34.

Table 34: Friction angle for interface cluster

<i>Time [years]</i>	<i>Cumul. time [years]</i>	<i>Friction angle [°]</i>	<i>Multiplier</i>
50	50	32.9	1
50	100	24.4	0.7
50	150	17.9	0.5
50	200	11	0.3
50	250	3.7	0.1
200	450	0.37	0.01
70	520	0.037	0.001
130	650	0.037	0.001

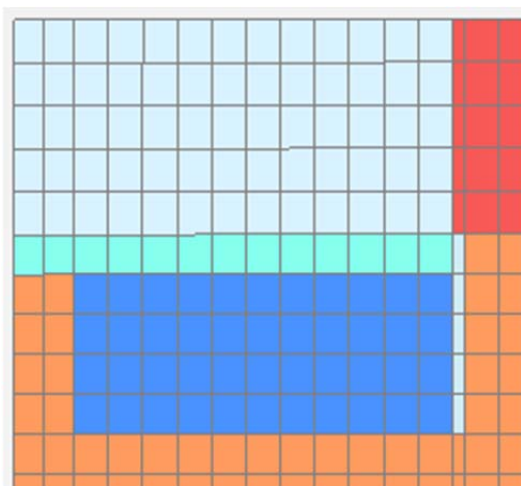
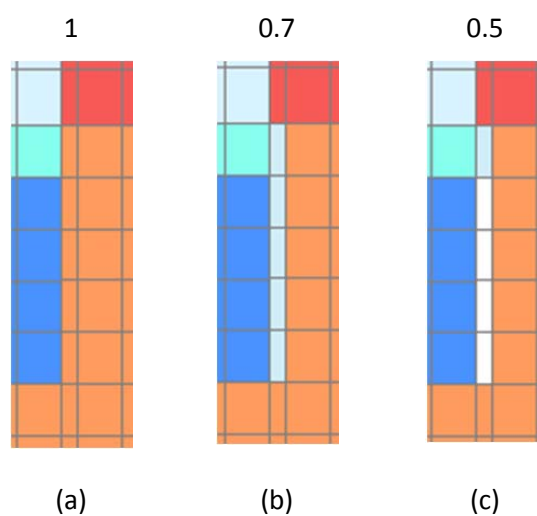


Figure 92: Detail on foundation and interface cluster



In Figure 92, a section of the foundation and the narrow cluster representing the interface between soil and pile respectively raft is illustrated. At the beginning, a tight bond between wooden elements and soil is assumed; therefore, the interface cluster bears the original soil properties. Compare Figure 93 (a). In the next phase, (b), the interface material of the pile and the raft are exchanged. In this way, the friction angle of the interface material is reduced to 70%. In (c), the pile’s interface is degraded further to 50%, whereas the interface material of the raft is kept from the previous phase. Thus, a further degradation of the raft is not considered. According to the example of ‘0.5’, the degradation is proceeding until the last phase, where the friction angle is practically zero. This implies a complete degradation of the interface.

Figure 93: Change of interface material during degradation

Results

In Figure 94, the Time-settlement for an OCR of 1.1 is shown according to the pure creep analysis, and is compared to the curve considering interface degradation. The graphs practically show the same development. A negligible difference can be seen from Figure 95, where the results of the creep phase of the pure creep analysis and those of the single degradation phases of the combined analysis are depicted.

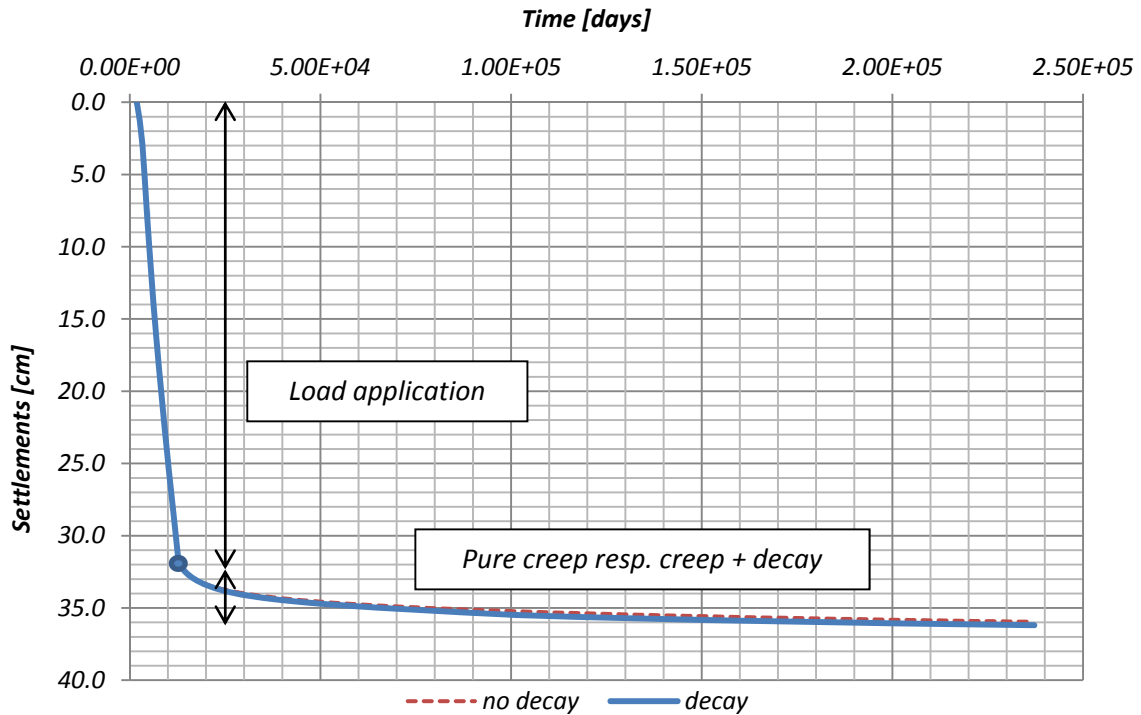


Figure 94: Time-settlement curves showing influence of interface degradation

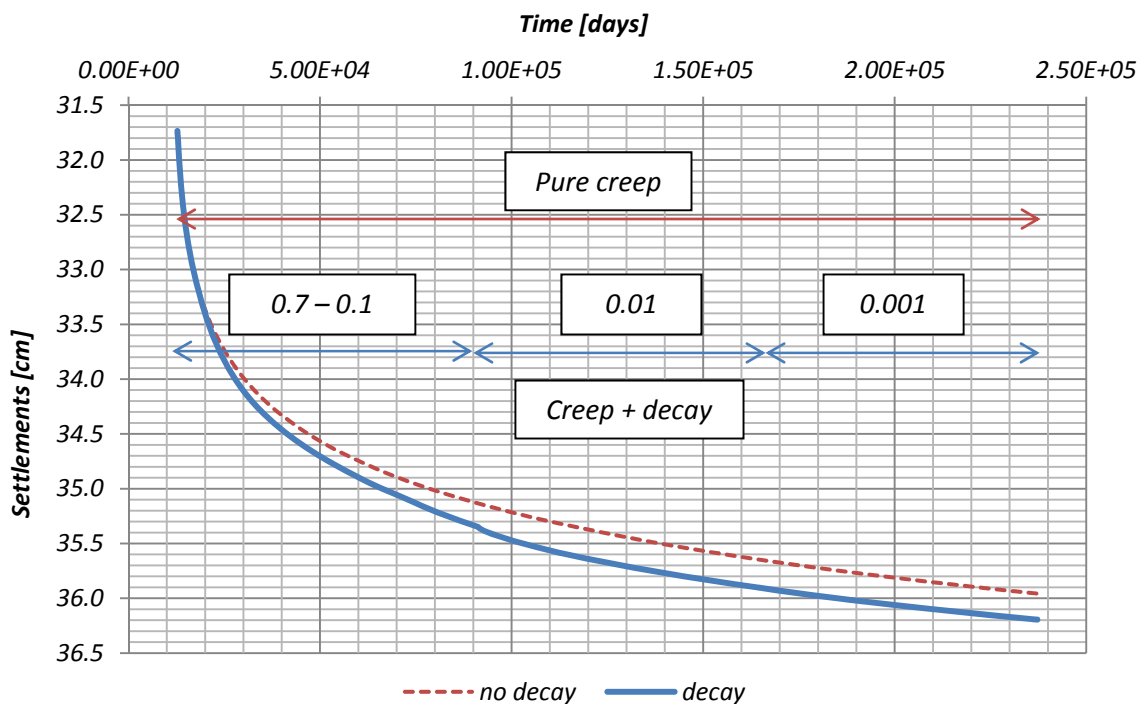


Figure 95: Detail on Figure 94

---

### *Summary of results and discussion*

Compared to the results of interface degradation deriving from the single-pile analysis, the impact of degradation is much smaller in the 3D model, especially regarding the degradation phase of '0.01'. In this phase, in the 2D analysis a rapid acceleration of the settlement-rate was observed. Compare Figure 68 on page 75. However, in the 3D analysis only a slight kink in the curve is visible at the beginning of this phase.

Consequently, in contrast to the 2D model the visco-plasticity of the soil has a larger impact on results (in the order of 4 cm during 615 years of pure creep) than the diminishing interface properties.

## 6.4.2 CONSOLIDATION ANALYSIS

Since the layers with a higher amount of silt and clay have a low permeability, the analyses would have to be performed in undrained conditions. However, due to the slow load application (the construction phase lasts 35 years), the assumption is made that the generation of excess pore water will, if at all, mainly be relevant for the construction phase. After the completion of the foundation, it is assumed that the development of excess pore water pressure will hardly influence the settlements. According to that, the estimation of settlements based on the drained analysis would be reliable despite the neglect of low permeability of certain layers. The scope of this analysis is therefore to quantify the error which is made through these assumptions.

The permeability coefficient,  $k$ , for the single layers is chosen as follows in Table 35.

Table 35: Permeability coefficients

<i>Layer</i>	<i>Permeability <math>k</math></i>	
	<i>[m/d]</i>	<i>[m/s]</i>
Clay	$8.64 \cdot 10^{-5}$	$10^{-9}$
Sand	0.432	$5 \cdot 10^{-6}$
Alternating layers	$8.64 \cdot 10^{-3}$	$10^{-7}$

Apart from that, the material parameters and constitutive models are kept as described on page 91, using the SSC model for the clay layer and the HSS model for deeper layers.

Due to the limited computational resources, the original 3D model has to be modified for conducting the consolidation analysis. Therefore, the number of elements is reduced to 37 386 and corresponding number of nodes to 101 896.

The consolidation analysis is performed neglecting the influence of degradation. Therefore, the sequence of calculation phases is principally the one of the pure creep analysis in drained conditions. After every single phase, a consolidation is carried out. The calculation phases can be seen from Table 36.

Table 36: Calculation phases for pure creep analysis in undrained conditions

<i>Identification</i>	<i>Phase no.</i>	<i>Start from Phase no.</i>	<i>Explanation</i>
Initial phase	0	N/A	K0-procedure
Activation of walls	1	0	Installation of support system to a depth of -6.2 m below ground level (1 day)
Consolidation	2	1	365 days
Ground-water lowering	3	2	Lowering of ground-water to a depth of -3.7 m (1 day)
Consolidation	4	3	365 days

---

Excavation	5	4	Excavation to a depth of -3.2 m (1 day)
Consolidation	6	5	365 days
Activation of block and raft	7	6	Installation of piles (represented by the block) from -3.2 m to -5.2 m and of the raft (1 day)
Consolidation	8	7	365 days
Deactivation of walls and activation of masonry	9	8	Deactivation of support system and activation of the foundation masonry of the tower with zero weight (1 day)
Consolidation	10	9	365 days
Rising of groundwater level	11	10	Rising groundwater level to original level of -1.0 m (1 day)
Consolidation	12	11	365 days
Load I	13	12	Application of 160 kPa on the raft, corresponding to 1/3 of the structural loads (1 day)
Consolidation	14	13	10 years
Load II	15	14	Application of further 160 kPa on the raft, corresponding to 2/3 of the structural loads (1 day)
Consolidation	16	15	10 years
Load III	17	16	Application of further 80 kPa on the raft (1 day)
Consolidation	18	17	5 years
Load IV	19	18	Application of 480 kPa on the raft, corresponding to the full structural loads (1 day)
Consolidation	20	19	Consolidation analysis for 619 years (Pure creep)

---

Results

In Figure 96 and Figure 97, the Time-displacement curve before load application respectively for the time period after completion of the foundation is illustrated. The settlements are again measured in the centre of the foundation (compare Figure 85 on page 95). During the construction of the foundation, the settlements of the consolidation analysis are smaller, whereas the difference before load application amounts to about 1 cm. The difference results mainly from the application of the support system, which is the first phase after k0-procedure. However, settlements after the completion of the foundation show a different development. In this case, the drained analysis in general provokes smaller settlements, whereas the difference at the end of the observation amounts to 3 cm.

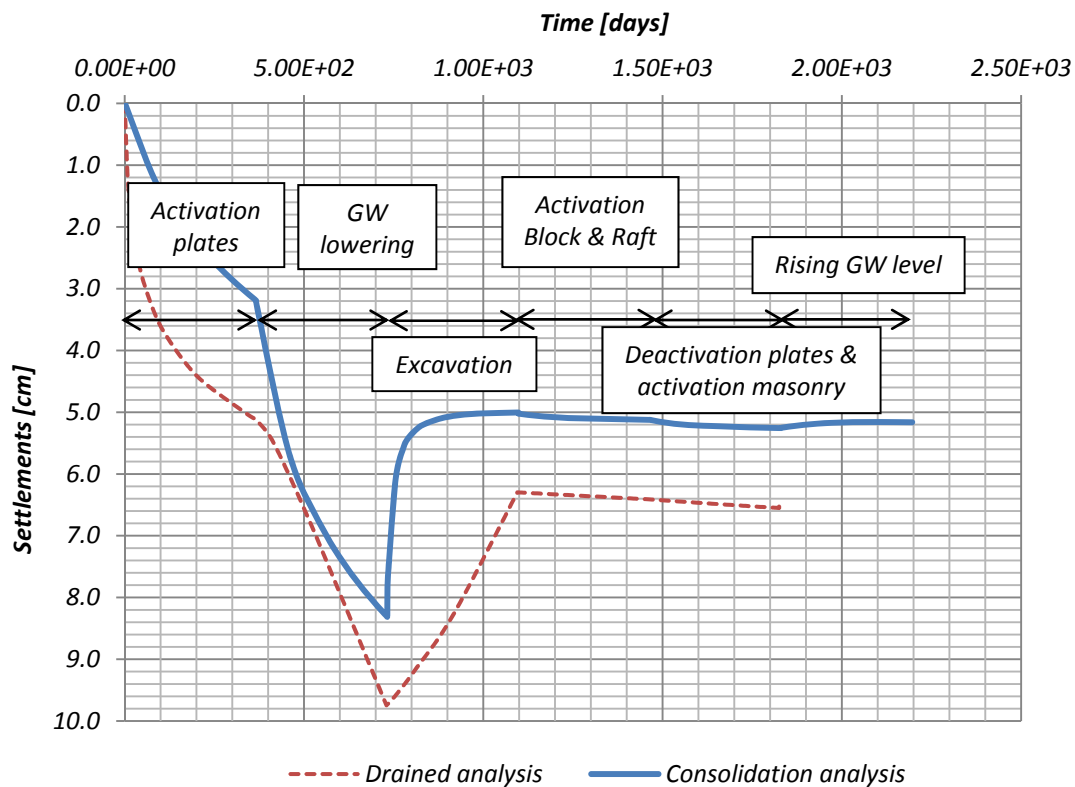


Figure 96: Time-displacement curve before load application

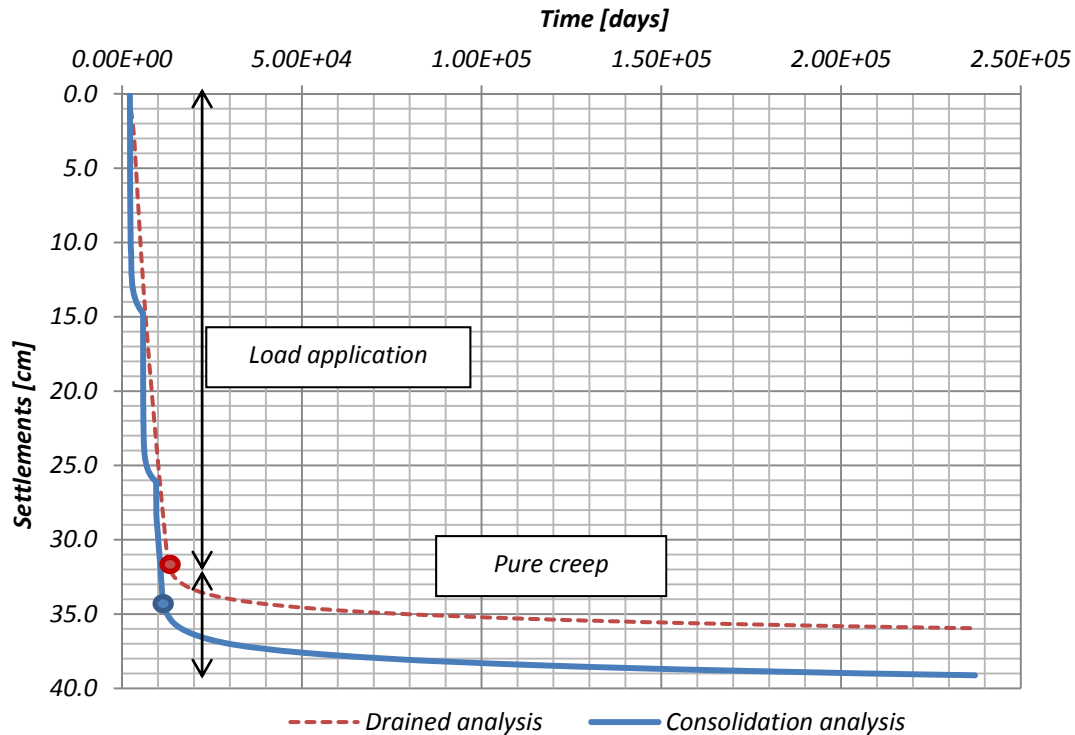


Figure 97: Time-displacement curve after construction of foundation

### Summary of results and discussion

During the construction of the foundation, it is shown that undrained conditions provoke smaller settlements, which derive primarily from the first year. As it was discussed before (see page 95), in drained conditions relatively high settlements due to the visco-plasticity of the soil occur in this period. In the consolidation analysis, however, the creep settlements are retarded during the installation of the support system, and can only fully develop during the subsequent consolidation phase. This causes a stiffer soil response, with a difference of 2 cm after the consolidation phase compared to only 3 cm of settlements in undrained conditions.

After the construction of the foundation, an inverse development is observed, since the settlements from the consolidation analysis result higher (difference of about 3 cm), with a final value of 39 cm. Comparable with the development of settlements during the drained analysis, these settlements are mainly generated during the phases of load application and intermediate consolidation phases.

### 6.4.3 CONCLUSION

During the 3D analysis, several factors were tested on their influence on settlement behaviour. These are the OCR, visco-plasticity and pile degradation. It was shown that the OCR has a very low influence on settlement behaviour in the time period of load application and the following creep phase. The effect of creeping itself turned out to be relevant mainly for the first years of constructing the foundation. Afterwards, the settlement-rate due to creeping is strongly decreasing. Further, it was illustrated that also through the interface degradation the general settlement behaviour is not changed. The main factor that guides the settlement seems to be the applied load. However, this does not explain the settlements of the tower which have been observed since the beginning of the 20<sup>th</sup> century.

Concerning the impact of degradation, the following difference between modelling in 2D and 3D was observed: During the single-pile analysis the effect of interface degradation caused a remarkable increase in settlements compared to the amount of settlements due to creep. In contrast, in the 3D analysis the interface degradation hardly affected the results. Moreover, those settlements resulted even smaller than the settlements due to creeping, which amounted to only 3 cm at the end of the final creep phase. This might be due to the fact that the whole group of piles is simulated as a block with smeared parameters; thus, the interface area of the block is smaller compared to the interface area of the pile in relation to their respective volumes. Further, the parameters of the block and the piles differ already in non-degraded state. Another reason might be that the interface degradation was simulated differently in the 2D and the 3D model: In the 2D model, the interface as it is provided within the calculation program is applied for simulating degradation. This was possible since to these interfaces different parameter sets can be assigned. However, in the 3D calculation this is not possible, as it was explained before. Therefore, the small element cluster was introduced acting as interface between block and soil.

According to the results obtained, the system reaction during degradation has to be verified, in order to ascertain whether the negligible small influence of degradation on behaviour is due to the chosen type of model or if the behaviour is indeed independent of the interface degradation.

## 7 FINAL REMARKS

The time-dependent behaviour of wooden pile foundations was simulated in this thesis within an axisymmetric 2D model and a 3D model. During the 2D analysis, the focus lay on finding a representative model for the decreasing material properties of wooden piles with time. For this purpose, different degradation methods were applied and compared amongst each other. Apart of the identification of a suitable degradation model, specific features of numeric modelling were recognized in the course of this study, such as the influence of the pile's strength on stress distribution and its predominance compared to the influence of stiffness concerning stress redistribution. Moreover, the study allowed understanding the program response when altering the pile's stiffness.

The conclusions of the 2D analysis were then applied within the 3D model. In this model, the foundation of a specific tower in Venice was investigated, which exhibits severe degradation due to the described bacterial attack. The influences of pile degradation as well as of soil viscosity were analyzed in this regard. The results obtained from the 3D model have to be treated with caution, since these results are valid solely under the made assumptions which were necessary for creating a simplified model. Such a preliminary model is needed for studying the basic system response and, in this way, to obtain a qualitative idea of the problem like in the 2D model.

One assumption concerns modelling degradation, which is for a start restricted to the interface. However, as it was mentioned previously, a verification of the results from the used degradation model is needed. For this purpose, one could exploit the interfaces of the wall elements provided by the 3DF program, as it was done for simulating the contact behaviour between the masonry footing and the soil. This time, however, various parameter sets would have to be created for modelling the diminishing contact properties between the piles and the surrounding soil. These parameter sets differ from each other only by the value of  $R_{inter}$ . For simulating degradation, the material sets are then assigned to the adjacent soil, so that the  $R_{inter}$  and consequently the interface parameters diminish, whereas the material properties of the soil itself remain the same.

Besides, also the pile-degradation, which was performed within the 2D analyses, could be performed in the presented 3D model. In this case, the parameters of the block itself would have to be reduced. However, it is most likely that this would not have a strong impact on the general load bearing behaviour, apart from an increase of settlements in the 'pile-head' area due to the elasto-plastic strains of the block. On the other hand, by using single piles in the 3D model instead of the smeared block, a change in system response may be observed if the pile distance is large enough.

Other assumptions concern for example neighboring buildings, which are neglected in the model, and the construction sequence, in particular in combination with the construction of the basilica itself. Further, the intervention at the beginning of the 20<sup>th</sup> century is not taken into account, and neither the rotation of the tower, which occurred since then and was originated most probably from that intervention (see page 9). These circumstances, however, cannot be easily implemented into the current model. This is due to the lack of information regarding the construction sequence of the tower, and also regarding preloading of the subsoil through the construction and existence of former buildings at this site (such as the former smaller churches), which is of major relevance for describing the mechanical behavior of the soil. Further, assumptions would have to be made for considering adjacent buildings, since the current model is based on double-symmetry. Therefore, also the

rotation of the tower is not simulated, which however could be done by modelling the entire tower instead of a quarter.

As mentioned in the introduction, similar studies have been and are performed at the University of Padova. In Baglioni (2009), the results of parametric studies within a 2D model are provided. These studies are carried out for modelling degradation of wooden piles of a typical Venetian foundation. According to the pile degradation method 'Method B' of the present thesis, Baglioni simulated the pile degradation by reducing stiffness and/or strength of the pile to 1/10, 1/100 and 1/1000 of the original parameters. The obtained results show modifications in system behaviour when reducing the pile's parameters to 1/100 ( $E=129\,000$  kPa,  $c=250$  kPa), and in an excessive way at a reduction to 1/1000 ( $E=12\,900$  kPa,  $c=25$  kPa). Modifications comprise an increase in settlements as well as a redistribution of stresses towards the soil. A reduction to 1/10, however, does not modify the system behaviour. Results in between the degradation steps of 1/10 to 1/100 are not included.

During the pile degradation analyses within the single-pile model, similar modifications are observed in the present work with Method A and B. These, however, are generated mainly between the degradation steps 1/10 ( $E=700\,000$  kPa,  $c=700$  kPa) and 1/100 ( $E=70\,000$  kPa,  $c=70$  kPa).

The excessive modification at 1/1000, observed by Baglioni, may be due to the application of Method B, not considering in this way the 'history' of the pile, but also avoiding specific features of the numeric calculation program (such as predominance of the effect of strength reduction compared to the one of stiffness reduction concerning stress redistribution, no response to a gradually reduced pile stiffness). It has to be discussed how such features could be treated in a more elegant way.

Besides, Baglioni reports that the piles and the intermediate soil move down as a whole, justifying the simplification made within the 3D model when representing the piles and the soil in between by a block.

In Ceccato (2012) further analyses are presented, which, however, are based on a more advanced degradation model assuming a linear reduction of stiffness and strength. According to Ceccato, the effect of the visco-plastic behaviour of the subsoil is predominant compared to the effect of pile degradation unless the piles have totally lost their mechanical properties.

A similar observation is made within the 3D analysis of the present thesis. However, the total settlements of the Frari tower after its construction cannot be explained solely by the observed secondary settlements, and the degradation model used, considering only interface degradation, has to be verified.

## 8 FUTURE PROSPECT

The current 3D model of the Frari bell tower is preliminary and very general. The advantage of this simplified model is that single mechanisms can be studied individually and through the information obtained universal conclusions can be drawn which can be applied also within other projects. However, in order to reproduce the development of settlements of this tower or similar buildings, more advanced models are needed for representing the behaviour of the wooden piles and of the soil and their interaction with time.

For describing the degradation of the wooden foundation elements per se, it is necessary to conduct further investigations in order to receive a larger quantity of data and consequently vaster information to rely on. In this way, it might be possible to relate measurable factors, like for example density and humidity of the wood specimen, with mechanical properties such as residual strength and stiffness. This relationship could then be used for assessing the mechanical properties at a certain degradation stage, which are needed within the numerical calculation. Besides, such a relationship was already set up for piles of historical buildings in the Netherlands, and was used within a prediction model [see Klaassen (2008)]. This model allows predicting compressive strength from moisture content.

For capturing the contact behaviour between pile and soil in degraded as well as in non-degraded state, mechanical tests with real-scale specimens are essential. Through these tests, it would also be possible to calibrate the present numerical model of the single pile.

Apart of the time-dependent behaviour of the piles, the visco-plasticity of the soft soil layers and corresponding creep settlements play a key role for describing the mechanical behaviour of the foundation. Therefore, the presented calculations should be repeated with a constitutive model which is well adapted for representing the characteristics of Venetian subsoil instead of the standard SSC model provided by Plaxis, such as the *Anisotropic creep model* or the *Visco-clay model*, mentioned in Chapter 3 on page 15.

In connection with the used SSC model, it has to be considered that lateral plastic outflow of soil from highly stressed regions near the foundation cannot be captured. This outflow may have been constrained in the first years or decades due to a specific construction method, which was described on page 6. This method comprehends the driving of the exterior piles for creating a confinement before installing the interior piles, limiting the outflow of the soil and receiving in this way a well-compacted subsoil. However, it is possible that this problem became relevant with time, as severe total as well as differential settlements occurred. Especially after the intervention at the beginning of the 20<sup>th</sup> century, the plastic outflow in combination with the one-sided reinforcement of the foundation might have been the reason for the leaning of the tower against the basilica. Moreover, this could also explain the increase of settlements observed in the course of the last century. Consequently, there is further need to investigate this phenomenon.

It is a future goal to clarify if the settlements of the past century are due to the degradation of the piles, or rather are provoked by plastic outflow. In case of the Frari tower, the settlements are already constrained through the soil improvement in 2003 (mentioned on page 9) and are monitored since then. Thus, there is no urgent or mandatory need for pursuing further investigations regarding this tower. However, results of such investigations would play a decisive role in evaluating if foundations in Venice fulfill the stability requirements and, if this is not the case, their need for safeguarding measures. Moreover, a further development of the degradation model would be

---

beneficial also for other European cities facing the same problem of wood pile degradation, such as for example Amsterdam.

## 9 REFERENCES

- Baglioni, A. (2009). Analisi del comportamento a lungo termine delle fondazioni dei palazzi di Venezia. Padova (Italy): Department IMAGE, University of Padova.
- Berengo, V., Leoni, M. & Simonini, P. (2008). Numerical Modelling of the Time-dependent Behaviour of Venice Lagoon Silts. *The 12th International Conference of IACMAG*, (pp. 929-936). Goa (India).
- Bertolini, C., Cestari, L., Marzi, T., Macchioni, N., Pizzo, B. & Pignatelli, O. (2006). New Methodological Approaches to the Survey on Timber Historical Foundations. (P. B. Lourenco, P. Roca, C. Modena, & S. Agrawal, Eds.) *Structural Analysis of Historical Constructions*, pp. 335-342.
- Biscontin, G., Izzo, F. & Rinaldi, E. (Eds.). (2009). *Il sistema delle fondazioni lignee a Venezia - Valutazione del comportamento chimico-fisico e microbiologico*. CORILA.
- Casoni, G. (1851). Sopra un singolare apparato di fondazione scoperto nell'occasione che fu disfatta un'antica torre in Venezia. Memoria del M. E. Ingegn. Giovanni Casoni. *Atti dell'Istituto Veneto, Vol. 1, Serie III*.
- Ceccato, F. (2011). Comportamento meccanico delle palificate lignee di Venezia (Master Thesis). Padova (Italy): Department IMAGE, University of Padova.
- Ceccato, F. (2012). Comportamento meccanico delle palificate lignee di Venezia nel tempo. *Atti del Incontro Annuale dei Ricercatori di Geotecnica 2012 (IARG 2012)*. Padova (Italy).
- Cola, S. & Simonini, P. (2002). Mechanical behaviour of the silty soils of the Venice lagoon as a function of their grading characteristics. *Can. Geotech. J.* 39 (4), pp. 879-893.
- Colombo, P. & Colleselli, F. (1997). Preservation problems in historical and artistic monuments. In C. Viggiani (Ed.), *Geotechnical engineering for the preservation in historic sites* (pp. 435-443). Balkema, Rotterdam.
- Donghi, D. (1913). The reconstruction of St. Mark's belltower in Venice. La ricostruzione del campanile di S. Marco a Venezia. *Giornale del Genio Civile*.
- Gottardi, G., Lionello, A. & Modena, C. (2008). Influenza delle caratteristiche di fondazione sulla stabilità dei campanili di S. Stefano e dei Frari a Venezia. In F. Zezza (Ed.), *Geologia e progettazione nel centro storico di Venezia* (pp. 79-98). Padova (Italy): Il Poligrafo.
- Jamiolkowski, M., Ricceri, G. & Simonini, P. (2009). Safeguarding Venice from high tides: site characterization & geotechnical problems. *Proceedings of the 17th International Conference on Soil Mechanics and Geotechnical Engineering (ICSMGE 2009)*, (pp. 3209-3227). Alexandria (Egypt).
- Klaassen, R. (2008). Bacterial decay in wooden foundation piles - Patterns and causes: A study of historical pile foundations in the Netherlands. *International Biodeterioration & Biodegradation* 61, pp. 45-60.
- Leoni, M., Karstunen, M. & Vermeer, P. A. (2008). Anisotropic creep model for soft soils. *Géotechnique* 58, No. 3, pp. 215-226.
- Lionello, A. (Ed.). (2008). *Il campanile di Santa Maria Gloriosa dei Frari in Venezia - Conoscenza, consolidamento, restauro*. Milan (Italy): Electa.

- Maggi, A. (Ed.). (2002). *John Soane e i ponti in legno svizzeri*. Mendrisio (Switzerland): Accademia di architettura Mendrisio, Università della Svizzera italiana.
- Marchi, M., Gottardi, G. & Lionello, A. (2006). Sulle fondazioni dei campanili di Venezia. *Atti V Convegno Nazionale dei Ricercatori di Ingegneria Geotecnica*, (pp. 177-193). Bari (Italy).
- Naldini, S., Trovò, F. & de Jong, J. (2010). Wooden Piles in Venice and Amsterdam: Characteristics, Damage and Interventions. *Restoration of Buildings and Monuments* (Vol. 16, No. 6), pp. 421-434.
- Plaxis bv. (n.d.). PLAXIS 3D Foundation Material Models Manual. Version 2. Delft (The Netherlands).
- Plaxis bv. (n.d.). PLAXIS 3D Foundation Reference Manual. Version 2. Delft (The Netherlands).
- Ricceri, G., Simonini, P. & Cola, S. (2002). Applicability of piezocone and dilatometer to characterize the soils of the Venice Lagoon. *Geotechnical and Geological Engineering* 20, pp. 89-121.
- Rocchi, G., Fontana, M. & Da Prat, M. (2003). Modelling of natural soft clay destruction processes using. *Géotechnique* 53, No. 8, pp. 729–745.
- Schickhofer, G. (Ed.). (2006). *Holzbau - Der Roh- und Werkstoff Holz* (Lecture notes, Part A). Graz, Austria: Institute for Timber Engineering and Wood Technology.
- Trovò, F. (2012). *I sistemi fondali dell'architettura storica di Venezia (Corso di Caratteri Costruttivi dell'Edilizia Storica)*. Retrieved August 2012, from <http://www.iuav.it/Ateneo1/docenti/architetto/docenti-a-/Trov--Fran/materiali/-/04--IUAV-Caratteri-09-10---I-SISTEMI-FONDALI.pdf>
- Wichert, H.-W. (1988). Einfluss der Alterung auf die Tragfähigkeit von historischen Spickpfahl-Gründungen. Braunschweig, Germany: Institut für Grundbau und Bodenmechanik, Technische Universität Braunschweig.
- Zeza, F. (2007). Geologia, proprietà e deformazione dei terreni del centro storico di Venezia. In *La Riqualificazione delle città e dei territori - Geologia e Progettazione nel centro*. Venice (Italy): Il Poligrafo.
- Zienkiewicz, O. C., Taylor, R. L. & Zhu, J. (2005). *The Finite Element Method: Its Basis and Fundamentals*. London: Butterworth-Heinemann.